Wireless modular multi-sensor systems for the analysis of mechanical coupling between respiration and locomotion in mammals

DISSERTATION

zur Erlangung des akademischen Grades

DOKTORINGENIEUR

(**Dr.-Ing.**)

vorgelegt der

Fäkultät für Maschinenbau der

Technischen Universität Ilmenau

von Herrn

M.Sc. Nelson Enrique Bances Purizaca

geboren am 10.01.1983 in Lambayeque/Peru

1. Gutachter: Univ.-Prof. Dipl.-Ing. Dr. med. (habil.) Hartmut Witte

2. Gutachter: Univ.-Prof. Dr.-Ing. Thomas Sattel

3. Gutachter: Univ.-Prof. Dr. Hans-Christoph Scholle

Tag der Einreichung: 10.01.2018

Tag der wissenschaftlichen Aussprache: 12.06.2018

urn:nbn:de:gbv:ilm1-2018000287

Dedication

This thesis work is dedicated to my wife, Alina, who has been a constant source of support and encouragement during the challenges of this work. I am truly thankful for having you in my life. I also dedicate to my son, Daniel, who is my inspiration to keep moving forward, and to my parents, Cesar and Agustina, who have always loved me unconditionally and whose good examples have taught me to work hard for the things that I aspire to achieve.

Zusammenfassung

Die Kopplung zwischen Fortbewegung und Atmung (Locomotion-Respiration-Coupling LRC) basiert bei Säugetieren nach den gängigen Modellvorstellungen sowohl auf mechanischen als auch neuromuskulären Bindungen zwischen beiden Prozessen. Zur artübergreifenden Analyse dieser Interaktionen fehlt es bisher an einfach anpassbaren, modularen Systemen. Damit fehlt es an belastbaren Messdaten zur Beantwortung der Fragen, wie Fortbewegungszyklen zum Atemfluss beitragen oder wie die Atemmuskelkontraktionen die Fortbewegung beeinflussen. Die meisten der bisherigen artspezifischen Studien konzentrierten sich auf LRC während des Laufens, aber einige analysierten auch andere Aktivitäten wie Radfahren, Fliegen (Vögel) oder Tauchen. In dieser Arbeit wurde basierend auf einem modularen Multisensor-Funksystem eine neuartige Methode entwickelt, die es ermöglicht, die Interaktion zwischen Fortbewegung und Atmung bei Säugetieren zu analysieren. Das entwickelte System besteht aus vier Komponenten für die LRC-Analyse: (1) einer Thoraxbinnendruckmessung basierend auf einem implantierbaren Gerät, (2) ein Volumenstrommodul zur Messung des lokomotorisch getriebenen Luftvolumens (LDV - Locomotor driven air volume) während des Atemzyklus, (3) ein Schrittidentifikationsmodul zur Berechnung des LRC-Verhältnisses (Schritt/Atem) und (4) ein Muskelaktivitätsmodul zur Analyse des Verhaltens des Atemmuskels während der Kopplung. Diese Module sind freizügig kombinierbar.

Die drahtlose Kommunikation erlaubt es, Untersuchungen im Freifeld durchzuführen, wobei sich das Tier (oder der Mensch) im Gegensatz zu früheren Studien, in denen sich das Subjekt mit einer konstanten Geschwindigkeit auf einem Laufband bewegt, frei mit einer selbstgewählten Laufgeschwindigkeit bewegen kann. Diese Möglichkeit könnte das Stressniveau von Tieren während der Experimente signifikant reduzieren, die Analyseergebnisse liegen absehbar näher am "natürlichen" Laufverhalten (unrestrained) als jene von Laufbandstudien (restrained).

Als experimenteller Test des Systems wurde die Methode am Menschen angewendet. Das Respiratory Flow Module (RFM) wurde basierend auf einer „ergonomischen Maske“ und einem Strömungssensor entwickelt. Das Respiratory Muscles Module (RMM) nutzte vier Oberflächen-Elektromyographie-Sensoren (sEMG) an der Bauch- und Brustmuskulatur. Am Knöchel jedes Beines befanden sich zwei Beschleunigungssensoren, um den Fuß-Boden-Kontakt zu erkennen. Fünfzehn Teilnehmer wurden bei einem Sprint-Lauftest in einem Sportzentrum (50 m x 30 m) der Technischen Universität Ilmenau beobachtet. Die erhaltenen Ergebnisse bestätigten ein variables LRC-Verhältnis von 2:1, 3:1, 4:1 wie in früheren Studien gezeigt wurde, zeigte jedoch zusätzlich im Falle des LDV die Nutzung der annähernd maximal möglichen Amplitude (Vitalkapazität) auf.

Das Experiment belegt, dass die neue Methode zur Untersuchung von Säugetieren verwendet werden kann.

Abstract

Locomotor-respiratory coupling (LRC) is a mechanical and neuromuscular link between respiration and locomotion in mammals. In the last several decades many researchers have developed studies in this field measuring LRC in different mammals. However, until now it was not exactly established how many locomotion cycles contribute to the respiratory flow or how the respiratory muscle contractions affect the locomotion cycles. Most of these studies were focused on LRC during running, but some also analyzed other activities like cycling, flying (birds), diving. In this work a novel method was developed based on a modular multi-sensor wireless system which allows analyzing the interaction between locomotion and respiration in mammals. The developed system consists of four modules for the LRC analysis: (1) a thoracic pressure measurement based on an implantable device, (2) a volumetric flow module to measure the locomotor driven air volume (LDV) during the breathing cycle, (3) a step identification module to calculate the LRC ratio (stride/breath), and (4) a muscular activity module to analyze the behavior of the respiratory muscle during the coupling.

The wireless communication allows performing studies in open field, where the animal can move freely with a self selected running pace, contrary to previous studies where the object moves at a steady speed on a treadmill. These characteristics could significantly reduce the stress level of animals during the experiments.

The method was applied to humans as an experimental test of the system, the Respiratory Flow Module (RFM) was designed based on an ergonomic mask and flow sensor. The Respiratory Muscles Module (RMM) had four surface Electromyography (sEMG) sensors located at the abdominal and thoracic respiratory muscles and two accelerometers were located at the ankle of each leg to detect the foot-ground contact. Fifteen participants were evaluated in a sprint running test at a sport center (50 m x 30 m) of Technische Universität Ilmenau. The obtained results confirmed a variable LRC ratio of 2:1, 3:1, 4:1, as was shown in previous studies. However, in the case of LDV it reached almost the maximum amplitude of the vital capacity. The performed experiment showed that our novel method could also be used to study other mammals.

Nomenclature

Greek Symbols

γ	a simply closed curve on a complex plane
Δ	differential
π	$\simeq 3.1415\ldots$
$\propto$	directly linearly proportional
ρ	density
σ	electric conductivity

List of Variables

$\dot{m}$	mass flow
$\dot{V}$	volumetric flow
C_p	specific heat of the fluid
H	heat power input
P	pressure
R	resistance of a central membrane
T	temperature
V	volume

Superscripts

j	superscript index

Subscripts

0	subscript index

Other Symbols

$\oint_\gamma$	integration around a curve γ

Acronyms / Abbreviations

ABS Acrylonitrile Butadiene Styrene

ACC Accelerometer

DAQ Data Acquisition

DAQ Data Adquisition

DCC Data Control Center

DG Diaphragm

EI External Intercostal *(M. intercostales externi)*

EIRP Effective Isotropic Radiated Power

EIRP Equivalent Isotropically Radiated Power

EMF Electromagnetic Field

EO External Oblique *(M. abdominis obliquus externus)*

ERV Expiratory Reserve Volume

EXA Experimental Area

FRC Functional Residual Capacity

GUI Graphic Unit Interface

I2C Inter-Integrated Circuit

ICNIRP International Commission on Non Ionizing Radiation Protection

iEMG Invasive Electromyography

IPD Implantable Pressure Device

IPM Implantable Pressure Module

IRV Inspiratory Reserve Volume

ITU International Telecommunication Union

LRC Locomotor Respiratory Coupling

LVD Locomotor Driven Volume

MCU Microcontroller

MLM Mechanical Linkage Mechanism

PA Post Analysis

PDMS *Polydimethylsiloxane*

PRx Pressure Receiver

PTx Pressure Transmitter

RFM Respiratory Flow Module

RF Radio Frequency

RMM Respiratory Muscles Module

RV Residual Volume

SAR Specific Absorption Rate

SA Serratus Anterior *(M. serratus anterior)*

SCL Serial Clock

SDA Serial Data

sEMG Surface Electromyography

SIM Stride Identification Module

SoC System on Chip

SPI Serial Peripheral Interface

SSC Sensor Signal Conditioner

TCU Trigno Control Utility

TLC Total Lung Capacity

TUI-AT Technische Universität Ilmenau - Athletics Track

TUI-SC Technische Universität Ilmenau - Sports Center

TV Tidal Volume

WCC Wireless Communication Controller

WHO World Health Organization

WLAN Wireless Local Area Network

Table of Contents

List of Figures

List of Tables

Chapter 1

Introduction

1.1 Introduction

This work shows the development of an experimental method for the study of the mechanical and neuromuscular interaction between respiration and locomotion during free-running mode in mammals. Unlike earlier experimental studies of locomotor-respiratory coupling (LRC) in several animals, here the focus is exclusively on the study of the LRC and its changes not only of air volume changes in lungs, but also on the pressure changes in the thoracic cavity, and the neuromuscular reaction of breathing muscles during the locomotion.

Additionally, this study has focused on the development of experimental tests with mammals moving in free spaces, where the running pace can be self-selected, differing from other studies that were done in laboratories with induced running speed by a treadmill. The implemented method consists of using a wireless system to collect data from different physiological parameters during locomotion. In this introductory chapter, we explain how our interest is to develop a modular multi-sensor wireless system to study the LRC; we describe the institutional concept of LRC and the mechanical link effects, and we give a brief outline of the analytical frameworks.

1.2 Background

The study concentrates on the mechanical interaction between locomotion and breathing of animals in movement, and its importance for the changes of abdominal and thoracic pressure as well as for air volume changes in lungs. It is a biological physical phenomenon that aroused the interest of several researchers in the decade of the 80s, the genre which Bramble (1983) described as "Locomotor-respiratory coupling (LRC)" [21]. Our own interest in LRC was first stimulated by the work of Alexander (1989), who explained the three mechanical its impacts in horses and wallabies: visceral piston mechanism, lumbar bending and loading of the rib cage by the forelimb [2]. He developed the first mathematical model of LRC based on the visceral piston mechanism, concluding that locomotor activity in hopping or galloping animals could drive all or a substantial parts of ventilation. Besides, our interest on the study

of Deban and Carrier (2002), who discussed the dual function (locomotor and respiratory) of many hypaxial muscles may produce conflicts during running [36]. However, a particular pattern of LRC in quadrupedal mammals may circumvent this conflict or minimize their impact on respiration. Additionally, our interest was increased when other researches like Boggs (1997) or Carrier (1987) developed studies in birds and lizards and concluded the existence of LRC in all the cases [16, 24]. Also, the work of Daley (2013), who shows the importance of the associated intrapulmonary dynamics instead of the volume driven by locomotion, is based on the evident coupling between locomotion and respiration in vertebrates, particularly in mammals [33]. Our interest was to focus on the methods, i.e. previously developed experimental studies, and how this information could follow a pattern to develop mathematical or statistical models of LRC in a specific species. These methods can be useful for a better understanding of breathing and locomotion interaction in any mammals, and it can be a powerful tool for a specialist in order to recognize patterns in the parameter's changes and to identify unexpected results.

The study started from the premise that there are three physiological parameter changes during a breathing cycle, driven by locomotion: (1) air volume changes in the lungs, (2) the thoracoabdominal pressure changes and (3) the electrical activities of respiratory muscles during locomotion. Our next step was to identify would quantify the mentioned changes. Although, all the previous studies mention how the volume changes or the electrical activity of the respiratory muscles during exercise were quantified, none of them quantified the pressure changes during those experiments. The latter becomes our greatest challenge in this work. On the other hand, unlike all previous studies using experimental tests in conditioned laboratories, inducing to a fixed speed of locomotion on a treadmill, we wanted to developed a study method considering the natural environment in the movement of any species, minimizing the stress of experiments on the animal and collecting data of parameters involved in the LRC for post analysis.

There was already a substantial body of work not only on the methods of how to measure the parameters changes during locomotion, but also on how to integrate different modules corresponding to each parameter measurement. Also, all the signals should be synchronized to get a better understanding of the LRC. We wished to develop a non-commercial wireless system which integrates several modules to study the LRC of a specific species, and for example, to subsequently build mathematical models based on statistical methods or a pattern recognition based on an artificial neural network (ANN) methods.

Finally, we had to avoid the difficulties of performing animal experiments such as on dogs or on horses in Thüringia due to long procedures to obtain the corresponding permissions.

This work seeks to show the functioning of a system that can be adapted to a specific species, considering previous analysis of its anatomy and physiology.

1.3 Analytical Framework

Concerning the previous studies, detailed references are given in Chapter 2: existing research on LRC in different animals have been based on the ratio between the number of strides per breathing cycle reached by the animals while running or galloping at a high speed pace. The results in most of the cases reach a ratio value of 1:1. In cases such as with human beings, this ratio is more adaptive, and several reasons related to the bipedal motion have been stated. Surprisingly, only few studies gave quantification of parameter values in their results. For example, the displaced air volume during the breathing cycle in each stride, or breathing muscle's electrical activity during the high speed movements were shown. Besides, literature mentions that during a breathing cycle based on Boyle's law, the pressure within the thoracic cavity changes inversely proportional to the volume, and some numerical values were given. However, all these measurement values were given in static experimental tests of breathing. In other words, they can not quantify the pressure changes that occur in a LRC during locomotion at high speeds. Even if some studies on a treadmill measured the air volume changes during motion, and then approximated the pressure changes of the thoracic cavity, the data reported has made it impossible to carry out satisfactory studies on pattern recognition, as example. On this basis two research questions were formulated:

1. If the method based on a modular multi-sensor system with wireless communication is a reliable tool for the analysis of the interaction between respiration and locomotion in mammals?

2. Will the experiments with exercising mammals in a free space with self-selected running pace have a considerable difference in the results compared to the typical laboratory experiments in the same field, using a treadmill with a steady set speed?

In order to answer these questions, this work performs careful analysis as an alternative method of the existing LRC studies. With this method we expect to drive our studies closer to the natural behavior of an animal in motion. To determine analytically if previous methods with animals in movement on a treadmill under controlled conditions were well conducted, this work proposes additionally to incorporate the thoracic pressure changes in our future analyses of LRC, and also, to quantify the pressure changes during the locomotion phases. Finally, this method collects data of each parameter along the whole experiments. This data

allows futures studies on the field of system identification, that uses statistical methods to build mathematical models. It also allows developing computational models in order to detect the patterns and relationships in data.

As already mentioned, our intention at the outset of this research was firstly, to propose a method based on a modular multi-sensor wireless system to measure changes in physiological parameters during a breathing cycle induced by locomotion; secondly, to implement four modules to measure the parameter changes: (a) to measure the volumetric flow during a breathing cycle (inhalation/exhalation), (b) to measure the thoracic pressure changes, (c) to measure the electrical activity of the respiratory muscles, and (d) a module to identify the foot contact on the ground in order to identify the number of steps during the exercises. This last module allows the synchronization of all other signals and recognizes a pattern of LRC during the experiments. Thirdly, to develop experimental tests of the system in humans, in order to prove the functionality of the system and to analyze the possible adaptation in other mammals; and fourthly, to synchronize the collected signals for the analysis of the relation between the signals during the tests.

1.4 Outline of Thesis

The remaining chapters are organized as follows. Chapter 2 contextualises the study in the relevant literature. In Chapter 3 the developed system and the technical information on each implemented module are described and illustrations depict the functional test of each working module. In Chapter 4, the experimental test of the integrated global system is described. As well, it shows the experimental results and discusses them according to the LRC analysis. In Chapter 5, we discuss the results of the implemented system. Finally, in Chapter 6 the summary of this thesis and the outlook are given.

Chapter 2

State-of-the-Art Review

This chapter gives an introduction to the principles of mammalian pulmonary ventilation from the mechanical point of view. This provides a better understanding of how the principal parameters (pressure and volume flow) are affected during locomotion. Also, it explains the mechanical and neuromuscular interaction between breathing and locomotion in quadrupedal and bipedal mammals. It also shows the effects of mechanical linkage mechanisms of locomotion upon breathing. In addition, we comment on a brief description of previous experimental studies and their developed methods in order to explain this interaction.

Finally, to analyze the volume flow changes, this chapter introduces methods based on transducers which measure the air flow rate during breathing. Furthermore, it shows alternative methods of using implantable wireless devices to measure any physiological parameter like pressure within the thoracic cage during locomotion, and the challenges in its design.

2.1 Mechanics of Breathing

The respiratory system aids in breathing, also called pulmonary ventilation. It can be described as the movement of air divided in two phases (inspiration and expiration). During each phase the body changes lung volume dimensions to produce a flow of air either in or out of the lungs.

The mechanics of breathing is illustrated in Figure 2.1, where the main organs and muscles involved in breathing are depicted. Also, in Cotes et al. [30] and Bates [8] the humans physiology and breathing mechanics are explained.

The mechanism of breathing can be explained in terms of Boyle's Law of gases (pressure is inversely proportional to volume): when the volume of thoracic cavity increases, pressure in the thorax decreases and, vice versa, when the volume of thoracic cavity decreases, pressure in the thorax increases. In other words, the action of breathing happens due to pressure changes within thoracic cavity and the atmosphere. This pressure difference is created by changing the volume of thoracic cavity. Mathematically, Boyle's law can be stated as:

$$P \propto \frac{1}{V}, \tag{2.1}$$

where P is a pressure, V is a volume.

What follows is a description of breathing cycle and how the main physiological parameters (pressure and volume) change during the breathing. In addition, it describes the amounts of air in the lungs associated with different phases of the breathing cycle. They are called lung volumes. This description was taken from the anatomy and physiology of humans as a reference. However, the process of respiration is similar in other mammals.

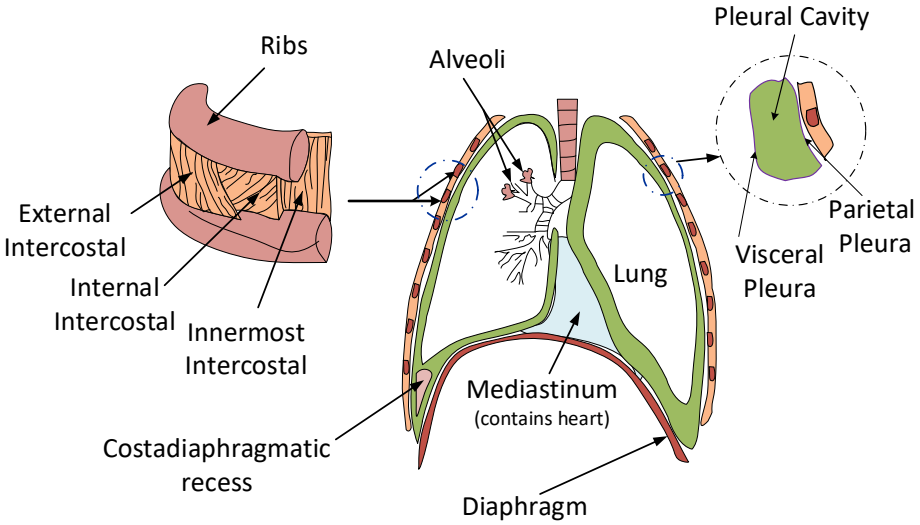

Fig. 2.1 Physiology of breathing: The lungs are separated from the thoracic cage by two thin layers: the visceral pleura that surrounds the lungs, and the parietal pleura, which is in contact with the chest wall, diaphragm and mediastinum. The space between these layers is called a pleural cavity. Intercostal spaces are located between the ribs and contain intercostal muscles. The costodiaphragmatic recess is a potential space in the pleural cavity. Diaphragm is the muscle which separates the thorax and abdomen. [82]

2.1.1 Pulmonary Ventilation

Pulmonary ventilation refers to the movement of air in and out of the lungs. Fig. 2.2 shows the action of inspiration and expiration, and it remarks the function of some ventilatory muscles as diaphragm and the intercostals. In resume, it shows how Bowle´s law works. During inspiration, the diaphragm contracts downward, lungs and parietal pleura are expanded, increasing the volume of pleural cavity. That means, it´s pressure (intrapleural pressure ($P_{pl} \approx 756$ mmHg)), as well the intrapulmonary pressure ($P_{al} \approx P_{atm}$) decreases according to Boyle´s law. The following pressure inside lungs (P_{pl}) decreases to a sub-atmospheric level ($P_{atm} \approx 760$ mmHg), producing air flow entering lungs and increasing it´s volume until the P_{la} rises to the atmospheric level again. In expiration, the cycle is opposite, the inspiratory

muscles relax, the pressure outside (P_{atm}) is lower than within the lungs, and volume is decreasing due to the air expelled from the lungs.

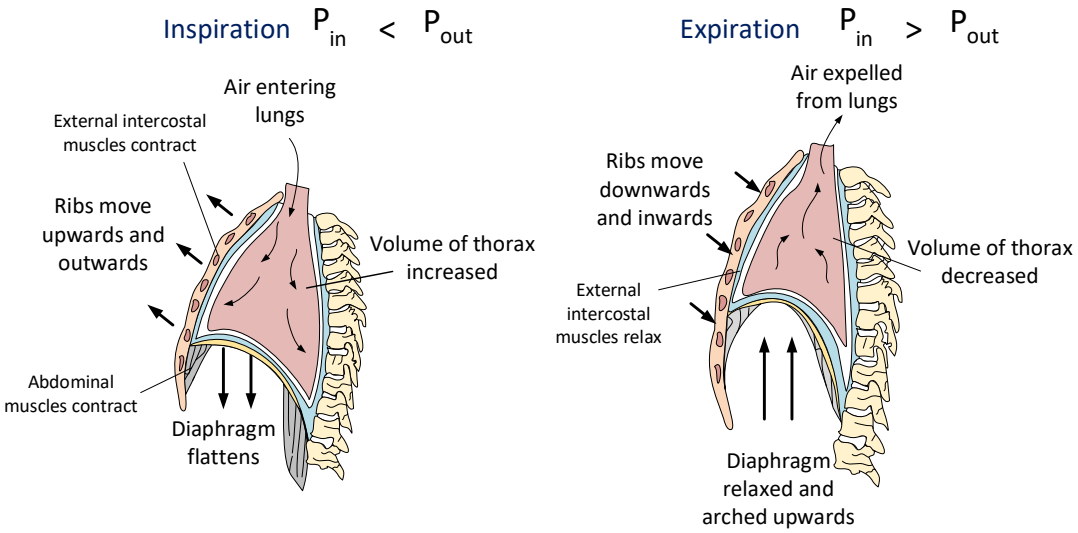

Fig. 2.2 Inspiration: The abdominal muscles help with the diaphragmatic contraction, and the external intercostal contraction makes rib movement upward and outward cause expansion of the thoracic cage. This is possible due to the atmospheric pressure (P_{out}) being greater than intrapulmonary pressure (P_{in}), allowing air to enter the lungs with the volume increasing. Expiration: The external intercostal muscles relax, the relaxed diaphragm moves upwards. The pressure P_{in} is higher than the P_{out}, and as a consequence, the air is expelled from the lungs. [8]

As additional information, Fig. 2.3 describes the changes in pressure, lung volume, and airflow that occurs during a single cycle of breathing. However, it is important to note that these values refer to a human physiology; the pressure and volume changes depend explicitly on the anatomy and physiology of each species.

2.1.2 Lung Volumes and Capacities

The amounts of air in the lungs associated with different phases of the breathing cycle are represented as lung volumes. Summing up, specific lung volumes produces lung capacities. Different animals exhibit different lung capacities based on their activities. For example, cheetahs have evolved a much higher lung capacity than humans, in order to provide oxygen to all the muscles in the body, allowing them to run very fast. Elephants also have a high lung capacity due to their large body mass and their need to take up oxygen in accordance with their body size. Duncker [38] explained the different lung structures and theirs topographic position in vertebrates like reptiles and birds, causing a direct influence in their breathing

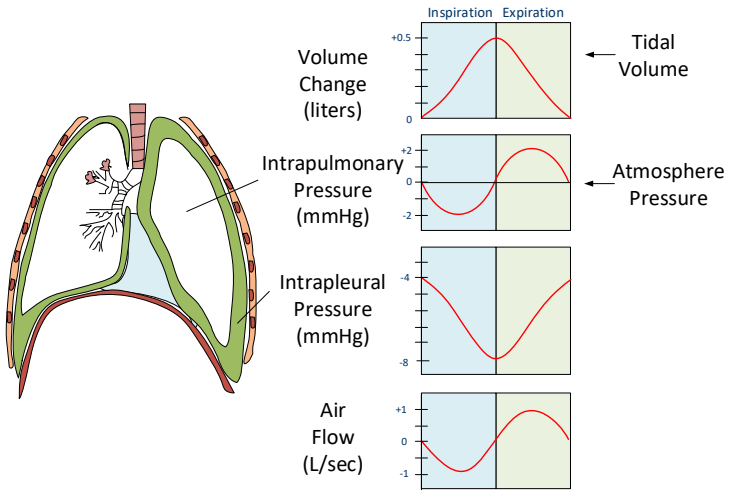

Fig. 2.3 The breathing cycle is a description of the changes in pressure, lung volume and airflow that occurs during a single cycle of breathing. The intrapleural pressure (P_{pl}) becomes more negative as the chest wall expands during inspiration. Its pressure returns to the initial value as the chest wall recoils. The intrapulmonary pressure (P_{al}) decreases, as lung volume increases during inspiration. During expiration, the elastic recoil of the lung declines as it contracts; consequently, the intrapleural pressure returns to its previous value of -4 $mmHg$ in humans, and (P_{pl}) increases [7].

cycle. The time-dependant changes of lung volumes can be seen on a spirogram in Fig. 2.4.

Total Lung Capacity (TLC) is the maximum volume of air contained in the lungs at the end of a full inspiration. This is divided into four primary volumes:

- Tidal Volume (TV) is the volume inhaled and exhaled during normal breath.
- Inspiratory Reserve Volume (IRV) is the maximum additional volume that can be inhaled with additional effort.
- Expiratory Reserve Volume (ERV) is the volume of air that can be further exhaled at the end of normal tidal breath.
- Residual Volume (RV) is the volume remaining in the lungs after maximal expiration.

The Functional Residual Capacity (FRC) is the sum of IRV and RV. This is the volume left in the lungs at the end of normal breath. It is determined by elastic properties of a lung and the chest wall [7].

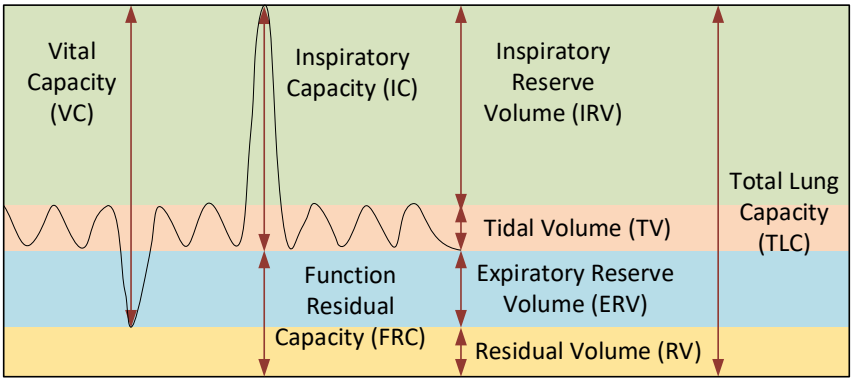

Fig. 2.4 Lung volumes: The average total lung capacity of an adult human male is about six liters of air. Tidal volume is the volume of air inhaled in a single, normal breath. Inspiratory capacity is the amount of air taken in during a deep breath, while residual volume is the amount of air left in the lungs after forceful expiration. [8, 30]

2.2 Locomotor-Respiratory Coupling (LRC)

In this section, we explain the concept of LRC, the mechanical and neuromuscular links between respiration and locomotion in mammals. Also, we report previous studies based on current technology to analyze the LRC. Finally, we mention some physiological effects due to LRC.

2.2.1 The Concept of LRC

Locomotor-respiratory coupling refers to phase locking of breathing and other motion activities. Most of the developed studies have focused on the action of running in different mammals (bipedal or quadrupedal). Furthermore, some researchers have been interested in studying other animals and other activities such as cycling (e.g. Kohl et al. [64]), rowing (e.g. Daffertshofer et al. [32]) in humans, or flying and diving in birds (e.g. Boggs [15, 16, 18]).

According to Boggs et al. [17], breathing and locomotion may be linked neurally and mechanically. It was mentioned that numerous neural mechanisms contribute to the coordination of both respiratory cycles and locomotor cycles, even in fictive locomotion in paralyzed decerebrated animals [66]. On the other hand, the mechanical links are presented in respiratory muscle's contraction, which could affect the locomotion cycle. However, most of the

developed studies refer to the hypothesis, that locomotion cycles contribute to respiratory flow.

2.2.2 Mechanical Interaction in LRC

Over the last 30 years, several theories have been proposed to explain mechanical interaction between locomotion and breathing in mammals. Particularly, studies showed mechanical impacts of locomotion upon **ventilatory pressures and volume flows**. These studies reported that different animals (bipedal and quadrupedal) synchronize their respiration with the movements of their limbs during fast locomotion. For instance, in various quadrupedal mammals, LRC **ratio** (strides/breaths) is 1:1 during their highest speed, such as galloping or trotting [20, 21, 84, 91]. However, the human breathing pattern is more flexible during running, showing ratios of 2:1, 2.5:1, 3:1, 4:1, 5:2 [20, 33]. Boggs et al. have published a complete review from several experimental studies of this interaction (LCR) in different species of mammals and birds. In Table 2.1 a summary of his review is given [17].

Table 2.1 Relation of locomotor cycle to respiratory cycle in mammals. The resume was made by Boggs [17].

Species	Gait or Speed	LRC ratios
Gerbil (rat)	Gallop	1:1
Hare	Half bound	1:1, 2:1
	Galloping	1:1
Domestic rabbit	Gallop	1:1
	Lower Speed	variable
Cat	Gallop	1:1
Dog	Trot	1:1, others
Sheep	Gallop	1:1
Horse	Trot	1:1, 3:2, 2:1, 5:1
	Gallop	1:1
Tammar Wallaby	Hopping	1:1
Humans	Running	3:1, 2:1 ,5:2, 3:2, 4:1, others

2.2.3 Mechanical Linkage Mechanism (MLM)

As was mentioned in Section 2.2.1, these two rhythmic (locomotion and breathing) activities with different frequencies become phase locked due to mechanical and neuromuscular interaction. In particular, many species exhibit a constant ratio of 1:1 (strides/breaths) at higher speeds [2, 20–22, 65].

Additionally, some studies suggested that LRC has some physiological effects such as: (i) reducing the energy cost of breathing [9, 11, 72], (ii) reduction of muscles conflict which are involved in both activities [25, 36], (iii) incremental pumping of air in and out of the lungs due to the inertial movement of some organs and tissues [20, 21], and (iv) body stabilization during motion as Simons [84] mentioned, according to the hypothesis of pneumatic stabilization.

Finally, four exercises-associated forces called MLM affecting respiration have been proposed as the responsible of these physiological effects. Fig. 2.5 gives an example of the mechanical interaction mechanism during locomotion in quadruped mammals.

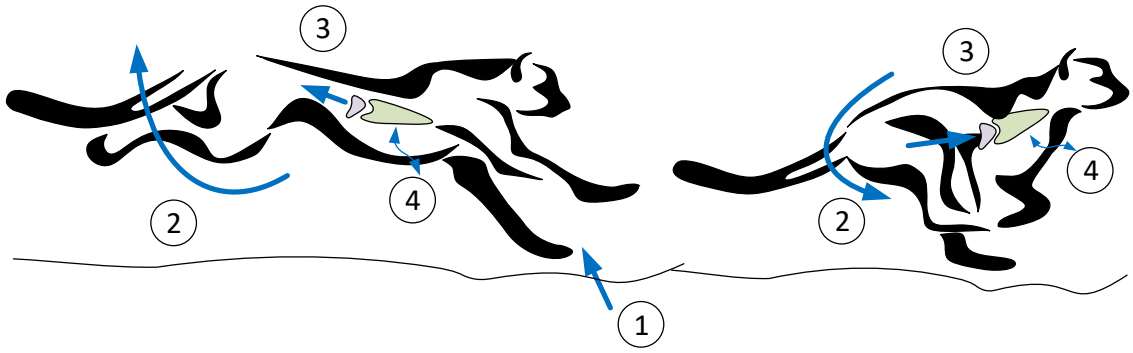

Fig. 2.5 Mechanical linkage mechanism (MLM). ① *Rib cage loading by forelimb:* Transmitted compressive forces to the rib cage due to impact with ground. ② *Lumbar flexion:* the trunk flexion and extension affects internal volume in the thoracic cavity. ③ *Visceral piston:* Inertial movements of the not firmly connected visceral mass. ④ *Ventilatory muscles:* In some vertebrates, many chest wall muscles contribute to both breathing and locomotion, ceasing respiratory action and becoming entrained with locomotor cycle during running.

Ribcage Loading by Forelimb

In quadrupedal species, the forefeet impact on the ground transmits compressive forces through the muscles to ribs cage, which changes pressures inside the thorax, driving air out of the lungs when the forefeet are on the ground. According to Young et al. [91], in this period the maximal expiratory flow is achieved.

Lumbar Flexion

During locomotion, the trunk flexion of the lumbar spine displaces the abdominal viscera (mainly the liver), which tends to push up against the diaphragm. This volume displacement

produces expiratory flows from the lungs, as well as the pressure changes within thorax and abdomen. The opposite situation occurs with the trunk extension producing inspiratory flows.

Visceral Piston

The visceral mass is suspended by elastic structures within the body wall. This loose attachment and accelerations of the trunk may impact the position of the diaphragm. Consequently it modifies volume changes in the thoracic cavity, causing airflows [21], as well as intrapleural and intrapulmonary pressure [17]. Bramble and Carrier [20, 21] suggested that these backward and forward movements could be regarded as a resonant spring-mass system called "visceral piston". Alexander [2] proposed a mathematical model of this mechanism, following the results of studies in wallabies and horses. In summary, both researchers proposed that during galloping cranial motion of the visceral mass upon landing would facilitate expiration. The caudal motion during forelimb flight phase would facilitate inspiration. Therefore, this model predicts that motion of the visceral mass during galloping will directly influence the respiratory cycle.

Years later, Simons [84], based on her studies in rabbits, proposed another model regarding the liver position and its relationship to locomotor and respiratory mechanics. She called the model pneumatic stabilization. This model explained that simultaneous expiration and forelimb support results in positive pressure in the pleural cavity. This pressure drives the visceral mass caudally and provides some mechanical support for the heart.

Ventilatory Muscles

There are three groups of ventilatory muscles: the diaphragm, thoracic cage and abdominal muscles. During motion the increased ventilation demands to determine an increased neural drive to the respiratory muscles. Consecutively, the mechanical power increases are developed by the muscles. Aliverti [3] affirmed that the diaphragm is a flow generator, and the rib cage and abdominal muscles are pressure generators.

In particular, hypaxial muscles (abdominal and rib cage) are used for both breathing and locomotion. Carrier [24, 26] showed that many hypaxial muscles produce functional conflicts during locomotion in lizards and dogs. In 2002, Deban and Carrier [36] made an experimental study on dogs. It was concluded that the LRC may circumvent these conflicts or minimize their impacts on respiration.

All these studies were based on the hypothesis proposed in 1960s. It was mentioned that breathing frequencies maximize flow rate, but minimize the work of respiratory muscles.

Experimental studies were done with some animals like guinea pigs and dogs to support this hypothesis [31, 68].

Effects of LRC

Based on several theoretical and experimental studies on LRC, researchers have concluded that LRC has a number of important physiological effects:

- Energy cost reduction of breathing [9, 11, 44, 72].
- Minimizing conflict in hypaxial muscles [25, 26, 36].
- Body stabilization [84].
- Increase of breathing performance [21, 20].

2.3 LRC in Humans

Previously it was explained that several numbers of studies have found the LRC ratio in most of quadrupeds during high speed of motion is 1:1 (strides / breath). However, it was also mentioned that in humans the ratio varies, e.g. 2:1, 3:1, 4:1. This variety in breathing patterns relative to locomotion most likely relates to an upright posture and striding bipedal gait [5, 21, 74, 76].

In contrast to quadrupeds, the trunk flexion of the lumbar spine during locomotion does not assist ventilation performance. Moreover, the forelimbs are not subjected to direct weight-bearing and impact loading. Daley et al. [33] mentioned, that transmitted forces through the thorax, abdomen and rib cage are smaller in humans, reducing mechanical interaction between locomotion and breathing. Also, the idea was supported that bipedal posture may reduce the mechanical and neuromuscular conflicts that constrain quadrupeds to a 1:1 LRC pattern [26, 36].

However, this flexibility does not mean that humans do not have any mechanical coupling. Some researchers suggested that the coupling occurs under some specific circumstances. For instance, humans couple breathing frequency with the low impact or movements such as fingers and arm tracking [39, 74, 76, 79]. Additionally, Daley et al. [33] explained that impact loading of the body at footstrike may cause compression of the thorax and downward displacement of the abdominal viscera. Also, the arm swing exerts compressive load on the

thorax during early to mid-stance[1], the effect is alteration of respiratory flow by changing volume and pressure in thorax and abdomen.

2.4 Previous LRC Experimental Studies

According to the brief explanation of the mechanical and neuromuscular LRC in mammals, it is evident that some respiratory flows occur with the stride. Nevertheless, the discussion is focused on whether the volume displaced is significant or not for breathing. At the beginning of the 80s, some research proposed that locomotor activity could drive all or a substantial part of ventilation in exercising animals [21]. Others have developed mathematical models based on the MLM, suggesting that this hypothesis is applicable in hopping and galloping animals [2]. However, measurements of volume change provided by stride in trotting and galloping animals range from 1% to 20% of tidal volume [43]. In humans it was from 1% to 2% of tidal volume [5], or in trotting dogs it was 3%-16% [13].

The following is a brief description regarding the experimental techniques used by researchers to analyze the LRC and its linkage mechanisms. There are some methods based on transducers to measure the volume and pressure changes during locomotion. Also, it describes methods to synchronize locomotion with breathing, based on the stride cycle detection (start and end) in order to calculate the LRC ratio. In addition, to get a better understanding of the coupling, some methods include the electrical activity of the ventilatory muscles to analyze the neuromuscular effects during motion.

2.4.1 Respiratory Air Volume

For several years, the discussion was focused on air volume displaced due to the LRC mechanism. Many researchers implemented methods based on transducers to collect data during breathing in order to obtain quantitative results of ventilation (movement of air in and out of the lungs) during locomotion. For instance, Lafortuna et al. [65] used an ultrasonic flowmeter in their experiment with horses to determine the effects of LRC. The other example was developed by Simons [84]; she had studied the viscera piston mechanism in domestic rabbits using pneumotachometer. Daley et al. [33] studied LRC in humans with the same method.

In order to determine the air volume moved by stride, first it is necessary to measure the respiratory flow rate during locomotion. The most common flow transducer is a pneumo-

[1] Phase of the normal gait cycle: Stance phase is the time when the foot is on the ground.

tachometer[2]. Different kinds of transducers also exist, like a turbine, vortex, ultrasound or a thermal mass flow meter[3]. The main advantage of thermal mass flow meters is higher sensitivity for very low flow rates ideal for medical applications (see Fig. 2.6).

In case of a pneumotachometer, the volumetric flow is calculated by:

$$\dot{V} = \frac{\Delta P}{R} \quad , \qquad [\mathrm{dm^3\,s^{-1}}] \tag{2.2}$$

where R is the known resistance of the central membrane and (ΔP) is the pressure differential (see Fig. 2.6).

In the case of a mass flow meter, mass flow ($\dot{m}$) is calculated using the measured temperature difference (T_2 - T_1), heat power input (H), and the specific heat of the fluid (C_p):

$$\dot{m} = \frac{H}{C_\mathrm{p} \cdot \Delta T} \quad , \qquad [\mathrm{kg\,s^{-1}}] \tag{2.3}$$

To calculate the volumetric flow ($\dot{V}$) in $\mathrm{dm^3}$ per minute, we must convert the mass in to kilograms to volume in $\mathrm{dm^3}$ using the density ρ (kg/L) of the gas. In case of the air the density is 1.184 kg/m^3 or 0.001184 $kg/\mathrm{dm^3}$ at a temperature of 25°C and an atmospheric pressure of 1 atm:

$$\dot{V} = \frac{\dot{m}}{\rho} \quad , \qquad [\mathrm{dm^3}] \tag{2.4}$$

Finally, for both cases the flow signal is integrated over time to determine the volume (V), as in:

$$V = \int \dot{V} \partial t \quad , \qquad [\mathrm{dm^3}] \tag{2.5}$$

where V denotes the inhaled or exhaled air volume, and $\dot{V} = \partial V / \partial t [\mathrm{dm^3}/s]$ is the measured volumetric flow.

2.4.2 Stride Detection and Synchronization

Conventional gait analysis techniques, such as optoelectronic motion capture systems[4], often are used as standard methods, thanks to their highly accurate three-dimensional measurements. However, these systems can only be used in a controlled laboratory environment.

[2] Pneumotachometer is a transducer that converts the air flow into a proportional signal of pressure difference via fixed diameter tube on either side of a central membrane.

[3] Mas flow meter measures the temperature changes of the flow as it passes through a heat source.

[4] Motion capture systems measure the motion of a body or object, using light (often infra-red) reflected from markers attached to its surface.

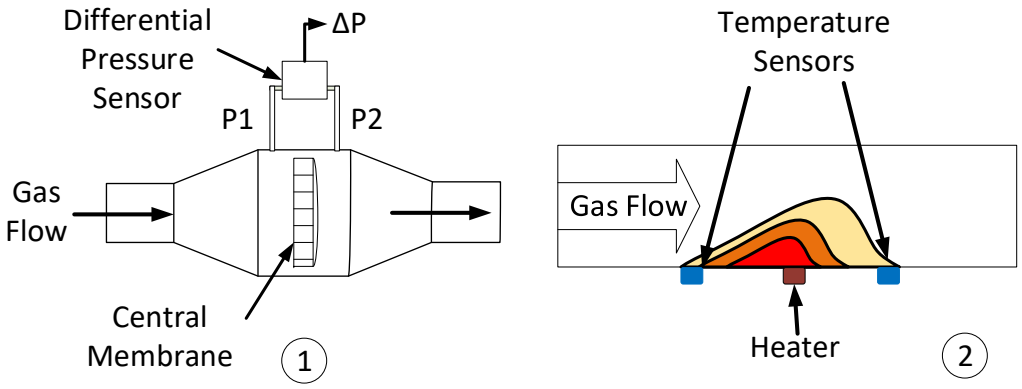

Fig. 2.6 A flowmeter transducer measures the rate flow of gases :① Pneumotachometer: The pressure gradient is directly related to flow, the central membrane has a known resistance. ② Mass flowmeter (thermal principles): An adjustable heating element is positioned at the center of a pressure-stabilized membrane, with a temperature sensor both upstream and downstream of the membrane in the direction of gas flow.

In previous studies of LRC, researchers have chosen to use more simple and economical methods, such as wearable sensor technology or video camera recording to reach the synchronization (stride cycle[5] and respiratory cycle must be aligned on the same time axis). Several studies were developed using these methods with several animals such as rabbits [84], horses [65], iguanas [23] and dogs [21].

Additionally, another device was used called a mechanoelectrical goniometer[6] fixed on the hips, indicating forward movements of the left leg ("one" signal) or right ("zero" signal) during running or cycling in humans. The whole step is detected as the difference between "zero" signal to the next "one" signal [11, 80].

Accelerometer-based systems have been proposed as the most popular ambulatory solution for stride detection during locomotion. These sensors allow continuous assessment of gait features outside the laboratory environment [19, 46, 57, 75]. In particular, some studies used accelerometers to perform analysis of human running cycles synchronized with breathing cycles [33]. It is important to note that all the previous experimental studies were done with animals or humans while running on the treadmills. Besides, the complexity to entice animals to run on treadmills or to breath normally through respiratory equipment is a considerable problem. Also, they faced some technical problems: for example, it is difficult to connect

5 Stride cycle is the period when one foot contacts the ground to when that same foot contacts the ground again.

6 Goniometer is an instrument for measuring angles.

measuring devices to an animal, motion artifacts may be misinterpreted as a locomotor contribution to breathing. Also, the mask holding a transducer to measure flow accurately must provide a good seal.

Brief description is included of the techniques and many problems (mentioned before) occurring during the discovered experimental tests. As a result, we opted to use wireless technology for data acquisition in order to reduce stress in animals during the test. Furthermore, wireless technology allows experiments outdoors or in free running environments.

2.4.3 Muscular Electrical Activity Durign Breathing

Several respiratory muscles (e.g. intercostal and abdominal) also have locomotor functions. These affirmations were inferred from their physical electromyography[7] **(EMG)** activity with the locomotor cycle [26, 36]. For example, Ainsworth et al. [1] studied the relationship between the respiratory muscle activity and esophageal pressure generation in exercising dogs, breathing at high frequencies. Hodges and Gandevia [53] studied the electrical activity of the abdominal muscles and the relation with the intra-abdominal pressure during the postural in humans. In general, the EMG technique is used to infer neural activities of respiratory muscles that occur during their contraction and relaxation cycles. At the beginning, this technique was invasive; the motor neurons[8] transmit electrical signals that cause muscles to contract. An EMG needle electrode inserted directly into a muscle and an amplifier chain record its electrical activity and convert these signals into graphs, sounds or numerical values. These values are then interpreted by a specialist [81].

Alternatively, these days there are surface EMG, that are used to obtain information about the time or intensity of superficial muscle activation [70]. However, the disadvantage of surface electrodes is the inability to specifically monitor deep muscles. Also, surface EMG requires high signal processing to obtain reliable information (see. Fig. 2.7) [29, 34]. Finally, according to the opinion of these authors, surface EMG technique can be used together with wireless technology. In this way, it is possible to perform experimental studies in free running, in order to analyze the neuromuscular coupling of ventilation muscle and their effects on locomotion.

[7] EMG is a technique for recording the electrical activity of muscles, used in the diagnosis of nerve and muscle disorders.

[8] In vertebrates, motor neurons (also called motoneurons) are nerve cell that conducts impulses to a muscle or gland

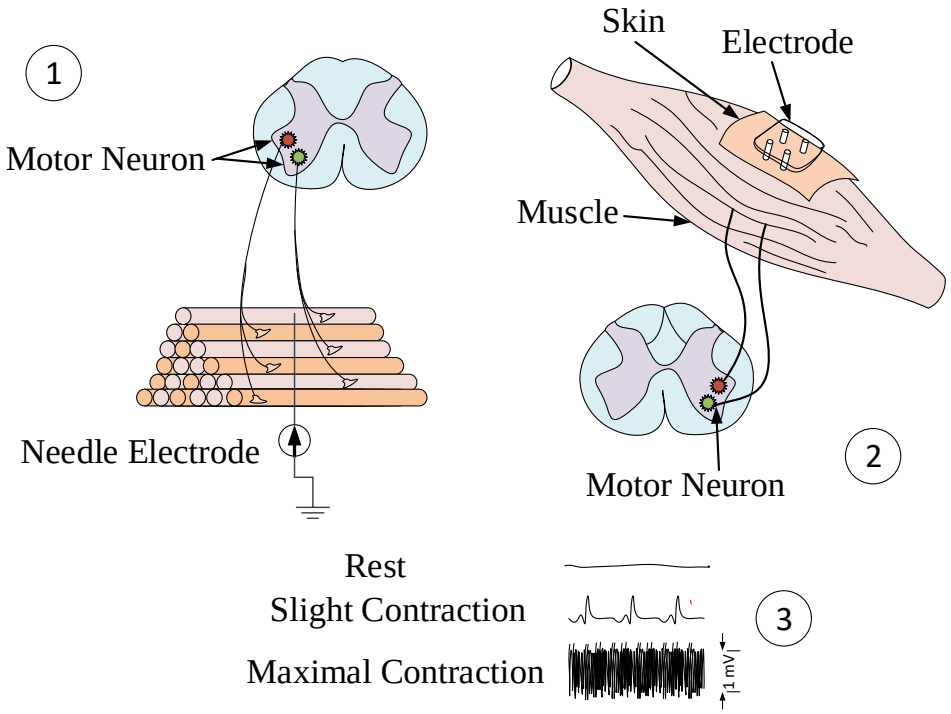

Fig. 2.7 Electromyography (EMG), invasive and surface electrodes: ① Intramuscular (**iEMG**): A needle electrode is used, inserted through the skin until it enters the muscle tissue. ② Surface (**sEMG**): uses a single or an array of electrodes placed on the skin surface over the muscles to be tested. ③ Outline of the signal decomposition [34].

2.4.4 Thoracic Pressure Measurement

In Section 2.2.2, it was explained that two physiological parameters are affected by the mechanical linkage between locomotion and breathing: (i) ventilation volume, (ii) thoracic and abdominal pressure. Nevertheless, the majority of previous studies does not provide any quantitative information about the thoracic pressure changes during locomotion, especially in the free running mode. However, a few studies showed some experimental results with humans or animals. For instance, Hodges and Gandevia [53] published a study about the pressure changes in an intra-abdominal cave during postural and respiratory activation of the human diaphragm. In this study, the pressure transducer was inserted via the nose and esophagus into the stomach of the person in static position. The electrical activity of the thoracic muscles during breathing was studied using EMG sensors.

Another experimental study was done by Ainsworth et al. [1]. Dogs were moving on a treadmill. Previously the dogs were tracheostomized[9], according to the methods of Milic-Emili et al. [71] for estimating pleural pressure from an esophagel ballon-catheter transducer. In other studies the pleural pressure was estimated from esophageal pressure [42, 52, 69]. However, Hedenstierna [49] mentioned that this method presents potential errors, because esophageal pressure is affected by the (i) elastance[10] and weight of the lungs, rib cage, diaphram and abdomen; (ii) weight of mediastinal[11] organs; and (iii) elastance of esophageal wall. Based on the literature analysis, this work proposes another method to measure the thoracic pressure. Based on Valdastri et al. [88], short term implantable devices that support wireless communication can be used.

2.5 Radio Frequency Implantable Pressure Device (IPD)

Over the last 60 years, implantable devices have been utilized in many applications. Nowadays, any physiological parameters can be monitored, becoming a valuable biomedical tool for telemetry *in vivo*[12]. In particular, for pressure monitoring *in vivo*, many researchers have proposed various methods. For instance, Tan et al. [85] developed a pressure device for short term urological studies and patient monitoring. Lin et al. [67] also developed a device to measure pressure changes in the upper urinary tract per degree of obstruction. Recently, Henrik Casimir Ahn [50] developed a wireless implantable pressure device for monitoring and study of cardiac function (intracardiac pressure) in humans. Another case for using IPD was reported by Johnson et al. [59]. They developed an intra-vaginal transducer to measure intra-abdominal pressure during physical activities, showing an improvement in the dynamic response when compared to a standard rectal balloon catheter. It is worth mentioning that all the presented devices, have the advantages that can be extended to measure other physiological parameters from different sensors and for specific applications, such as Valdastri et al. [88] has proposed.

In this research an implantable device to measure the pressure within the thoracic cavity during locomotion in mammals was developed. In order to achieve the technical requirements

[9] Tracheostomize is a surgical procedure in which an incision is made into the trachea through the neck. A tube is inserted also in the trachea to make an artificial opening to assist breathing.

[10] Elastance is a measure of a structure tendency to return to its original form after removal of a deforming force.

[11] The mediastinum is the central compartment of the thoracic cavity, it contains the heart and its vessels, the esophagus, trachea, phrenic and cardiac nerves, the thoracic duct, thymus and lymph nodes of the central chest.

[12] The term in vivo refers to a medical test, experiment or procedure that is done on (or in) a living organism, such as a laboratory animal or human.

for our system, during the device design international standards were taken into account despite the limitations of using only commercial components.

2.5.1 Properties of Implantable Devices

Several requirements should be considered during the design of implantable devices, such as minimal size and weight, low power consumption, good reliability, high compatibility, reduction of pain sensation and discomfort to the host during the application [10].

2.5.2 Communication Frequency Range

Radio Frequency (**RF**) technology plays an important role in the development of medical implant communication system (**MICS**). The international organizations such as Federal Communications Commission **(FCC)** and the European Telecommunications Standards Institute **(ETSI)** are focused on supporting new frequency bands associated with biomedical communications [28]. In particular, the FCC established 402-406 MHz Medical Device Radio Communication **(MedRadio)** band just for implantable medical device applications [41]. It allows low power transmission (output power maximum is 25 μW **EIRP** [13]). Furthermore, the FCC also established the Industrial, Scientific, Medical **(ISM)** bands (e.g. 433 MHz). These have become a reliable alternative for short-range and low power communication systems. Therefore, due to the limitation of commercial antennas designed for MedRadio band, our design was implemented considering only commercial ceramic or PCB antennas designed for ISM band. However, our device also allows communication in MedRadio frequency range.

2.5.3 Antenna Effects

Whereas advances in semiconductor and micro-electromechanical systems **(MEMS)** have been developing rapidly in the last decades, new pressure sensors have been created for medical applications. Also, new transceivers with very low power consumption which work with MICS frequencies have been developed [27, 45, 47, 56]. However, the antenna and battery size are still a challenge to overcome. Nevertheless, recent designs in patch antennas have been proposed by Kiourti and Nikita [62]. The patch antenna is preferred for implantable antenna design, due to their high flexibility in the shape [61]. However, at this time point these antennas are not commercially available.

[13] Equivalent Isotropically Radiated Power : The measured radiated power in a single direction. The EIRP is related to the power transmitted from the radio (Ptx), the cable losses (L) and the antenna gain (G) as in EIRP = Ptx-L+G [μW].

Another characteristic to consider in the IPD design are the effects of electromagnetic field generated by the device upon body. The specific absorption rate (**SAR**) is a measure of how transmitted RF energy is absorbed by tissues. It can be expressed as:

$$SAR = \int_V \frac{\sigma(r) \cdot |E(r)|^2}{\rho(r)} \mathrm{d}r \quad , \qquad [\mathrm{W\,kg^{-1}}] \tag{2.6}$$

where σ is the electric conductivity of the material, E is the electric field as function of position, ρ is the mass density of the measured material and r is a position vector. Finally, V is the volume over which the SAR is measured.

Since this parameter is important for the health of implant carriers, many organizations have established limits and regulations approving safety guidelines. IEEE C95.1-2005 [55] standard specifies the safety level of human RF exposure from 2 KHz to 300 GHz. Also, the International Commission on Non Ionizing Radiation Protection (ICNIRP) [54] published its guidelines for limiting exposure to the time-varying and electromagnetic field (**EMF**). It was established that the local SAR averaged over a cube of **10 g** of tissues should not exceed **2** W/kg for head and trunk and **4** W/kg for limbs. These guidelines have been accepted by the International Telecommunication Union (ITU) [58] and by the World Health Organization (WHO) [89]. In spite of IEEE C95.1 and ICNIRP guidelines, they are not explicitly designed for regulating EMF exposure implantable devices. Many implantable system designers follow these guidelines. For example, Xu et al. [90] made simulation studies of ingestible wireless devices (IWD) with different communication frequencies (430, 800, 1200, 2400 MHz), which showed that radiation intensity depended on orientation and position of the antenna. The obtained results showed the maximum of the averaged-10 g SAR can reach 1.37 W/kg at the input of 25 mW. These results are below the allowed standard (2 W/kg).

Finally, researchers as Fang [40] suggested that these guidelines are not sufficient for implantable medical devices.

2.5.4 Power Supply for IPD

The remaining challenge in the design of implants is the battery life, high efficiency and the battery size (especially with long term implants). The battery must provide service over many years to minimize surgical frequency to extract or replace batteries. The most utilized battery type is the lithium/iodine (L_2/I_2) cell, used in the beginning to power an implantable cardiac pacemaker. However, lithium ion batteries have also been developed for medical applications where the batteries are charged while remaining implanted [14]. For short term implants with low power consumption it is common to use cell lithium batteries, as will be done in this work.

2.5.5 Biocompatibility

The term of biocompatibility is related to the interaction between an implantable medical device and the surrounding host tissues. The main goal of the material is coating of the device and avoiding or minimizing infections, especially for long term implants. Bhunia et al. [12] mentioned that the designed device needs to consider the chemical composition of the material, biodegradation and changes in physical properties of the device, such as a shape, size and surface morphology. Another important factor is the position of the implant. Some of the commonly used materials for coating are metallic alloys, polymers and ceramics. Teo et al. [87] and Qin et al. [78] presented an extended review of Polydimethylsiloxane (PDMS), commonly referred as a silicone. It is preferred to metals and ceramics because of its biocompability, chemical resistance, mechanical flexibility and optical transparency. Furthermore, PDMS is well recommended for packing sensors, electronics and biomedical technology to develop integrated systems at low cost. In particular, Kirsten et al. [63] made an experimental study using a pressure sensor equipped with wireless communication. Different biocompatible polymers were chosen, investigating their barrier properties for a stent graft[14]. Also, Kim et al. [60] reported the advantages of using PDMS, such as mechanically stability and biocompatibility when encapsulating cables for long term implantable devices.

[14] A stent is a tiny tube placed into a hollow structure of human body, e.g. a blood vessel.

Chapter 3

System Overview and Features

In Section 2.4 it was shown that the techniques which study and analyze the LRC are based on the use of several transducers. These transducers measure parameters during locomotion such as the ventilation volume flow, thoracic pressure and the step identification for the synchronization. Also, the previous experimental studies analyzed the LRC in laboratory using treadmills with controlled speeds. The proposal of this work is to develop a system capable of studying the mammal's LRC under normal conditions during locomotion. The developed system is based on wireless communication to achieve the free-movement mode in free space. Furthermore, it will reduce stress of the animals under test and will allow animals to move at a preferred speed. Finally, this approach represents a valuable alternative to study the LRC in mammals.

This chapter gives the detailed description of the implemented system. The systems structure is based on the client-server communication model. This model describes the server component as a hub[1] dedicated to managing several peripherals (clients). For the data transmission wireless technology, namely Wi-Fi, was used. It primarily provides short range wireless high speed data transmission between the clients and a server. In particular, the used Wi-Fi operates in the 2.4 GHz radio band, and the network components are based on the **IEEE 802.11 a/b/g/n** standards with a maximum data rate of 300 Mbps.

The implemented system also may be described as a multi-modular sensor platform. The server called Data Control Center (**DCC**) manages the data transfer from the clients or sensor modules. Four clients were implemented in this work. Each module is responsible for the data acquisition of a specific parameter in LRC study: (i) the respiratory flow module (**RFM**) measures the air volume flows during the breathing cycle, (ii) the stride identification module (**SIM**) measures the acceleration of each step during locomotion, (iii) the implantable pressure module (**IPM**) measures the thoracic pressure, (iv) the respiratory muscle module (**RMM**) measures the electrical activity of the thoracic cage muscles. The system structure is shown in Fig. 3.1.

[1] A Hub is a central device that connects multiple peripheral devices to a single network

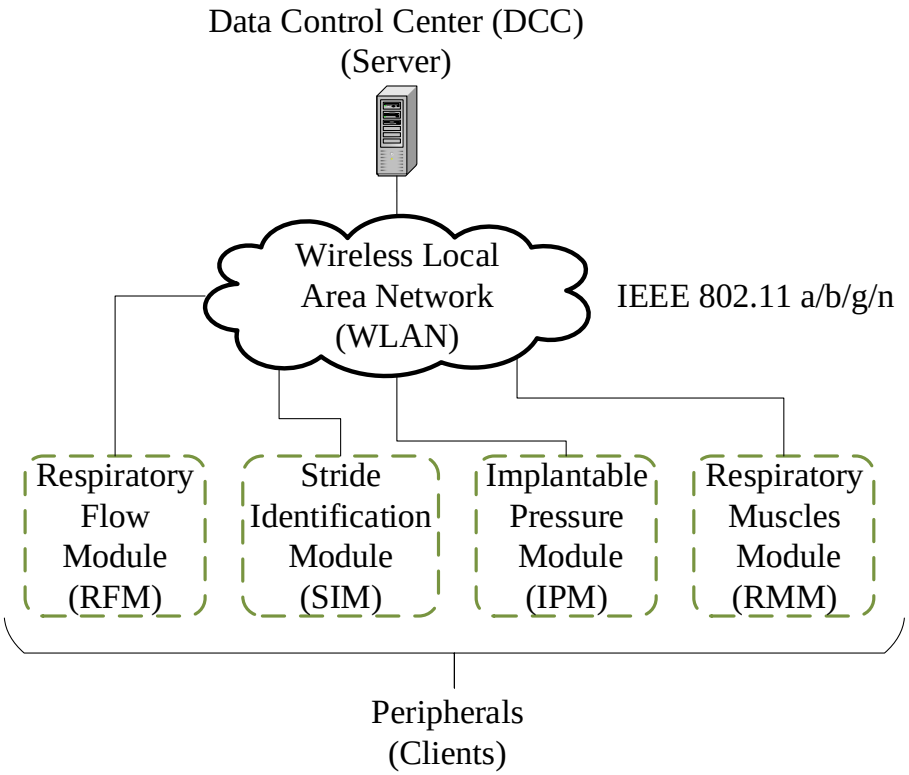

Fig. 3.1 Structure of the multi-modular sensor platform.

The following sections present the servers and each module´s technical description, and the module specific characteristics of electronics hardware, firmware, software and communication, as well as the mechanical implementation of adaption to any test. It is important to mention that the aim of this work is to develop an alternative and complete system to study the LRC in any mammal during free-motion mode.

3.1 Data Control Center (DCC)

The used server is a laptop (DCC) with the following characteristics: Processor Intel® Core™ i7, 16 GB DDR3 SDRAM and WLAN 802.11 a/b/g/n transceiver. The Wi-Fi technology is based on the standards IEEE 802.11 a/b/g/n. A graphic unit interface (**GUI**) is installed on the DCC to process data. All data processing was performed offline using a commercial software package MATLAB® *R2016b*. The GUI was programmed based on the modular functions structure. This characteristic allows adding extra sensor modules to the system. For example, the heart rate measurement module during locomotion. The GUI has two main functions or operation modes: (i) data acquisition mode when data sent by all

sensor modules is received by the DCC via Wi-Fi and saved, (ii) post data analysis mode which manages saved data.

In Fig. 3.2 two operation panels of each mode are shown. The following description of each panel explains the methods to obtain and to analyze the saved data.

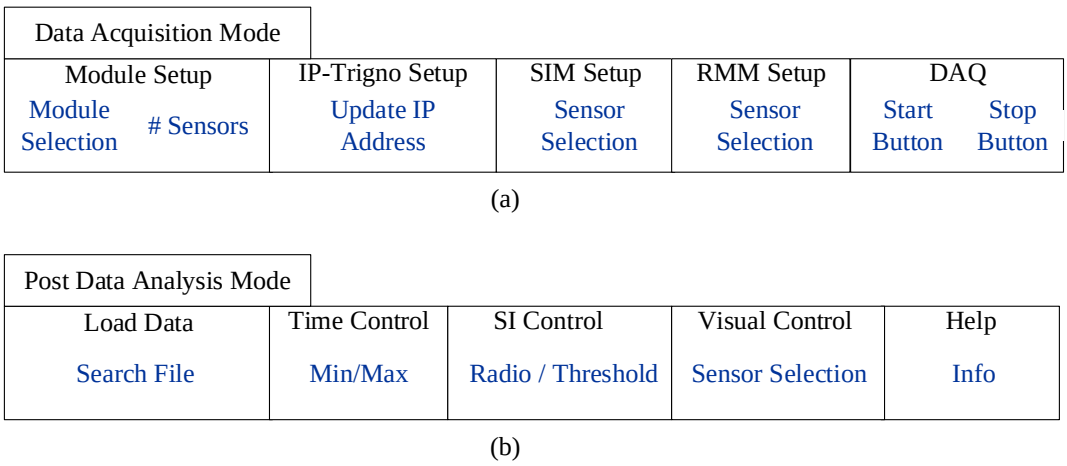

Fig. 3.2 GUI operation panels: (a) Data acquisition mode allows data acquisition and storing, (b) Post processing mode, allows the analysis of the saved data.

3.1.1 Data Acquisition Mode (DAQ)

The operational flowchart of data acquisition mode is shown in Fig. 3.3. The developed GUI allows data acquisition of all the sensor modules in parallel (complete system) or each module independently. The raw data is saved in a file with *.txt* extension. The data is organized in arrays and saved in a file (time and sensor values).

The DAQ mode can be explained in three main steps: (1) The GUI allows selection of one or more sensor modules for the study. The developed system includes four modules (RFM, SIM, PIM, RMM) as was explained in Fig. 3.1. It is possible to select the number of sensors in SIM and RMM in particular. After the module selection, (2) the sensor setup sub-panel is activated. For example, the RFM allows sensor calibration function in this sub-panel. In the case of SIM and RMM, a commercial wireless system called Trigno^{TM} based on 16 hybrid acceleration and EMG sensors was used. This system is explained in the following sections. However, Trigno system works with its own receiver. The GUI allows the connection between Trigno and the DCC through an IP-address. (3) Finally, the DAQ

is activated by the START button to plot the signal in real time and can be stopped with a STOP button.

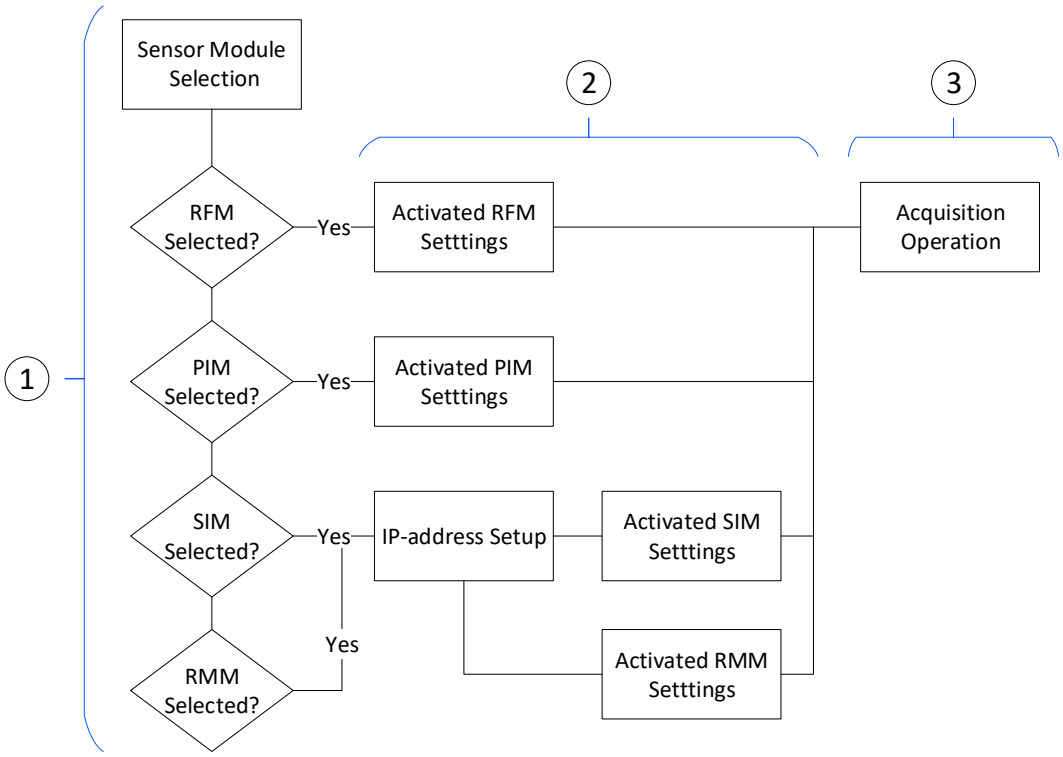

Fig. 3.3 Flowchart of operation panel for data acquisition mode

3.1.2 Post-Analysis (PA) Mode

Post-analysis mode allows the user to load saved raw data of a previous study and to visualize the signals for analysis. The operational flowchart of the PA mode is shown in Fig. 3.4. To start data analysis, the saved file of a previous experiment is loaded. Automatically, the GUI reads the file arrays (sensor values and time) and plots the sensor values. After the sensor data is loaded, the PA panel allows managing the graphics. (i) Time control: it allows zooming on the graphics. (ii) Step identification control: For LRC analysis, these functions allow filtering data of acceleration sensor. The filtered data facilitates identification of the highest peak of acceleration. It corresponds to the foot contact with the floor; in particular, the ratio and the threshold. These characteristics are illustrated in Fig. 3.5. (iii) Visual control: This function shows or hides the sensor signal from the graphic. (iv) Help: It gives general information how to manage the graphics.

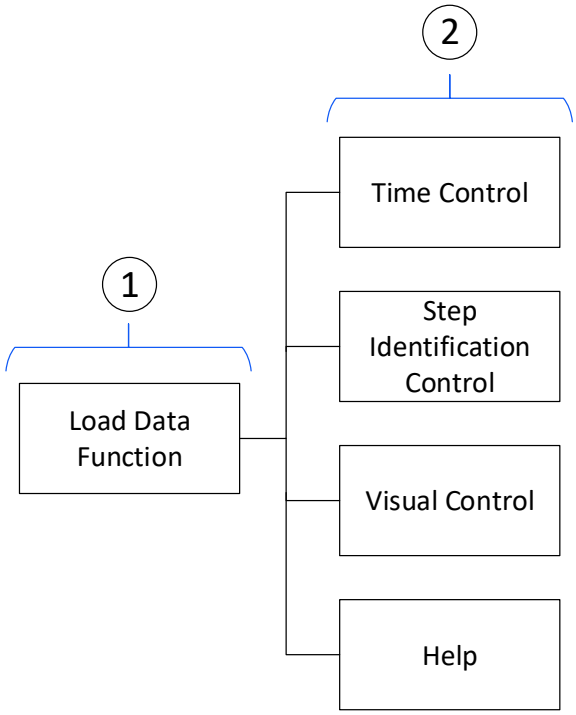

Fig. 3.4 Flowchart of operation panel for data post-analysis

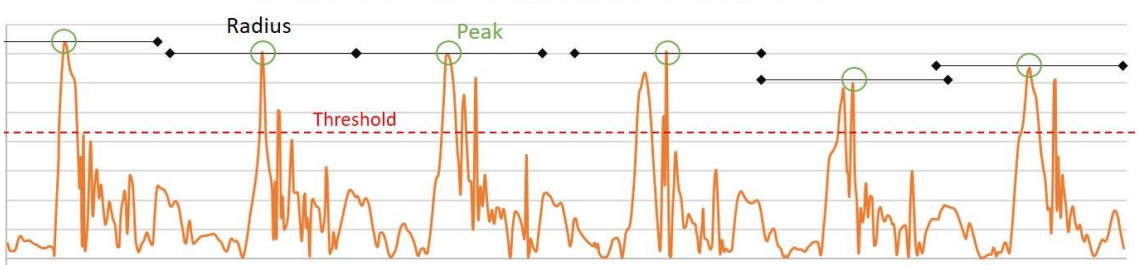

Fig. 3.5 Example of post analysis of an acceleration signal. The radio function defines the minimum peak separation, selecting the highest peak value in the range. The threshold function defines the minimum height difference between a peak and its neighbors.

As follows the complete characteristic of each sensor module will be explained.

3.2 Implantable Pressure Module (IPM)

Nowadays, any physiological parameters could be monitored by a telemetry tool like an implantable device. For this application a new implantable device was implemented to monitor thoracic pressure *in vivo* during locomotion in any mammal. Nevertheless, testing this system in real animals requires an arduous anatomical and physiological study of the animal. In addition, to obtain the corresponding permission to work with animals can take several months, depending on the country. Thus, in vivo tests of the IPM are not within the scope of this thesis. Hence, the main goal of this development module is a proper functionality of the wireless system, which includes the pressure data acquisition. In order to achieve the technical requirements of our system, this device was developed considering international standards despite the limitations of using only commercial components as was explained in Section 2.5. Biocompatibility was assured as this is possible in the design phase.

3.2.1 Commercial Implantable Telemetry - Pressure Devices

In addition to the multiple research and development of implantable devices in the academy, there are companies which develop wireless implantable devices. All of them are orientated to analyze in vivo some physiological parameters like pressure. These devices present characteristics like limited battery life and range of operation. The main characteristics of these devices are the size, which depends on the mass of the animal under study. Table 3.1 shows some commercial product's characteristics for implantable telemetry for animal masses bigger than 2.5 kg.

Table 3.1 Commercially available implantable pressure measurement devices for animal research.

Manufacturer	Model	Parameters	Volume* (cm^3)	Op. range (m)	Mass (g)
emka Technology	easyTel+	Pressure, Temp	25	4-6	35
DSI™	Series M	Pressure, Temp	29	3-5	37
TSE systems	Stellar Telemetry	Pressure, Temp	26.2	3-5	-

* The device volume corresponds to animals of medium and large body size.

3.2.2 IPM Hardware Design

The IPM consists of two main components, the pressure transmitter **(PTx)** and the pressure receiver **(PRx)**. As was mentioned in Section 2.5.2, the implantable devices are designed to

operate in MedRadio (402-406 MHz) band. The DCC does not directly receive the signal from the IPM. The PRx receives the signal from PTx and then re-transmit the data to DCC. This characteristic is due to the whole system works with Wi-Fi technology (transmission frequency 2.4 GHz) as was explained in the previous section. Fig. 3.6 shows the communication line between the PTx and DCC through the PRx.

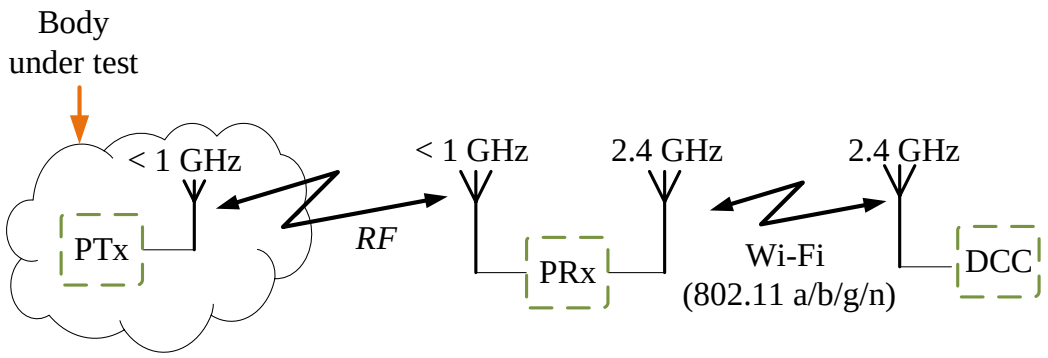

Fig. 3.6 Wireless communication structure of the IPM. The implanted transmitter (TRx) sends data via radio frequency ($f < 1$ GHz) to the pressure receptor (PRx). It saves and retransmits the data via Wi-Fi protocol to the data control center (DCC).

Pressure Transmitter (PTx)

The transmitter structure is based on three electronic elements ensuring the proper functioning as shown in Fig. 3.7. Firstly, the sensor signal conditioner (SSC) adapts the sensor signal, so the microcontroller (**MCU**) can process it. The SSC functions are amplification, filtering and digitalization of the signal. The SSC model ZSC31014 was chosen for this particular IPM. It works at a sampling rate of 1MHz or 4MHz. Depending on the rate used, the current consumption is between 7 μA and 2 mA. The SSC sends digital data (14 bits per sample) to the MCU via SPI[2] bus. Finally, the SSC has other characteristics, such as digital signal offset compensation, sensitivity, temperature drift and non-linearity accomplished by an internal signal processor. The second component is the microcontroller. It manages and controls all the data flow between the SSC and the wireless transmission. Finally, the third component is the transceiver. It manages the RF communication, allowing wireless data transmission and reception.

In the system presented here, the design of the device includes an MCU and a transceiver coupled in the same chip, called System on Chip (**SoC**). It allows programming the RF

[2] The Serial Peripheral Interface bus (SPI) is a synchronous serial communication interface used for short distance communication.

communication and the data acquisition on the same chip. This technology was developed by Texas Instrument and has the advantages of low power consumption. Furthermore, it allows programming the output power from -30 dBm up to 10 dBm. CC11110F32 was chosen as the SoC in this particular design. Due to the limitation of commercial tiny antennas which operate in the MedRadio band of frequencies, the SoC is set to operate to transmit data at 433 MHz and 868 MHz, with an external oscillator of 26 MHz. Additional technical details of the hardware circuit schematics are shown in Appendix A.1.1.

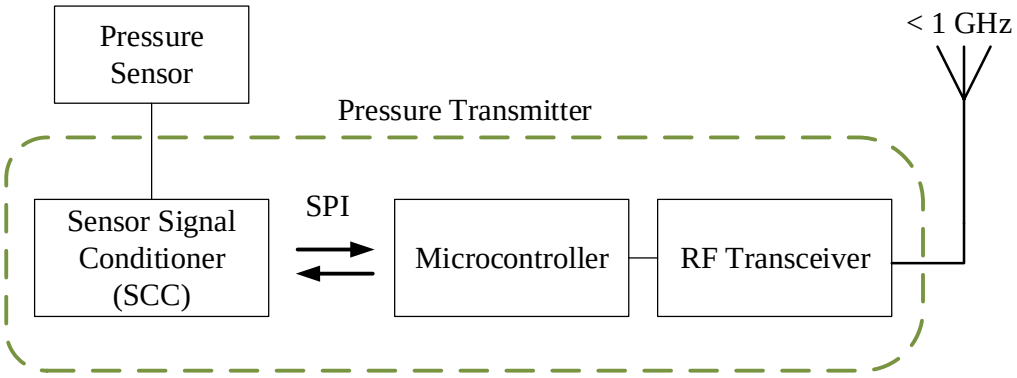

Fig. 3.7 Structure of Pressure Transmitter. The MCU and RF transceiver are couple in a single chip (SoC). The SCC allows digitalization of the pressure values.

Pressure Receptor (PRx)

The PRx has two main functions. First, it receives data packets from the TRx. Second, the saved data is retransmitted to the DCC via Wi-Fi protocol. According to the hardware, the PRx uses the same SoC for the communication with the PTx. As shown in Fig. 3.8, the Wi-Fi transceiver is connected to the SoC via serial port (UART[3]). The receiver has to be located on the body during motion, as this position reduces the limitation of distance range in case of RF communication between the PTx and PRx at frequencies less than 1 GHz. Additional technical details of the hardware circuit schematics are shown in Appendix A.1.2.

[3] An universal asynchronous receiver/transmitter (UART) is a hardware device for asynchronous serial communication.

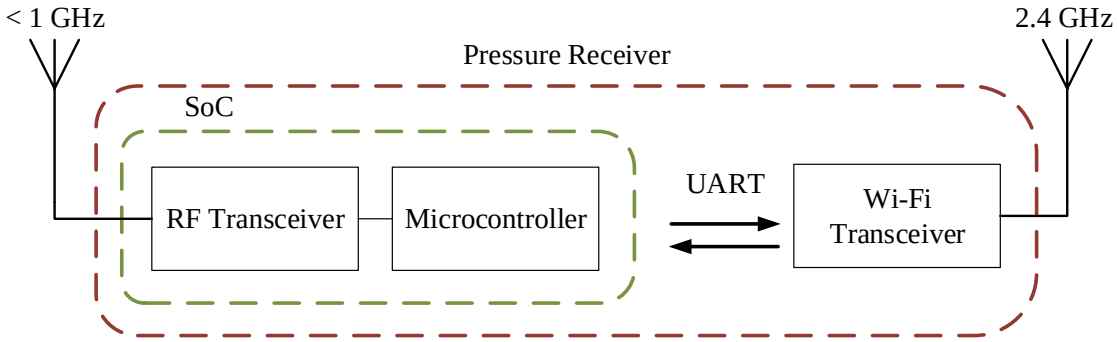

Fig. 3.8 Structure of the pressure receiver. The system has two antennas installed, one for communication frequencies less than 1 GHz. The other is used for Wi-Fi communication at the frequency of 2.4 GHz.

3.2.3 Piezoresistive Pressure Sensor

The pressure sensor has four piezoresistive strain gauges[4] placed in a wheatstone bridge arrangement. They hold a thin membrane called the diaphragm. Generally, the output signal of the sensor has limited amplitude and high external noise (difficult to read by conventional measuring instruments). As shown in Fig. 3.9, the piezoresistive effect[5] causes resistance changes in strain gauges, thereby affecting the output voltage. Finally, the output is converted into a reading format via a signal conditioning circuit (SSC).

The sensor pressure values measure in mmHg and are scaled from a digital value (Z) given by the SSC. To perform the scaling following equations are used.

$$V_{out} = \frac{P \cdot S}{10^6} \cdot V_{in}, \qquad [\mathrm{V}] \tag{3.1}$$

where V_{out} is the voltage difference of the sensor output terminals, P is the pressure, S is the sensor sensitivity and V_{in} is the sensor input voltage.

According to the SSC data sheet (ZSC31014), the digital value of the current pressure is given by:

$$Z = 2^{14} \cdot (GAIN \cdot \frac{V_{out}}{V_{in}} + A2D\_Offset) \tag{3.2}$$

4 A strain gauge is a device used to measure strain on the surface of an object.

5 The piezoresistive effect is a change in the electrical resistivity of a semiconductor or metal when mechanical strain is applied.

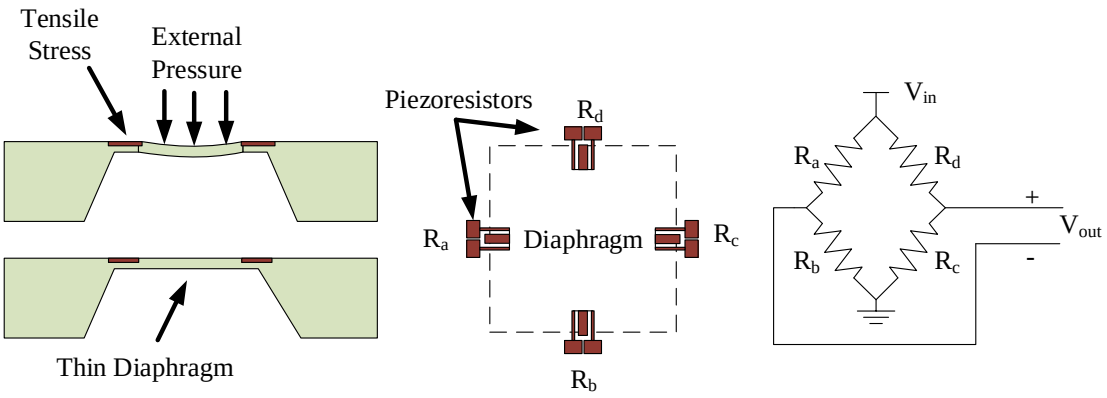

(a) Side View (b) Top View (c) Wheatstone Bridge

Fig. 3.9 Pressure sensors piezoresistive effect causes a change only in electrical resistance. The electric circuit representation is called a wheatstone bridge.

where GAIN and A2D_offset are parameters of the SSC. They are programmed for the analog to digital (ADC) conversion. Solving the Eq. 3.1 and 3.2, the pressure is given by:

$$P = \left(\frac{Z \cdot 10^6}{2^{14} \cdot GAIN \cdot S} - \frac{A2D\_Offset \cdot 10^6}{GAIN \cdot S}\right), \quad [mmHg] \tag{3.3}$$

The selected sensors (NovaSensor NPC-100) range is between -50 mmHg and 300 mmHg, and the sensitivity is 5 μV/V/mmHg. Furthermore, the SSC parameters are the A2D_offset = 1/16 and the GAIN =192. According to these values, the pressures is calculated as:

$$P = (0.0636 \cdot Z - 65.1), \quad [mmHg] \tag{3.4}$$

In this particular application, a catheter lead houses the pressure sensor and connects it to the sensor node of the SSC (see Fig. 3.10). The sensor measures the absolute pressure[6]. The sensors size is 10 mm $\times$ 7 mm, and it was designed specifically for medical applications in humans. Finally, the catheter is wrapped with a biocompatible silicone Nusil MED-4011.

[6] An absolute pressure is the measured relative pressure to the perfect vacuum (0 Pa).

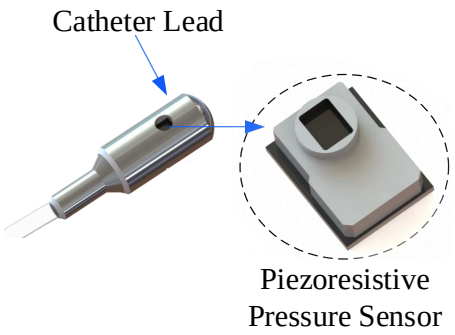

Fig. 3.10 Implemented pressure catheter lead.

3.2.4 IPM Communication Protocol

As it was explained before, the communication between the SSC (ZSC31014) and the SoC is performed through the SPI bus. The SSC sends a data frame of four bytes (see Fig. 3.11). However, the digitalized sensor data is represented in the 1^{st} and 2^{nd} byte of the frame. The SPI configuration has a baud rate of 9600 and negative clock polarity. Other important setup characteristics of SSC is the analog Gain = 192. This gain is the factor for the sensor analog signal amplification. Finally, the SoC extracts the sensor data and forms the RF transmission frame.

STATUS BITS [7-6]	BRIDGE DATA UPPER BITS [5-0]	BRIDGE DATA LOWER BITS [7-0]	TEMPERATURE UPPER BITS [7-0]	TEMPERATURE LOWER BITS [7-6]	NO RELEVANT BITS [5-0]
1st Byte		2nd Byte	3rd Byte	4th Byte	

Fig. 3.11 ZSC31014 serial data frame [86].

The SoC (CC11110F32) communication frequency is set to 433 MHz with data rate of 1.2 KBaud and -6 dBm of transmission power. As shown in Fig. 3.12, the communication packet frame is set to have four preamble bytes, two synchronization bytes and two CRC bytes. The data packet has the length of 17 bytes that can be used. The first byte shows the packets number of bytes. The next two bytes show network identification numbers in case there are other IPMs. The next 14 bytes are used to store the transmitted data. In this particular application, the sensor values are represented by the first two bytes in the case of the transmission. The receiver stores the value 0x2424 by the request function. Finally, the rest 12 bytes can be used to send more information for future applications.

PREAMBEL BITS	SYNC BYTES (0xD391)	PACKET LENGHT (0x11)	NETWORK ID (0x5AA5)	USED BYTES	FREE BYTES	CRC
4 Bytes	4 Bytes	1 Byte	2 Bytes	2 Bytes	12 Bytes	2 Bytes

Inserted automatically by the PTx / Processed and removed by the PRX
Identification bytes
Bytes for sensor data or free space for another sensor values.

Fig. 3.12 Sef-developed data frame for the RF communication.

3.2.5 IPM Operation Programm

As it was explained before, the implantable device can not send sensor data directly to the DCC. This is due to the different frequencies between them. For this reason it is necessary to put an intermediate device that receives data from the transmitter and retransmits data to the DCC. In Fig. 3.13 the system operation is explained. To start the data acquisition, the system follows fours steps: (1) the DCC sends a request command to the PRx. (2) Automatically, the PRx sends a request command to the PTx. The command is validated by the PTx. (3) It sends the pressure values to the PRx. This full duplex communication between the PTx and PRx responds to the explained protocol. (4) Finally, data is stored in a serial buffer, the PRx forms a packet frame to transmit the sensor data via Wi-Fi protocol to the DCC.

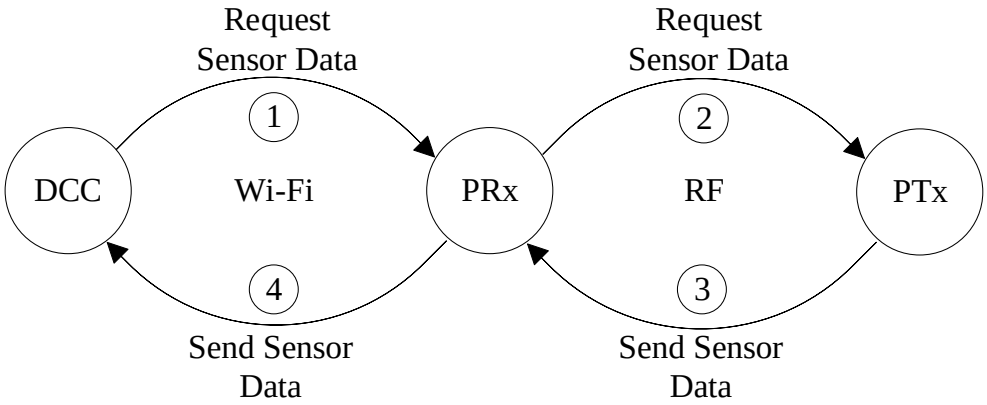

Fig. 3.13 Data acquisition cycle of the pressure module.

The operation algorithm of the pressure transmitter and receiver are explained in the Appendix A.2.

3.2.6 IPM Implementation

The implemented prototypes were designed under the requirements explained above. A functional test was developed to examine the RF communication performance. Besides, it confirms the sensor sensibility and reliability.

As shown in Fig. 3.14, the implemented functional prototype includes a reed switch to power on-off device. It is activated by an external electromagnetic field. Thus, in the thoracic cavity the sensor system can be switched on exclusively during data transmission. Furthermore, the power supply is a coin cell lithium battery of 3 VDC (CR2032). This prototype intentionally includes multiple connectors to monitor any signal in the circuit. It includes also a connector to program the SoC firmware and to debug. Also, a connector for the piezoresistive pressure sensor is considered. The RF module CC1110EM allows working with operation frequency **(OF)** of Sub-1 GHz. In this prototype the tested operation frequencies were 433 MHz and 868 MHz.

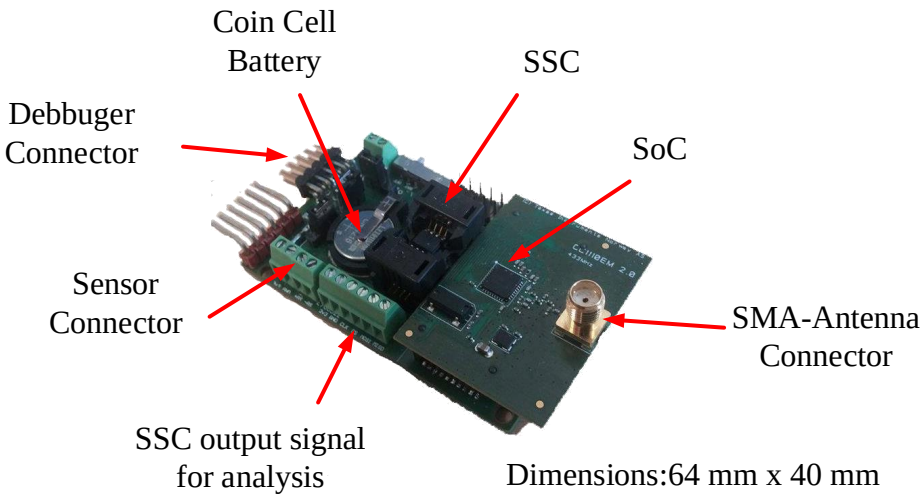

Fig. 3.14 Functional prototype of the implantable pressure module - transmitter.

After a series of tests of the first prototype, successful results were achieved. The device was scaled and tested to measure pressure in thoracic cavity. Fig. 3.15 shows two models based on the tested electronic design. The device works with commercial ceramic antenna of 433 MHz and 868 MHz. Both devices integrate the pressure catheter and an external board for power supply (see Fig. 3.16).

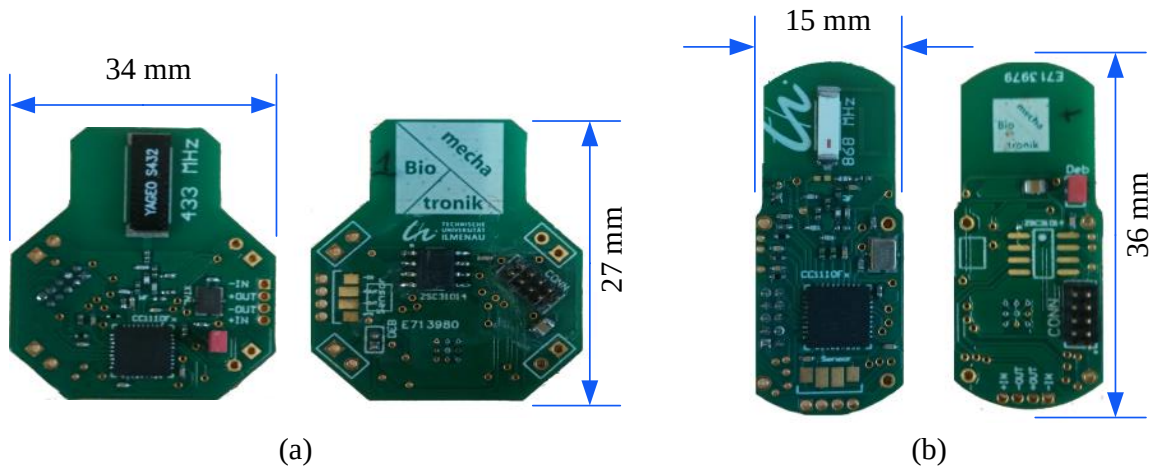

Fig. 3.15 Implemented implantable pressure devices. The device is controlled by the SoC CC1111 from Texas instruments with operating frequencies <1 GHz. In (a) the operational frequency is 433 MHz and in (b) 868 MHz.

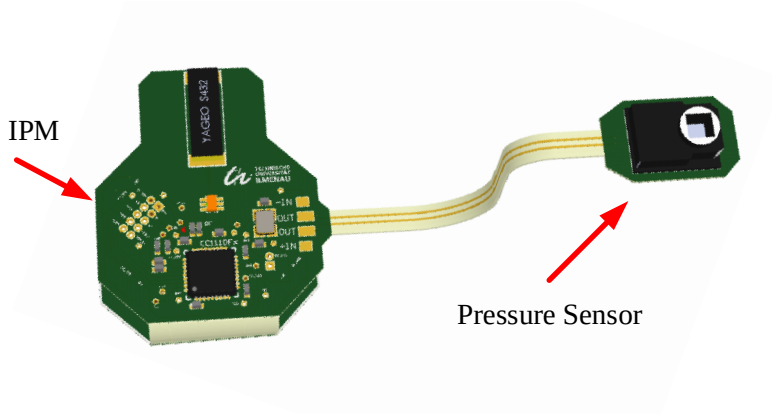

Fig. 3.16 IPM assembled: Power supply based on a coin cell holder, reed switch to power on-off device and pressure sensor.

3.2.7 Transmitters Electrical Parameters

According to the standards of implantable devices design explained in Section 2.5.2, the maximum RF output power is 25 μW EIRP. The selected SoC can be programmed to transmit between -30 dBm and 10 dBm of output power. In this application, the SoC was programmed to transmit at -20 dBm (10 μW). Also, with the following parameters (see Table. 3.2), the transmitter power consumption (P) in mW is given by the product of applied voltage (U) and the electric current (I) given by our own measurements.

The total current during the operation is between 15.12 mA and 16.12 mA for transmission frequency of 433 MHz and 868 MHz respectively. Therefore, the power consumption of the transmitter is $\approx$ 45.36 mW. A lithium coin cell of 240 mAh was selected. The theoretical autonomy of the device is $\approx$ 15 hrs in case of continuous operation.

Table 3.2 Electrical parameters of the IPM transmitter in normal operation mode. The operation frequencies were 433 MHz and 868 MHz.

Operational Parameter	Tx at 433MHz	Tx at 868MHz	Units
Power Supply	3	3	*V*
SoC Current	15	16	*mA*
SSC Current	0.12	0.12	*mA*
RF Power Output	-20	-20	*dBm*
Battery Capacity	240	240	*mAh*
Crystal Power dissipated	10	10	μW

3.2.8 Receiver Implementation

The implemented IPM receiver uses a Li-Po battery of 3.7 VDC (1000 mAh). In order to maximize the data transfer range, a standard SMA antenna is used for the communication with the PTx. Besides, the device uses a Wi-Fi transceiver (*XBee S6B*) for the communication between DCC and PRx. This transceiver works at an operation frequency of 2.4 GHz. The receptor design is shown in Fig. 3.17. More technical information about circuit schematics and firmware algorithm is given in Appendix A.1.2.

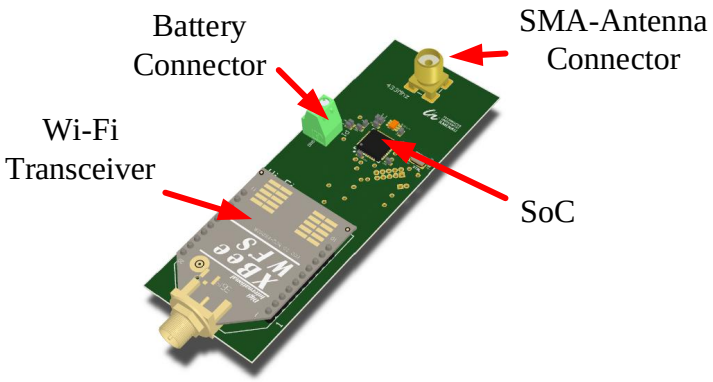

Fig. 3.17 Functional prototype of the IPM receiver.

3.2.9 IPM Experimental Test

In order to test the IPM transmitter and receiver, a test bench was designed, based on a sphygmomanometer[7]. The bench consists of: (i) a pressure chamber with two hose connectors, (ii) a digital manometer as a reference, (iii) a pump bulb used to change the pressure within the chamber. The sensor catheter is located on the bottom surface of the chamber. The manometer and the pump bulb are connected hermetically to the chamber through the hose connectors (see Fig. 3.18).

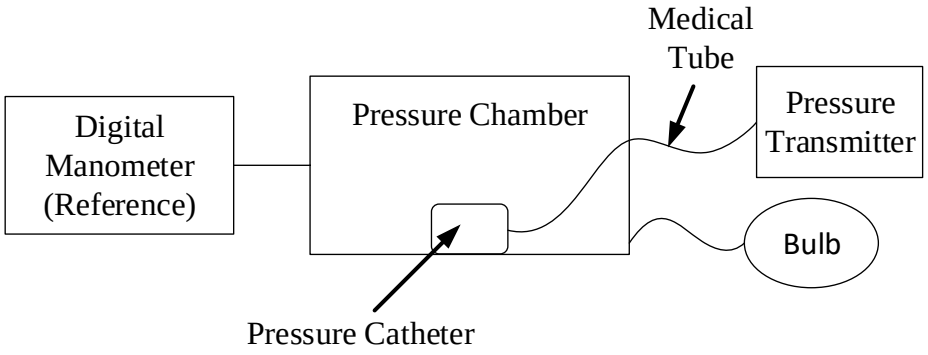

Fig. 3.18 Graphical illustration of the experimental test setup.

IPM Sensor Calibration

The implemented calibration method for the pressure sensor is based on an Pearson's method (linear regression). It is explained by the following steps (see Fig. 3.19):

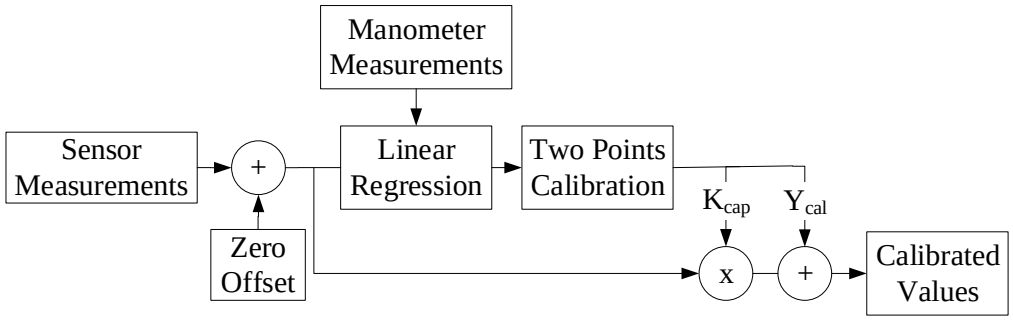

Fig. 3.19 Pressure sensor calibration method.

[7] A sphygmomanometer is a device used to measure the blood pressure.

1. Take n values read from the manometer (X) and the tested pressure sensor (Y).

2. The pressure values with zero correction are given by: $Y_z = Y - Y_0$,

   where (Y_0) is a value when p = 0 and Y is the value of the measured pressure.

3. The NPC100 is a linear measuring device. The corrected sensor values (Y_z) with the corresponding manometer values (X) can be used to estimate a linear model. A linear regression line (Y_l) is calculated as: $Y_l = A \cdot X + B$,

   where A and B are calculated using the least squares estimation for linear regression.

4. In addition, two calibration points are used to correct the slope and the new zero correction. The relation between the calibrated sensor value (Y_f) and the sensor value with zero correction is given by: $Y_f = K_{cal} \cdot Y_z + Y_{cal}$,

   where K_{cal}=1/A and Y_{cal}=-B/A

5. Finally, for each sensor value:

$$Y_f = A_{cal} \cdot Y + B_{cal} \tag{3.5}$$

   where A_{cal}= K_{cal} and B_{cal}= Y_{cal}-$Y_0 \cdot K_{\text{cal}}$,

IPM Experimental Results

The main goal of the experimental test is to test the sensor catheter and the transmitter performance. To test the sensor, the obtained analog data by the sensor is converted by the SSC as was explained in Eq. 3.4. The collected sensor data during the calibration proceeding can be seen in Fig. 3.20. Also, the numerical values are listed in Table 3.3.

Table 3.3 Comparison between pressure sensor measurement values and digital manometers values. The differences between the measured data by the manometer and the sensor respond to two factors: (1) the calibration parameter of the sensor needs to be adjusted and, (2) the digital value of the manometer was measured visually. This data corresponds to Fig. 3.20.

	Number of measurements[†]					
Pressure Measurement Device	1st	2nd	3rd	4th	5th	6th
Sensor [mmHg]	-4.93	54.74	39.87	92.07	35.99	84.50
Manometer [mmHg]	0.00	59.0	48.7	103.1	43.9	93.6

[†] Number of measurements for sensor calibration

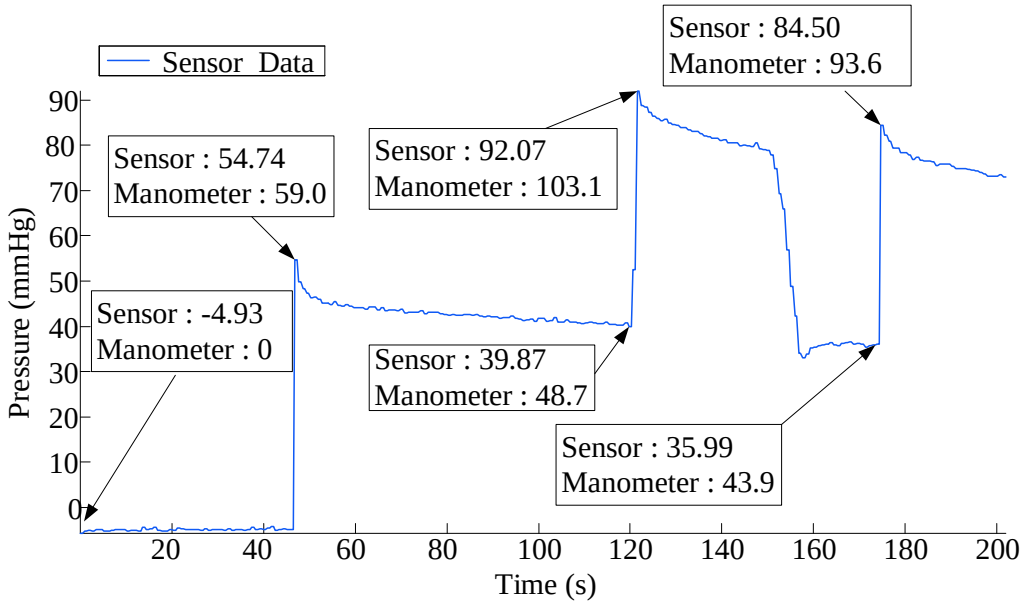

Fig. 3.20 Pressure sensor values taken for calibration and manometer values as a reference. All pressure values are given in [mmHg].

Using the explained calibration method, the calculated parameters for this particular example are A_{cal}=1.052 and B_{cal}=5.056.

Finally, Fig. 3.21 shows the sensor data read out before and after the calibration.

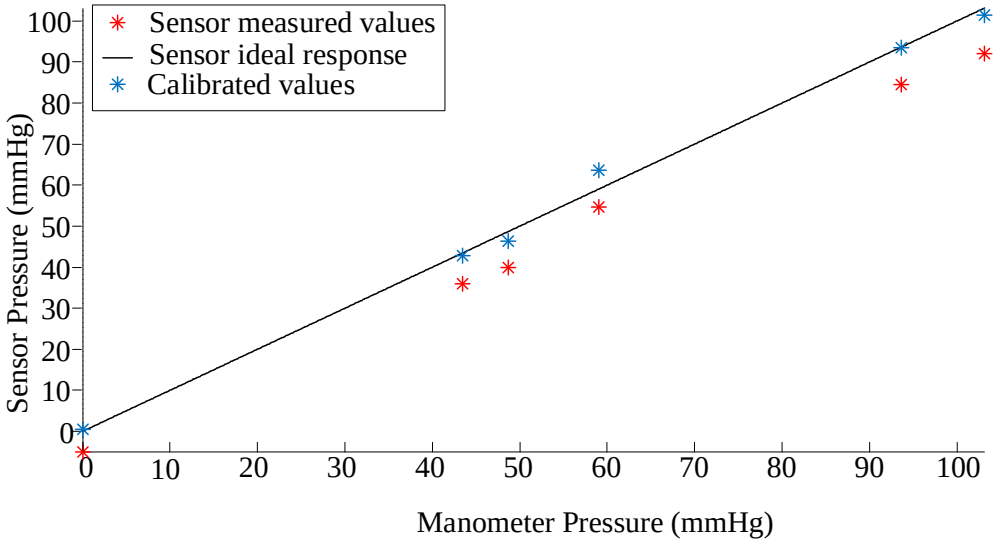

Fig. 3.21 Pressure sensor accuracy before and after the calibration method.

After the calibration, the pressure chamber was filled with a bio-material such as pork meat. Externally, a rubber bulb was connected to change the pressure within the chamber. As shown in Fig. 3.22 the pressure changes within the chamber are produced by the pump bulb.

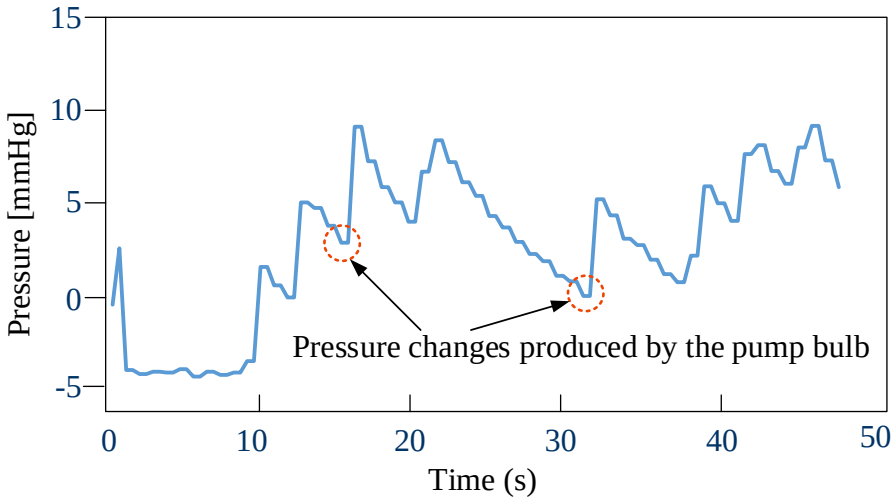

Fig. 3.22 Pressure measurements within a chamber filled with pork meat.

Finally, after several tests were developed, the following summary explains the IPM performance. The linearity of the NPC-100 sensor guarantees a correct measurement with an mean error of $\pm$ 1 mmHg of the pressure. The system presents a continuous data transfer rate between PTx and PRx. During sensor calibration, the RF communication range between the PTx and PRx reached $\approx$ 10 m with continuous data transfer. However, when the device was placed within the bio-material, the range decreased to $\approx$ 1.5 m.

3.3 Respiratory Flow Module (RFM)

For many years, researchers have studied the interaction between breathing and locomotion. It is evident that a respiratory flow occurs with a stride during locomotion in any vertebrate. Besides, the discussion was focused on the amount of air volume displaced in the lungs due to this interaction. Hence, the main goal of this module is to measure the volumetric (respiratory) flow of a breathing cycle (inhalation and exhalation) during free mode running. This module allows the user running under the condition of a self-selected (preferred) pace in free spaces.

3.3.1 Commercial Volumetric Flow Measurement Devices

The commercial devices adaptable to our application would be a wireless spirometer. However, this device is made for respiratory diagnostics in static position and not for outdoor testing. Attaching this device to a mask could cause error in the acquisition of data. However, there are applications like sport medicine, human performance and cardiac rehabilitation which make use of outdoor spiroergometry[8] systems for the simultaneous examination of a person´s reactions of the heart, lungs, circulatory system and metabolism to physical stress. This complex device allows the breathing analysis that our method needs. Normally, these devices are not compatible with external systems. Table 3.4 shows some commercial spiroergometry system characteristics for cardiopulmonary analysis.

Table 3.4 Characteristics of commercial spiroergometry devices.

Manufacture	Model	Communication	Flowmeter*	Flow range (l/s)	Flow resolution (ml)
CORTEX	METAMAX 3B	Bluetooth	Turbine, digital	0.1 - 12	8
COSMED	K4 b^2	Bluetooth	Turbine, digital	0.08 - 20	7

* Sensor type.

3.3.2 RFM Hardware Design

The RFM module (transmitter) is based on one mass flow meter (sensor) transducer with a hermetic mask attached. The selected sensor (Sensirion® $SFM3000$) is a bidirectional digital flow meter designed for medical applications in humans to measure the volume flows at rates up to 200 slm[9]. The sensor is connected by the serial bus I2C[10] to the wireless communication controller (**WCC**), and it operates at 5 VDC of supply voltage.

The selected WCC ($ESP32$) is based on a Dual-core $Tensilica\ LX6$ microprocessor with integrated 802.11 a/b/g/n Wi-Fi transceiver. The data transmitted via Wi-Fi protocol is received by the data control center (**DCC**) (see Fig. 3.23).

8 Spiroergometry is a diagnostic method in which by measuring respiratory gases during exercise, the response of the heart, circulation, respiration and the cardiopulmonary performance are monitored.

9 Slm: liters per minute measured at standard temperature of 0°C and pressure of 1 atm. The equivalence of slm is given by 1 $slm = 1,68875(Pa \cdot m^3)/s$ in International System of Units [DIN 1343].

10 The I2C bus is a bidirectional two-wire serial bus that provides a communication link between integrated circuits (ICs).

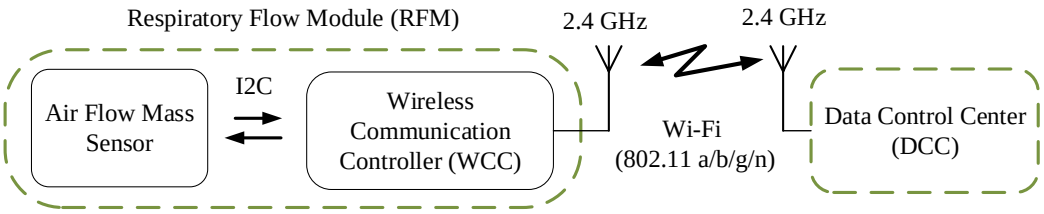

Fig. 3.23 Structure of respiratory flow transmitter. The air flow mass sensor transmits data through I2C bus to the WCC.

3.3.3 RFM Communication Overview

Regarding the communication between the sensor (slave) and the WCC (master), the sensor has a digital output and uses the I2C protocol for data transmission. I2C requires two wires to transmit data: SCL (serial clock) and SDA (serial data); each wire has to be pulled up[11] with the resistor to power supply. The detailed calculation of the pull up resistor is shown see Appendix B.1.1.

In I2C communication protocol, each slave device has its own seven bits address. In this particular application, only one slave was considered. However, the system can support more than one mass flow sensor in parallel, if it is required. The detailed schematic circuit is shown in Appendix B.1.

Wireless Communication

The system structure is based on a client-server communication model. The WCC firmware defines the wireless network (WLAN) setting as a name and a password. Also, the server's IP-address and the chosen hostports[12] allow the data transmission between the client and the server. The data is received and shown in the GUI. It saves data for post processing tasks. Finally, for data transfer of more than one client, it is recommended to use different hostports for each device. The firmware algorithm is explained in Appendix B.2.

[11] A pull-up resistor is connected in between a signal conductor and a positive supply voltage to ensure that the signal will have a valid logic level, if external devices are disconnected or high-impedance is introduced.

[12] A port is always associated with an IP address of a host and the protocol type of the communication. Thus it represents the destination or origination network address of a communication session.

3.3.4 Volumetric Flow Measurement

The measured digital value of volumetric flow rate is represented by four bytes. However, the real volumetric flow rate is given by:

$$\dot{V}_m = \frac{measured\_value - offset\_flow}{scale\_factor\_flow}, \qquad [\text{slm}] \tag{3.6}$$

where the parameters according to the sensor data-sheet [83] are $offset\_flow$ = 32000 DEC and the $scale\_factor\_flow$ = 140 [1/slm].

According to DIN 1343[13], the standard volumetric flow measurement in slm is accomplished under standard conditions of temperature and pressure. The standard temperature is T_n=273,15 K or 0 °C and the pressure P_n = 1atm or 1013,25 hPa. These reference values differ from the "room" values (environmental parameters) used in functional tests. The calculated volumetric flow ($\dot{V}_n$) expressed in ℓ/min based on the combined gas law is described as:

$$\dot{V}_n = \frac{P_m}{P_n} \times \frac{T_n}{T_m} \times \dot{V}_m, \qquad [\ell/\text{min}] \tag{3.7}$$

where P_m and T_m are the environmental pressure and temperature.

3.3.5 RFM Implementation

The respiratory flow transmitter (WDC + battery) was attached to a specially designed cover. The complete device has the following characteristics: (1) the sensor is placed on a cylindrical holder made of ABS[14]. The holder has the characteristics of diameter = 40 mm and length = 10 cm. It is linked with the commercial mask (Polimask 330) through a standard mechanical thread (DIN EN 148-1). (2) The transmitter has a trapezoidal holder (ABS) where the electronics circuits and the battery of 3.7 VDC (1000 mAh) are located. (3) A voltage regulator of 5 VDC (AMS117) is used to power the sensor and the WCC. (4) The complete module weight is ≈ 250 g including the mask (see Fig. 3.24).

[13] DIN 1343:1990-01: Reference conditions, normal conditions, normal volume, concepts and values.
[14] Acrylonitrile butadiene styrene (ABS) is a common thermoplastic polymer.

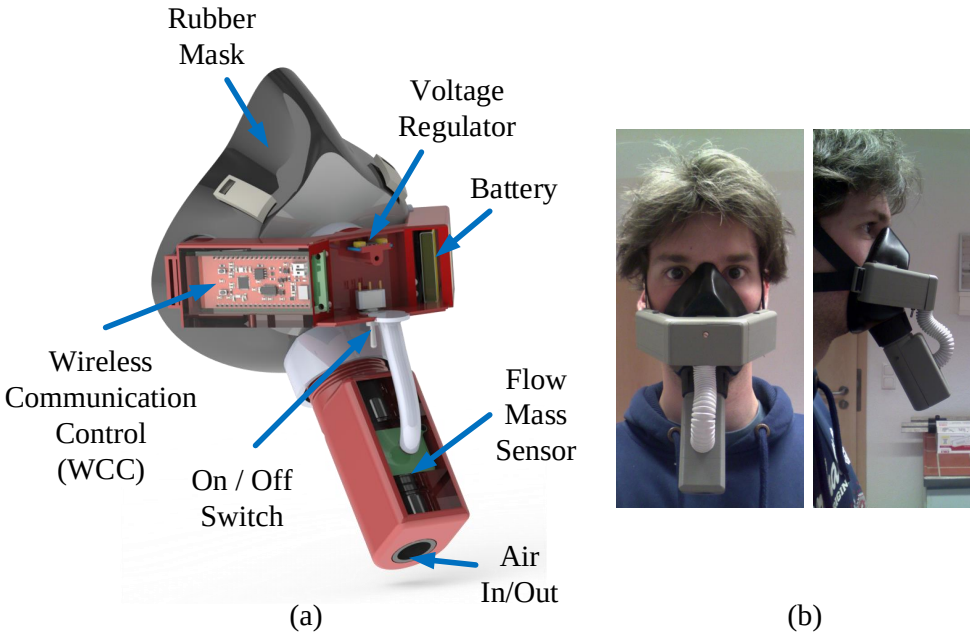

Fig. 3.24 (a) Design description and (b) implementation of the respiratory flow transmitter.

3.3.6 RFM Calibration

The method to calibrate the RFM sensor was based on a certificated three liter precision syringes developed by Vitalograph®. The calibration syringe provides an accurate and repeatable volume. The following steps are used to calibrate the sensor:

1. Pull up completely the syringe plunger handle (zero position).
2. The sensor holder is connected with the calibration syringe through a syringe adapter (see Fig. 3.25).
3. The whole system has to be located in a horizontal position before the calibration starts.
4. From the GUI panel, a RFM module is selected. A sub-panel is enabled to start the DAQ for the calibration.
5. Move the plunger handle fully from end to end when performing a calibration. Firm contact between the plunger and each end of the syringe should be felt. Repeated three times.

6. The DCC calculates the volume and GUI plots the graphic of volumetric flow vs volume.

7. The linearity is considered to be acceptable, if the injected volume does not vary by more than $\pm$ 3%. If adjustment is necessary, this is done by software correction.

As an calibration example, Fig. 3.26a shows the air flow measurement from the syringe. The plunger was moved three times emulating the respiration cycle. Furthermore, DCC calculated the volume in liters as is shown in Fig. 3.26b. Finally, the GUI shows the graphic air flow vs volume (see Fig. 3.26c) and calculates the error in percentage to determine the calibration factor given by:

$$PercentError = \frac{Vol\_Calculated - Vol\_Accepted}{Vol\_Accepted} \times 100, \qquad [\%] \tag{3.8}$$

In this particular example, the volume measurement was 2.87 liters and the error calculated was 4.33 %. This error is adjusted by software to the flow measurement in the next experimental test.

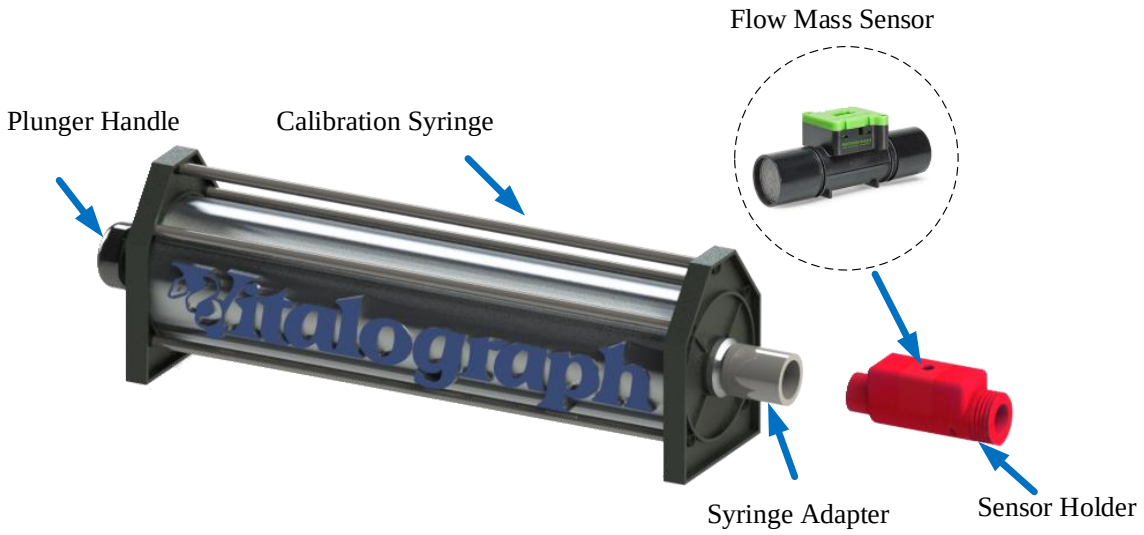

Fig. 3.25 Flow meter sensor. Description of calibration method .

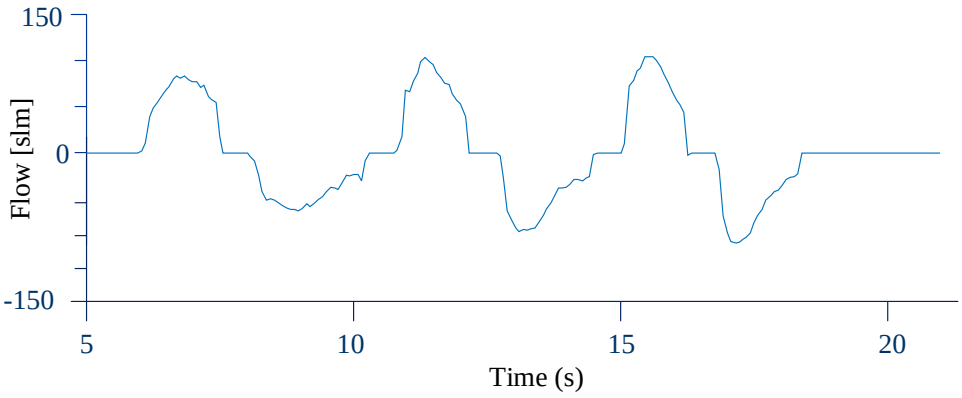

(a) Air flow calibration signal.

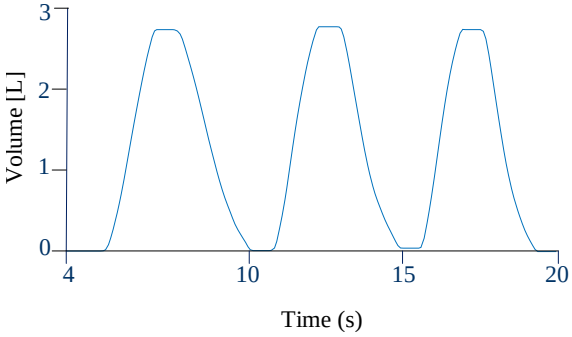

(b) Calculated volume.

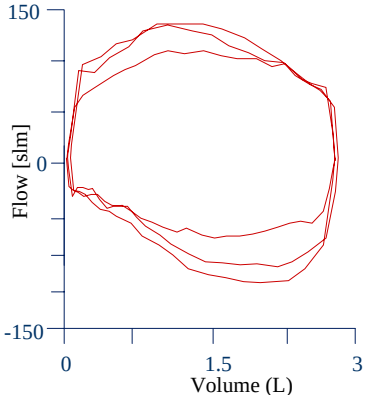

(c) Flow vs Volume.

Fig. 3.26 Calibration Graphics: (a) Calibration signal taken from the precision syringe, three cycles of calibration. (b) Calculated volume, based on the numerical integration (trapezoidal algorithms). (c) Graphic of flow vs volume during the calibration period, the maximum volume reached is three liters (capacity of the precision syringe).

3.3.7 Experimental Test of RFM

The designed system was implemented to measure the air flow during the free running mode. The system was tested in three different environments to evaluate its performance: (1) indoors on a treadmill, (2) indoors in free-running mode and (3) outdoors in free-running mode. Participants wore the respiratory flow system located on the face, covering the nose and the mouth. The system was fastened up firmly by elastic bands behind the head. Finally, participants were instructed to perform a running activity under normal conditions of ambient temperature and self-selected (preferred) running pace. The test description is:

1. The indoor test on the treadmill was developed to adjust the parameters of the airflow sensor. Thus, the indoor test allows setting the maximum value range of the sensor during the analysis of data. For example, when the running speed was 5 km/h, the maximum limit of flow was 130 slm. However, when the participant was running with a speed over 8 km/h, it was necessary to increase the limits of the maximum value of the sensors range to 220 slm.

2. The free-running mode indoor test took place in the closed sports center (SC) of the Technische Universität Ilmenau (TUI). The TUI-SC area has a size of approximately $30 \times 50\ m^2$. To facilitate the communication and to reach the best results in terms of system reliability, the TUI-SC WLAN was used.

   The experiment area was divided into three parts corresponding with three motion phases as seen in Fig. 3.27. The participant increases or decreases speed during the first and the third phase. These phases allow reaching a running speed over 10 km/h while running in a straight line (speed was constant). Finally, the purpose of these tests series was to evaluate the communication performance of the air flow sensor. The maximum transmission distance was approximately 60 m, reaching the whole workspace limited by the TUI-SC area. Furthermore, the packet transmission rate of the module had only a minor delay (< 50 ms).

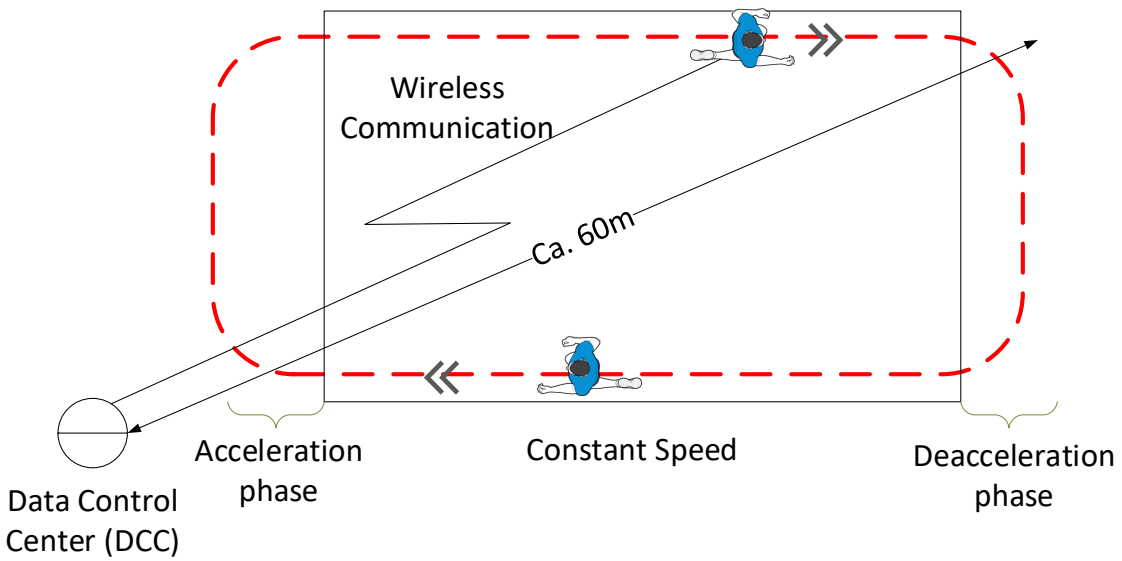

Fig. 3.27 Experimental area characteristics for free-running mode

One of the tests was made for the purpose of controlling breathing. The participant holds the air in straight segments. These irregularities can be well seen in real time and recorded for later analysis, shown in the Fig. 3.28.

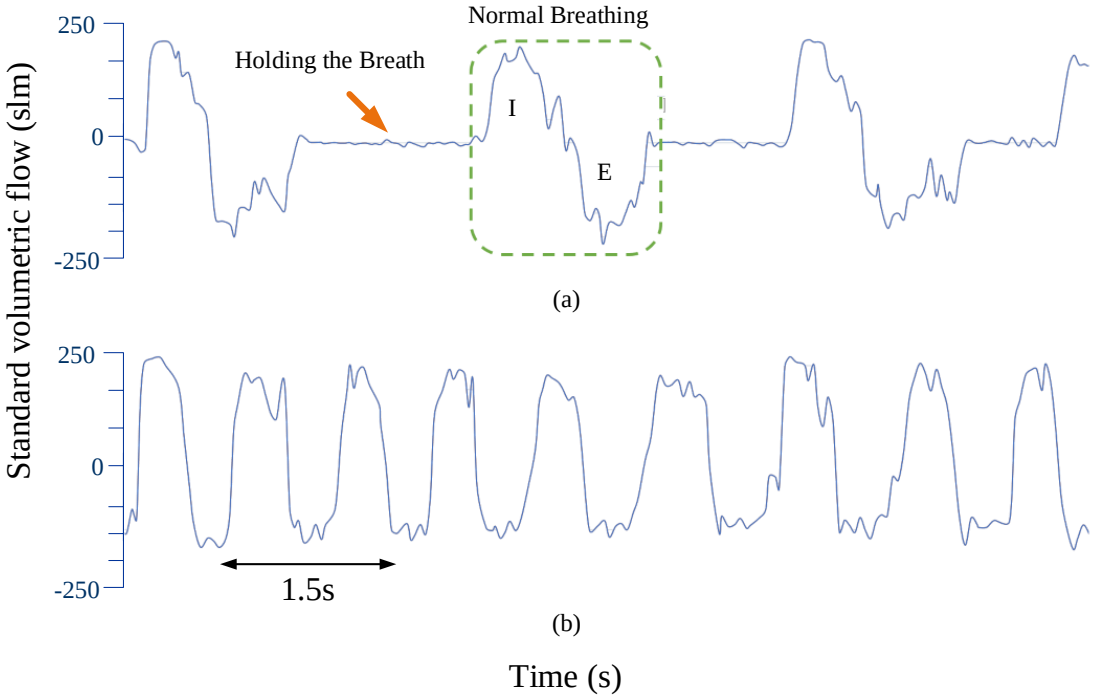

Fig. 3.28 Continuous data acquisition of volumetric flow during free running mode. The breathing cycle is one sequence of inhalation (I) and exhalation (E). (a) Controlled breathing and (b) normal breathing.

3. The free-running outdoor test was developed on a stadium ($\approx$ 40 m) of the university athletics track (TUI-AT). The participant ran straight at a moderate speed of $\approx$ 5 km/h. The communication range decreased significantly; this limitation restricts the acceleration/deceleration phases. Furthermore, the time of each test was below 30 seconds. It was observed that the amount of information received was not sufficient to identify a pattern of breathing. Due to the open field, the university WLAN range was limited; a hotspot from the DCC was created.

   Another test was developed in order to increment the data acquisition time. To increase the breathing rate, a warm up of 400 m jogging was included. The experimental method was similar to the TUI-SC explained above. The participant was jogging in a circular area of ($20 \times 5\ m^2$). In some cases, the transmitted data had a delay. However, the packets were saved for post analysis. This delay is due to the processing speed of the WLAN (hostpot).

Finally, after many tests, the following summary explains the RFM performance. In outdoor free-running mode, the system is affected by environmental conditions like wind, humidity and temperature. These factors decrease the communication range between a transmitter and the DCC. The range varies between 15 and 20 meters and it generates delays in the transmission. The opposite happens in indoor free-running mode. This environment (closed area without obstacles) is ideal for wireless transmission (range and data-transfer rate). Besides, controlled conditions of environment (temperature and no wind resistance) increase the range of communication between central and peripheral devices. In this case the system reaches a communication range of $\approx$ 60 m. The solution for this problem is to implement a router or multiple access points with a powerful antenna for the Wi-Fi network. This will improve the range significantly. Therefore, it allows a more stable transmission rate, avoiding delays and posterior corrections of signals.

3.4 Stride Identification Module (SIM)

The main task of this module is the identification of the foot-ground contact. The selected transducer was a wearable accelerometer. The accelerometer-based method measured the triaxial accelerations of the foot. Fig. 3.29 shows the location and orientation of the sensor above the ankle and its cartesian coordinate system.

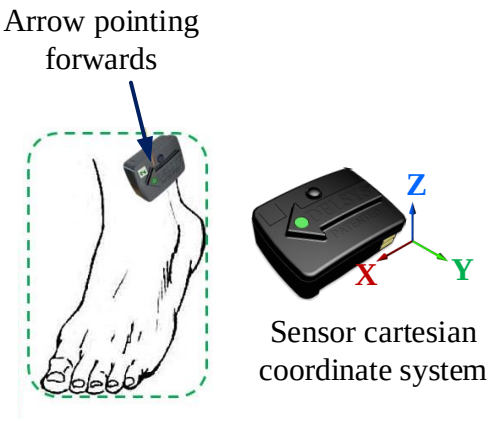

Fig. 3.29 Triaxial accelerometer - Cartesian coordinates system.

Purcel et al. [77] has implemented this method. They explain that two events were used to define contact time (between the foot and the ground) from the triaxial accelerometer data. The first event was the minimum in the X acceleration trace which corresponds to the peak of triaxial acceleration resultant. This occurred near the beginning of contact time. The

second event was based on the X and Z accelerations, which experience local minimum and maximum respectively near toe-off [15]. The acceleration-based method is shown in Fig. 3.30.

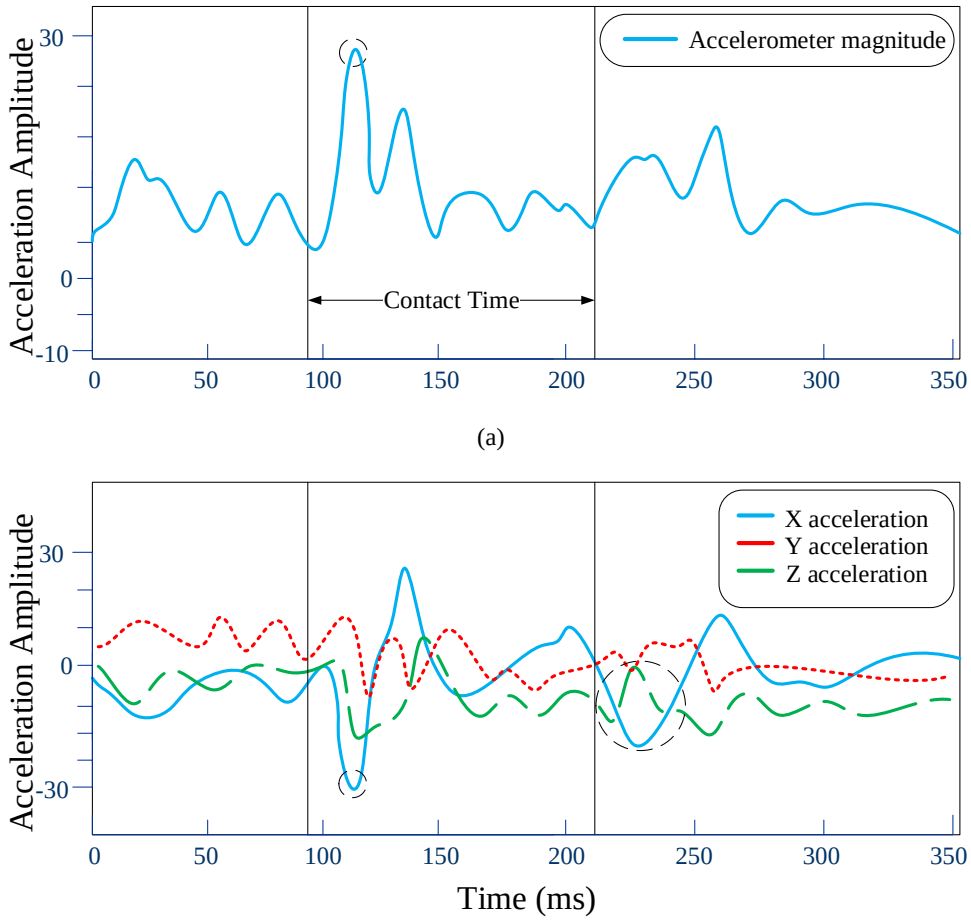

Fig. 3.30 Triaxial accelerations for a representative sprint trial. The accelerometer magnitude is depicted in (a) with the three acceleration components (X, Y and Z) shown in (b). Vertical lines define the foot-ground contact time. The beginning of contact time was obtained from the minimum in the X acceleration trace identified by the small circle in (b). The large circle highlights the local minimum and maximum in the X and Z accelerations that were used to define the end of the contact time. Vertical scale units are arbitrary. This graphic was adapted from [77].

[15] Toe-off (TO) is the final period of foot contact during stance phase (of gait) preceded by forefoot loading and followed by swing.

3.4.1 SIM Description

A certified commercial wireless system was used to identify the stride during free running-mode. This system is called Trigno™ and it was developed by the company Delsys©. This system consists of two main components: (1) 16 hybrid transducers (Trigno™ sensor) that combine a surface EMG and a triaxial wireless accelerometer. In our developed system, the first to eighth sensor are assigned for use as an accelerometer and the ninth to sixteenth sensor as an sEMG. (2) A central receiver base called Trigno™ Lab receives the measurements from the corresponding Trigno™ sensor. The following Table 3.5 shows some characteristic of Trigno™ System.

Table 3.5 Trigno™ System Characteristics

Trigno Lab	
Full-charge Operation Time	8 hrs
Typical Operating Range	40 m
Number of supported Trigno sensors	16
Trigno Sensor (EMG / ACC)	
ACC Number of axis	3
ACC range	$\pm$ 1.5 g, $\pm$ 6 g , $\pm$ 9 g
Mass	<15 g

The Trigno™ wireless system offers integration with the third-party measurement technologies while synchronizing the data recording. However, to make the integration possible with in our developed system, a licensed software has to be installed on the computer to which the Trigno™ Lab is connected. This software is called Trigno Control Utility (TCU). While the TCU is running, any other software can be connected to the command port and may instruct the base to begin streaming data. The command port is 50040 on the host (running the Trigno Control Utility) computer. Fig. 3.31 shows the integrated Trigno™ system with the developed DCC.

3.4.2 Operational Function of SIM

The data acquisition from the SIM module starts with the setting of the IP-Address of the computer where the Trigno™ control utility is installed. The hostports for accessing the Trigno Lab and the accelerometers from DCC are 50040 and 50042 [37]. In the GUI panel,

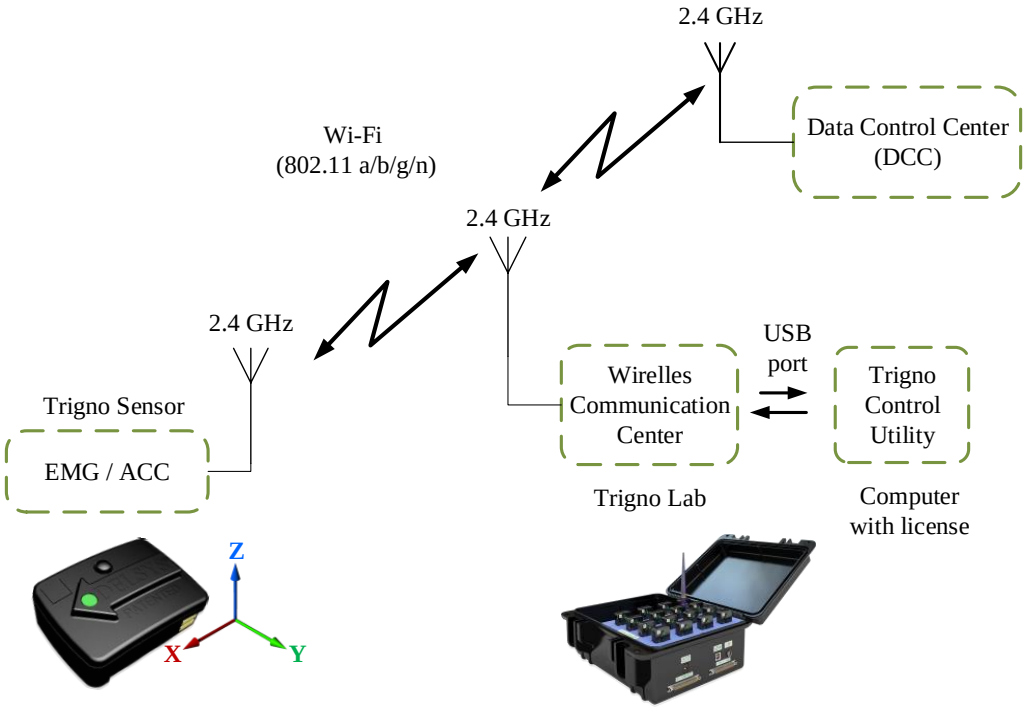

Fig. 3.31 Integration of Trigno™ wireless system with the DCC developed.

the number of sensors is selected for the test. Two sensor are selected to identify the stride during running.

Listing 3.1 Matlab code – hostport to access the Trigno Lab and accelerometers.

```
%TCPIP Connection.
S.commObject = tcpip(S.HostIP,50040);
%TCPIP Connection to stream ACC Data.
S.interfaceObjectACC = tcpip(S.HostIP,50042);
```

After the number of sensors is selected for the test, the GUI starts with the data acquisition sending a command 'START\r\n\r' to the Trigno Lab.

Listing 3.2 Matlab code – Open COM and read data avaliable from Trigno Lab.

```
fopen(commObject); %%Open the COM interface
data = fread(commObject,commObject.BytesAvailable);
% Send the commands to
fprintf(commObject, sprintf(['START\r\n\r']));
```

3.4.3 SIM Experimental Test

Different series of tests were programmed to analyze three main characteristics of the accelerometers. first, determined the sensor location on the legs. second, identified the number of sensors necessary to determine the foot contact. third, to identified the operation range of the sensors, as the maximum range of Trigno sensor is $\pm 9g$. The experimental tests were developed indoors and outdoors as was explained in Section 3.3.7.

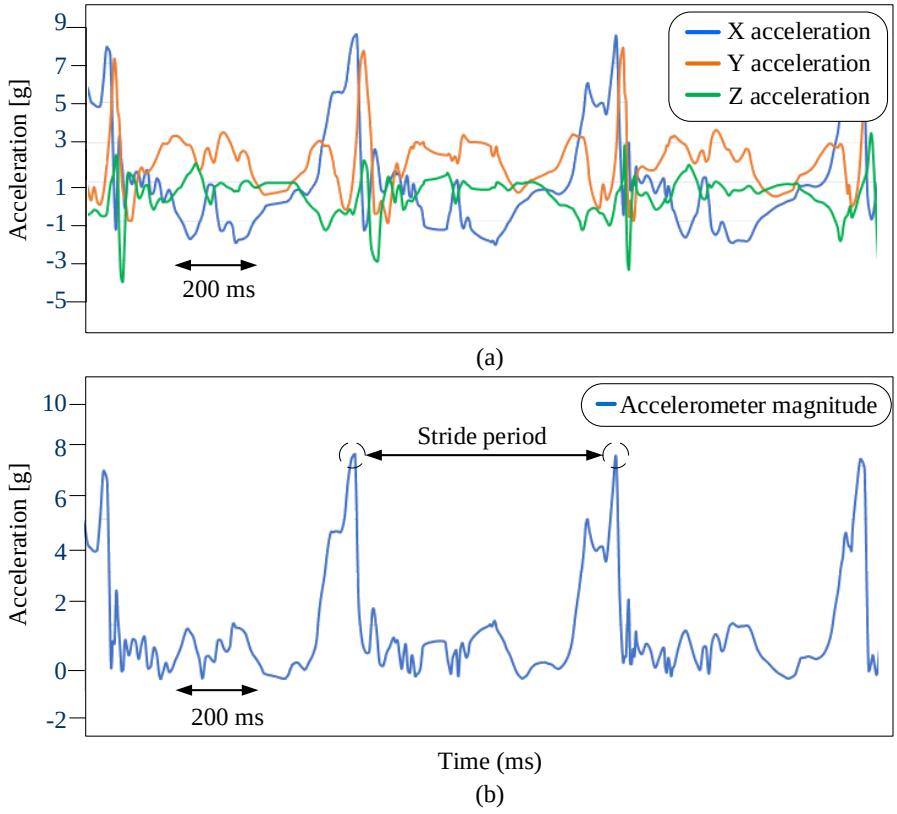

Fig. 3.32 (a) Triaxial signal from Trigno Sensor (right foot) while jogging; (b) Magnitude of the acceleration.

To determine the foot contact in humans based on the accelerometer method, one sensor is placed a few centimeters above each ankle. With these sensors it is possible to establish a pattern, to identify when the foot touches the ground. To simplify this identification, the magnitude of the acceleration was evaluated by:

$$a = \sqrt{x^2 + y^2 + z^2}, \quad [g] \tag{3.9}$$

where x,y,z are the axial accelerations expressed in $1g \approx 9.81 m/s^2$. Fig. 3.32 shows an example of the triaxial raw values, and the acceleration magnitude are both plotted by the

GUI. The maximum peaks in the graphics show the foot contact with the ground. Therefore, one simple stride cycle (two steps) can be identified when the same foot touches the ground twice.

To conclude, the Trigno system is a reliable device to identify the stride during running-mode based on accelerometers. However this system has the same problems of communication range (max $\approx$ 20 m), as the RFM in outdoor areas. Over the range of 20 m it causes delays in the transmission and accumulation of data (see Fig. 3.33). In indoor test the range was $\approx$ 50 m with the continuous data transfer.

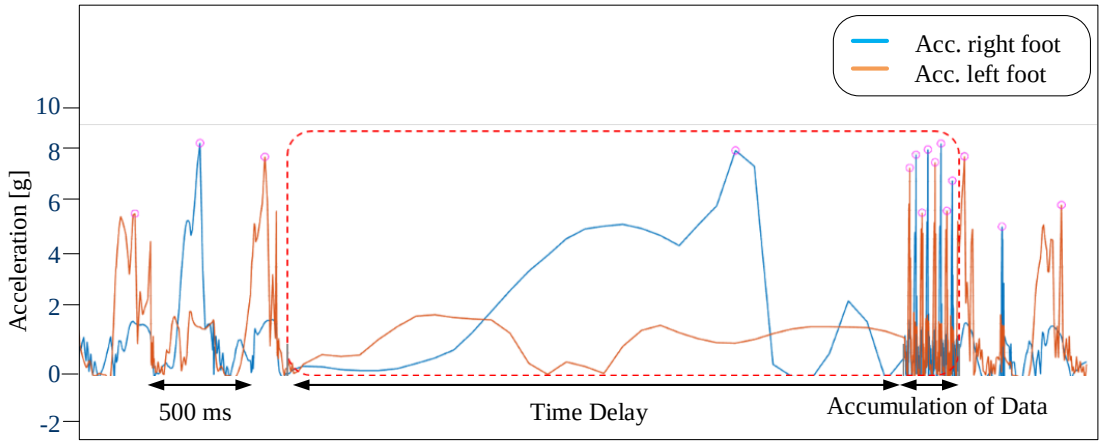

Fig. 3.33 Time delay of outdoor wireless communication.

3.5 Respiratory Muscles Module (RMM)

A method to estimate the muscular activity is provided by surface electromyography (sEMG). These sensors record potential from the electrodes placed close to the selected muscle. This method was used by other researchers to analyze the breathing muscle activation pattern in different mammals during locomotion. For example, Zsoldos et al. [92] studied the muscular activity of the M. rectus abdominis (RA) and M. obliqus externus abdominis (OEA) muscles in horses during walking and trotting on a treadmill. They used sEMG sensors to conclude that muscles activities were around three times smaller while walking than trotting. Furthermore, Anders [4] studied the trunk muscle activation during human walking at different speeds (2 to 5 km/h). He also showed that the muscle activation increases with the speed. Based on this method, this module records the muscular activity of some thoracic muscles and abdominal muscles during free-running mode. The muscles description is shown in Chapter 4.

3.5.1 RMM Description

This module used the four Trigno sensors to analyze the electrical activity of the respiratory muscles. This sensor also features sEMG electrodes with the following characteristics.

Table 3.6 Trigno™ Sensor - EMG Characteristics

Trigno Sensor (EMG / ACC)	
EMG resolution	16 bits
Number of contacts	4
Range	11 mV

3.5.2 Operational Function

Similar to the accelerometers, the data acquisition from the RMM module starts setting the IP-Address of the computer where the Trigno™ control utility is installed. The hostports to access the Trigno Lab and the sEMG from DCC are 50040 and 50041 [37].

Listing 3.3 Matlab code – hostport to access the Trigno Lab and sEMG.

```
%TCPIP Connection.
S.commObject = tcpip(S.HostIP,50040);
%TCPIP Connection to stream EMG Data.
S.interfaceObjectEMG = tcpip(S.HostIP,50041);
```

Chapter 4

Global System Experimental Evaluation

This chapter describes the series of experimental tests in order to evaluate the performance of the implemented system. Three of the implemented modules were used in these tests, the RFM, RMM and SIM. The module IPM was not considered because it is a prototype of an implantable device without any permission to be used in living beings. The tests were executed on humans in order to determine the pattern of LRC in free spaces at sprint running mode. The chosen participants for the test were 15 healthy persons between 23 and 35 years old. The analysis of all data showed what the relation is between locomotion and respiration in human beings. The developed system also allows measuring muscular activity of some respiratory muscles during locomotion and the direct relation between thoracic muscles, respiration cycle and the step identification of locomotion. As follows, we explain the implementation of this method in humans, the complete description of the developed experimental test and finally the analysis of the obtained LRC results.

4.1 Applied Methodology

We methodologically based the analysis on different sensor modules in order to establish the interaction between respiration and locomotion in mammals. 15 healthy (12 men and 3 women) persons participated in the experiment (23-35 years, median 28 years). Characteristics of the participants are summarized in Table 4.1. All participants were students from the Technische Universität Ilmenau. They denied having any respiratory illnesses or problems before the experimental tests. The modules were attached to the participants to measure their physiological parameters during the tests. The recorded data was analyzed using a graphic interface in post processing. All module's output signals were synchronized to the same time scale, such that each signal could be analyzed independently.

4.1.1 Experimental Setup

The experiments took place in the closed sports center of the Technische Universität Ilmenau (TUI-SC). The temperature was measured with a digital room thermometer. The experimental area (EXA) is described in Fig. 4.1. A starting (start) and an ending (finish) mark were

Table 4.1 Personal physical characteristics of participants

Subject	Gender	Age (yrs)	Mass (kg)	Height (cm)	Training
1	M	23	70	171	Nonrunner$^{\circ}$
2	M	28	66	162	Casual†
3	M	27	81	173	Nonrunner
4	M	27	75	175	Casual
5	M	34	90	175	Casual
6	M	25	70	168	Trained*
7	M	27	82	175	Trained
8	M	30	77	178	Trained
9	M	30	80	174	Nonrunner
10	M	26	74	171	Nonrunner
11	M	35	91	186	Trained
12	M	24	76	176	Trained
13	F	29	62	160	Casual
14	F	27	53	157	Casual
15	F	30	60	165	Casual
	mean	28	73	171	
	s.e.m*	0.22	0.71	0.50	

* standard error of mean.
* training more than three times per week
† training once per week
$^{\circ}$ training once per month

located in the area. The whole experiment was recorded with two video cameras, with the purpose of supporting the analysis of the recorded data in the post processing. One camera was placed at a higher position (second floor) of the EXA, the other camera was on the same level as the running area.

Each participant warmed up for 5 min, trotting around the experimental area and then performed 12 sprint tests, running with the fastest constant speed that could be reached along 30 m in straight line. The DCC and the Trigno Lab were located in the center of the area in order to obtain continuous data transfer rate. The environmental parameters (room values) were temperature of $T_m \approx 20$°C (measured) and atmospheric pressure of $P_m \approx 1008$ hPa (data taken from http://www.wetter.com). These parameters were used to calculate the volumetric flow expressed in ℓ/min from the measured volumetric flow [slm] based on the combined gas law, as was described in Section 3.3.4.

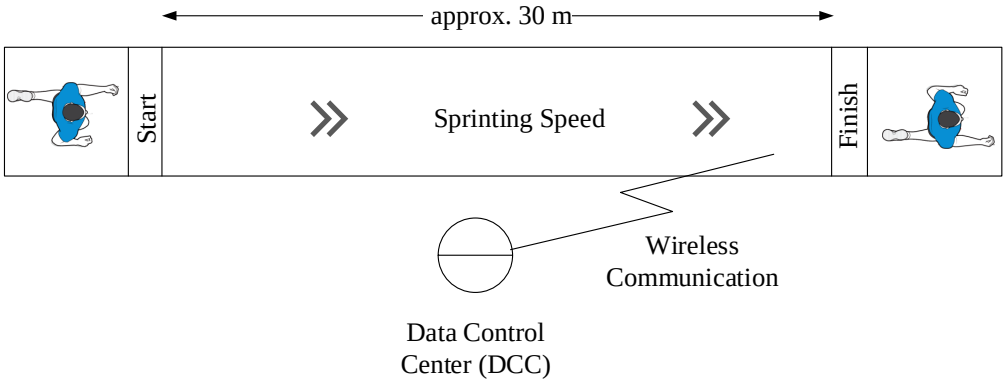

Fig. 4.1 Experimental area: characteristics of the sprint running test.

Three modules were attached to the participant: (1) To identify the foot-contact on the ground, two accelerometers were placed on the external lateral part of legs, 2 cm above the ankle. (2) To measure the electrical activity of the respiratory muscles, four sEMG sensors were attached with a special skin-tape. Two sensors were placed on the right side of the body in the midcavicular line. To record the contraction of the *diaphragm* (DG), an EMG sensor was placed in the seventh or eighth intercostal space. For the *M. intercostalis externus* (EI), the sensor was placed on the *M. pectoralis* major in the 2nd or the 3rd intercostal space. The other two sensors were placed on the left side of the body. One sensor was placed in the fifth or sixth intercostal space at the posterior axillary line, to record the *M. serratus anterior* (SA). The other sensor was placed on the *M. abdominis obliquus* (EO). Fig. 4.2 shows positions of all sEMG sensors described above. (3) To measure the flow, the participants wore the respiratory flow module (RFM) located on the face, covering the nose and the mouth. The module mask was fastened up firmly by elastic bands around the head. Fig. 4.3 shows a participant with three attached modules.

4.1.2 Data Recording

The DDC was embodied in a laptop with the following characteristics: Processor Intel® Core™ i7, 16 GB DDR3 SDRAM and WLAN 802.11 a/b/g/n transceiver. To initiate the data acquisition, a new test is created with the personal data of the subject. Then, the desired modules are selected. This option activates the Trigno system setup and the RFM calibration mode. (1) The Trigno setup includes the update of the Trigno Lab IP-Address, as it was explained in Section 3.4.2. Trigno system has 16 hybrid sensors in total. For the LRC study six Trigno sensors were used, two acceleration sensors for the SIM and four EMG sensors for

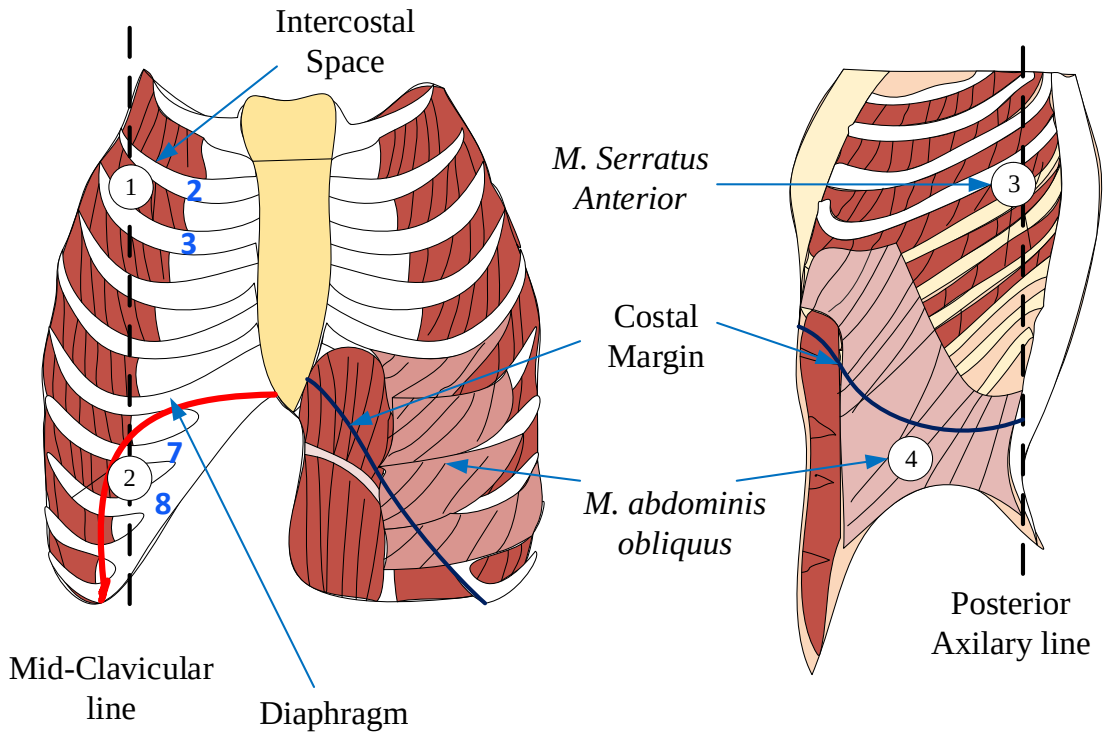

Fig. 4.2 Representative description of sEMG sensors location in human respiratory muscles. ① *M. External Intercostal* (EI): Between the second and the third rib (second intercostal space). ② Diaphragm (DG): intercostal space (between the seventh and the eight ribs) at mid-clavicular line. ③ *M. serratus Anterior* (SA): Fifth intercostal space at the posterior axillary line. ④ *M. abdominis obliquus externus* (EO): Directly below the most inferior point of costal margin. All the selected positions are based on the studies [4],[35],[48].

the RMM. (2) The RFM can be calibrated using the method based on a certificated precision syringes, as it was explained in Section 3.3.6. Finally, after the module's setup was complete, the DCC was prepared to record data. More details regarding the GUI panel functions are shown in Appendix C.1.

4.1.3 Experimental Procedure

Before the session recording (one session = one sprint), participants jogged for five minutes around the TUI-SC without any equipment. They also attended at least one further familiarization session with the RFM. Each participant ran (sprint mode) six times around the EXA (three round trips). This experiment was performed twice with a 5 to 7 min break in between.

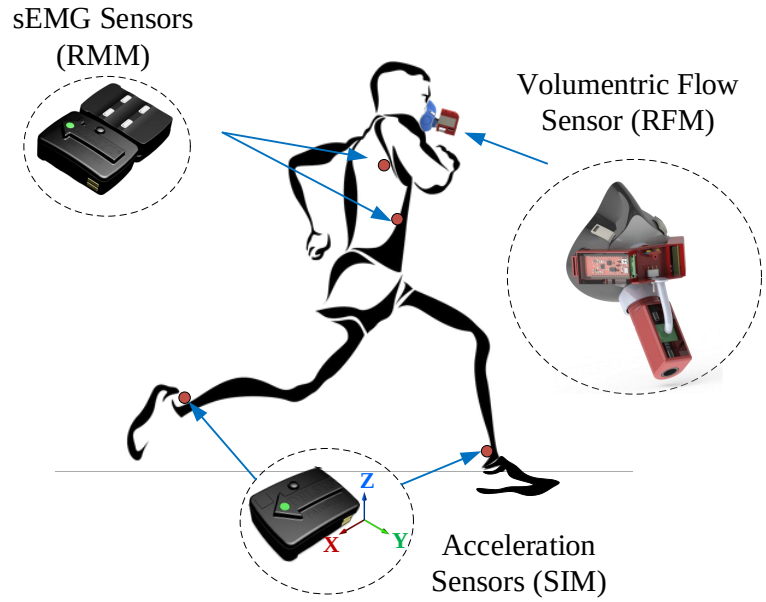

Fig. 4.3 Referential of the experimental test including the RFM, SIM, RMM. One accelerometer sensor is located at each leg, 2 cm above the ankle. Four sEMG sensors are located on the thoracical and abdominal muscles. A volumetric flow sensor is located in a mask, covering the nose and the mouth of the subject under test.

During the break, the proper attachment of modules was controlled to avoid any delay or incorrect data transmission.

4.1.4 Data Analysis

The measured data was saved in three different files with $*.txt$ extension (ACC, EMG, FLOW). The time values and the raw data of each sensor were recorded into the files. To analyze the data, the GUI run in a post processing mode. It allows the user to load saved data and to visualize the raw signals.

The measured accelerometer signals allow to identify the steps during locomotion. The GUI uses a function that improves the accuracy of step identification. Matlab® function called "findpeaks" identifies the values and the location of a local maximum in a set of data. This local set of data was based on two parameters, "threshold" and "radius". The threshold defines the minimum amplitude differences between a peak and its neighbors. The "radius" defines the minimum peak separation, choosing always the highest peak in the range and ignoring other peaks within this radius. These two parameters can be modified manually in the GUI panel. Besides, the peak identification during acceleration of the subject was

considered to determine the foot-ground contact and consequently to determine when a step has been taken (see Fig. 4.4). Another main objective of the accelerometer is to calculate the participant speed. It is calculated based on the relation between the time and running distance (30 m).

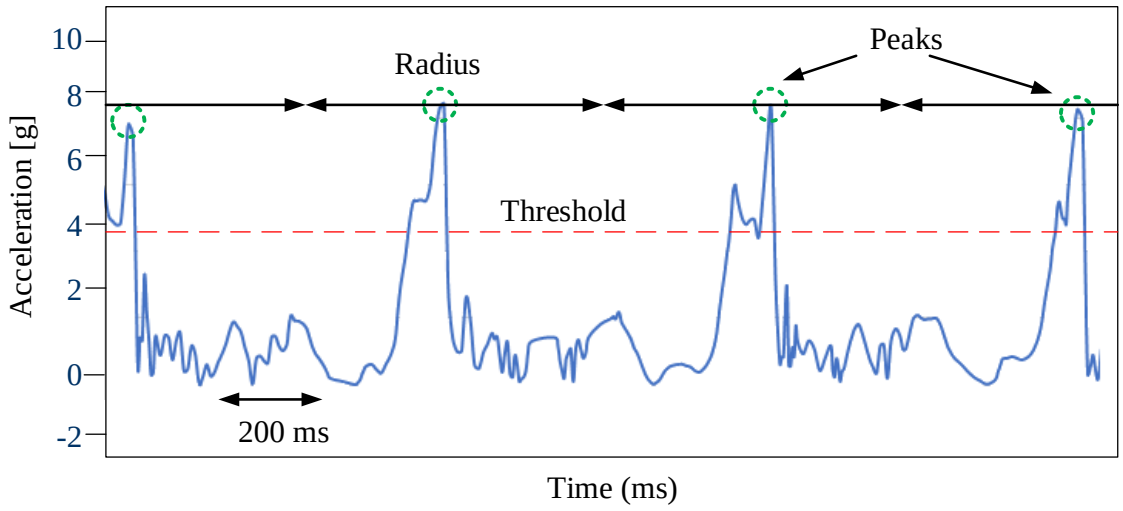

Fig. 4.4 Step identification based on maximum values (shown in a green circle) of a data segment generated by a radius and a threshold. Both are defined by the user manually trough the GUI.

Regarding the volumetric flow signal, it allows the identification of breathing cycles. The fact that humans are able to control their breathing is taken into account in the signal analysis. The results are influenced by the physiology of the subjects and their training status. Controlling the breathing is used by athletes to improve their performance by the economy of energy during the LRC coupling [6]. Also, this signal allows calculating the average air volume displaced in and out of the lungs during inhalation and exhalation respectively. The maximum amplitude represents the breathing strength of the subject. Also, along the tested distance it is possible to determine the LRC coupling with the number of strides. The example of such a signal is shown in Fig. 4.5.

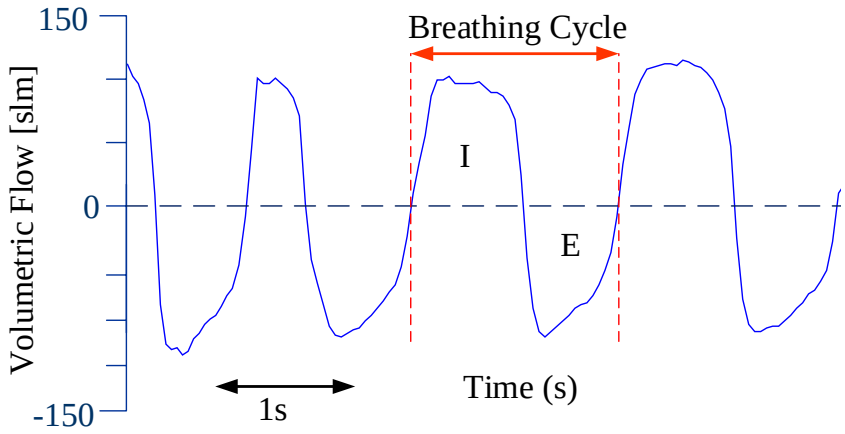

Fig. 4.5 Representative average volumetric flow signal. Breathing cycle is constituted by inhalation (I) and exhalation (E). The air volume moved during a breathing cycle is calculated based on the numerical integration (trapezoidal algorithm) of this signal.

On the other hand, regarding the electromyography signals, they represent the electrical activity of the respiratory muscles. The signal tension increased during locomotion, due to a greater muscle activation as shown in Fig. 4.6. Also, the amplitude of tension during locomotion reached the maximum values regarding the foot-strike.

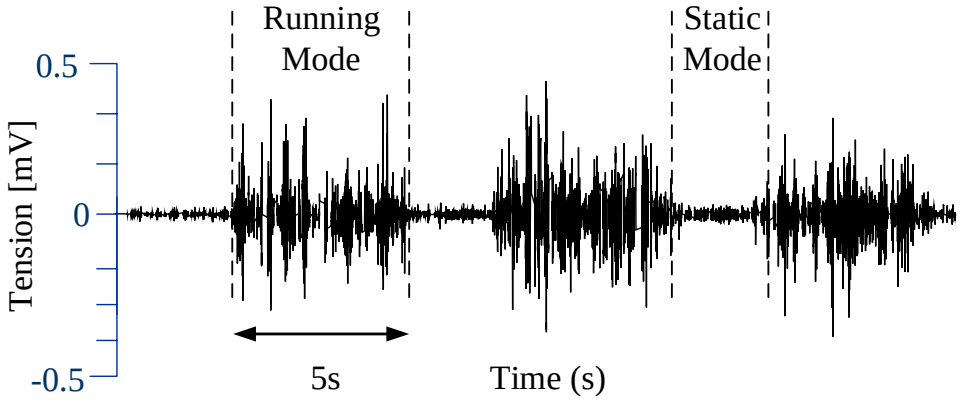

Fig. 4.6 Exemplary electromyography signal of a respiratory muscle (*M. pectoralis major*). Differences occur between running mode and static mode.

4.1.5 Data Synchronization

Each module has its own timeline during one data acquisition. However, due to the resolution of the sensor, the number of values in each module is not the same in one time interval. The intersection of them is taken to synchronize both timelines (RFM and SIM). As an example (see Fig. 4.7), the timeline from Trigno sensors (TT) starts before the flow sensor timeline (FT). As it was observed, the first time value in common is 1.2 seconds. This value is considered as the first value for the new "virtual" timeline (VT). As a consequence, the transfer data rate in the Trigno system is faster than in RFM, and the TT has more samples than the FT. In this example TT owns 11 samples and the FT has just five in common. The VT combines the values between both timelines. Finally, the VT ends where one timeline has no more values. In this example, the last sample value of Trigno is 2.2 sec, meaning that VT also ends after 2.2 sec. More details about the post analysis functions of the GUI panel are shown in Appendix C.1.

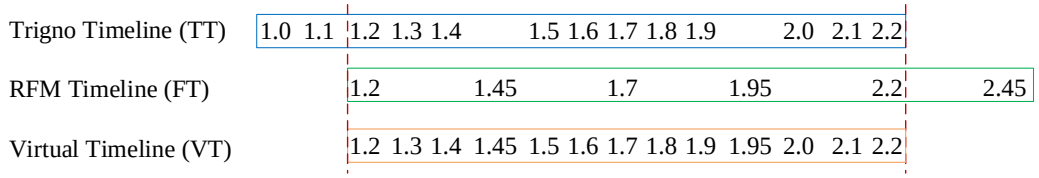

Fig. 4.7 Timelines interception of sensor signals.

As next the results from the experiment are described.

4.2 Obtained Results

The presented results focused on two physiological interactions: (1) the LRC ratio (strides/-breath) in humans during locomotion, (2) the relation between electrical activity of some respiratory muscle with the breathing cycle during locomotion. To determine the LRC ratio, the synchronization between the accelerometer signal and the respiratory flow signal was analyzed. As it was explained before, the accelerometer allows determining the foot-contact (step), and the flow signal determines the breathing cycle during the measured time. Table 4.2 presents the final results of the experimental tests in TUI-SC with fifteen participants.

Table 4.2 Obtained values during experimental evaluation

Subject	Number of trials†	Speed [m/s]	Number of Strides	Breathing Cycles	LRC ratio	Max I Flow [slm]	Max E Flow [slm]	Vol Insp [liter]	Vol Exp [liter]
1	12	5.55 ± 0.53	10 ± 0.58	5 ± 0.52	2:1	54.54 ± 30.95	-90.77 ± 27.33	1.60 ± 0.68	-2.19 ± 0.73
2	12	6.05 ± 0.43	8 ± 0.48	2 ± 0.50	4:1	163.08 ± 39.77	-167.42 ± 34.09	3.45 ± 0.80	-3.32 ± 0.77
3	12	6.39 ± 0.49	9 ± 0.52	3 ± 0.48	3:1	138.50 ± 13.88	-169.79 ± 35.46	2.81 ± 0.27	-3.50 ± 0.58
4	12	6.36 ± 0.20	8 ± 0.20	2 ± 0.22	4:1	102.00 ± 14.52	-72.00 ± 46.52	2.16 ± 1.33	-3.07 ± 0.21
5	12	4.97 ± 0.22	10 ± 0.69	5 ± 0.55	2:1	166.47 ± 29.78	-174.46 ± 28.37	3.45 ± 0.67	-3.79 ± 0.77
6	12	7.61 ± 0.54	10 ± 0.75	5 ± 0.95	2:1	136.68 ± 51.42	-145.70 ± 45.47	3.00 ± 1.08	-2.96 ± 0.88
7	12	5.82 ± 0.35	10 ± 0.35	5 ± 1.16	2:1	145.25 ± 46.40	-152.68 ± 43.77	3.15 ± 1.04	-3.31 ± 1.04
8	12	7.14 ± 0.38	8 ± 0.32	3 ± 1.13	3:1	184.73 ± 36.00	-185.17 ± 26.09	3.99 ± 1.02	-3.55 ± 0.78
9	12	5.57 ± 0.35	8 ± 0.50	4 ± 0.52	2:1	144.50 ± 40.96	-124.56 ± 35.99	2.74 ± 1.04	-3.68 ± 0.77
10	12	6.48 ± 0.79	9 ± 0.57	3 ± 0.84	3:1	148.50 ± 32.85	-164.14 ± 52.08	2.36 ± 0.93	-3.06 ± 1.01
11	**12**	**5.69 ± 0.58**	**9 ± 0.52**	**3 ± 1.05**	**3:1**	**184.42 ± 36.00**	**-205.75 ± 6.37**	**3.90 ± 0.68**	**-4.23 ± 0.18**
12	12	5.60 ± 0.26	10 ± 0.35	5 ± 0.74	2:1	162.18 ± 46.58	-152.00 ± 52.77	3.62 ± 0.83	-3.13 ± 1.07
13	12	5.69 ± 0.20	9 ± 0.68	3 ± 0.84	3:1	55.51 ± 38.92	-65.43 ± 23.05	1.15 ± 0.76	-1.16 ± 0.59
14	12	5.54 ± 0.46	12 ± 0.52	3 ± 0.89	4:1	153.17 ± 25.84	-175.37 ± 26.91	3.46 ± 0.74	-3.66 ± 0.88
15	12	6.05 ± 0.79	10 ± 0.76	2 ± 1.15	4:1	133.67 ± 44.63	-134.00 ± 20.00	2.46 ± 0.9	-2.49 ± 0.33

* All values are given in mean standard deviation (mean ± sd)

† Trial : One sprint test (30 m of distance)

4.2.1 Analysis of LRC ratio

Regarding the analysis of LRC, the experimental results are compared with related comparable work developed by Daley in 2013 [33]. Daley performed an experiment with fourteen healthy participants, running at a steady speed of 2.6 m/s on a treadmill. To track the step cycle, a single accelerometer located at the top of the head was used and a commercial pneumotachograph measured the volumetric flow. The calibration method of the pneumotachograph used a similar precision syringe of 3 liters, as in our case. To calculate the ensemble average (EA) of ventilatory flow or "step-driven flow" as designated by Daley, we considered the step cycle for each participant, including at least 50 steps per subject. Furthermore, the locomotor driven volume (LDV) is calculated from the trace of the ventilatory flow EA. The inhalation (positive) and exhalation (negative) volumes were integrated separately to assess the relative magnitude of each as is shown in Table 4.2.

The first observation focused on the speed reached by each participant running at a self selected speed in free space. The obtained mean speed was 6.03 m/s (21.73 km/h) compared to 2.6 m/s (9.36 km/h) in case of [33]. However, the calculated LRC ratio (stride/breath) was between 2:1 and 4:1, which mirrors similar results in both experiments according to the histogram shown in Fig. 4.8.

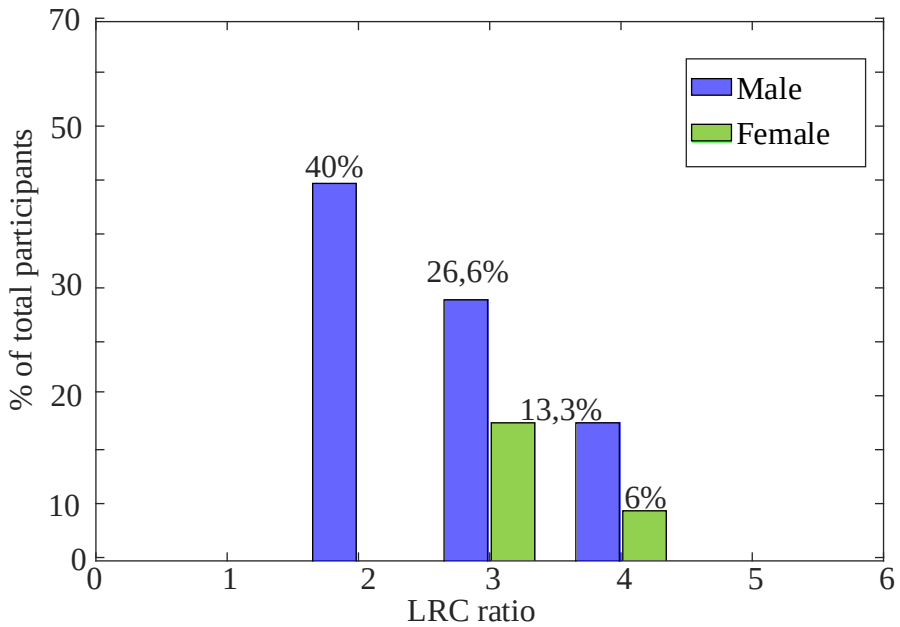

Fig. 4.8 The distribution of obtained experimental LRC values.

As an example, Fig. 4.9 shows a relation between the breathing cycle and the steps for the subject # 11 according to Table 4.2. This data represents the average of 12 sprint running tests over 30 meters. The subject under test showed good physical shape. Moreover, he trains at least twice per week. His results show an average stride number of 9 and an average number of breathing cycles of 3. The average time of the test was 5.27 sec running at a speed of 5.69 $\pm$ 0.58 m/s. A mean breathing cycle presents an average time of inhalation for 0.7 s and exhalation for 0.8 s. The average LRC ratio for this participant is approximately 3:1. He was not the fastest participant in this experiment. However, his volumetric flow during the breathing achieved the highest value and therefore the highest LDV. The average maximum respiratory flow is 184.42 slm for inhalation and -205.75 slm for exhalation. The calculated volume for this participant reached values of 3.9 liters during inhalation and 4.23 liters for exhalation. The estimated vital capacities for a man of 175 cm to 185 cm body height is 4.3 liters [51].

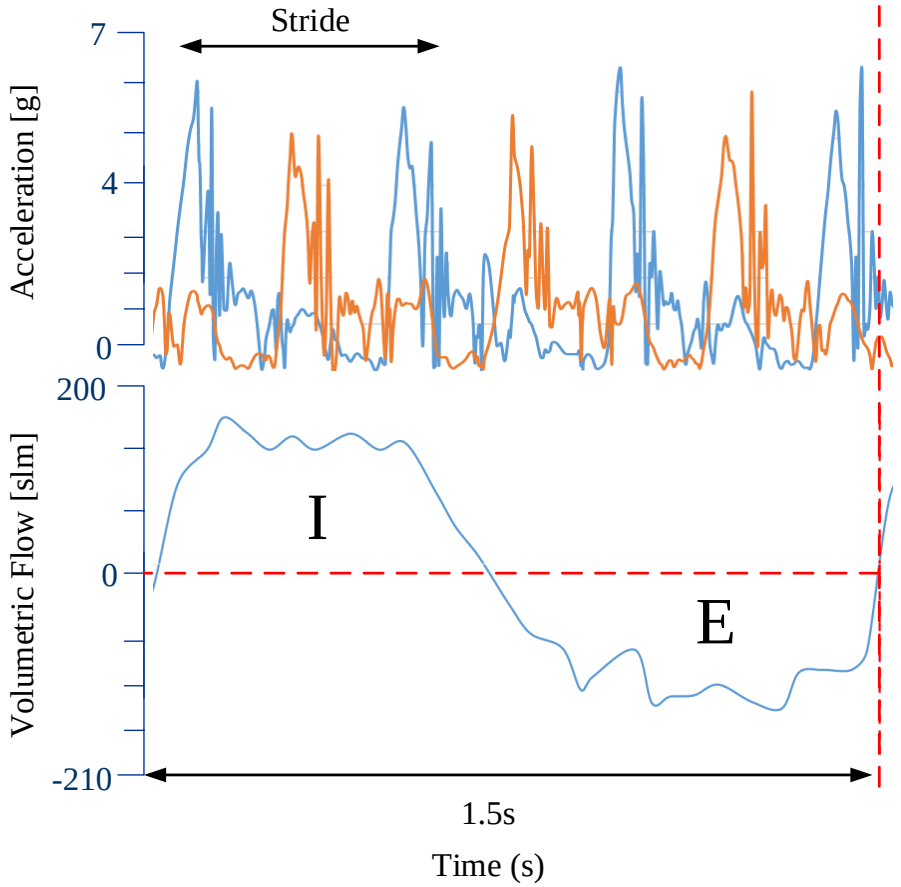

Fig. 4.9 Representative trace of the participant # 11. During a single breathing cycle (inhalation (I) and exhalation (E)), the subject make three stride (blue signal). The LRC ratio is 3:1 (strides/breathing).

Applying the same procedure to all participants, it is possible to determine tendencies of 2:1, 3:1 and 4:1 for the LRC ratio, and it confirms what other studies affirmed, LRC is flexible in humans. The ratios for this experiment are shown in the histogram in Fig. 4.8. However, we can only determine tendencies for the performed experiment. No global conclusions regarding LRC ratio can be made, as the number of participants is not high enough. However, as was stated before, the performance of biomechanic studies was not the initial purpose of the presented experiment. Results only serve to show the feasibility of the developed method and to show its potential, as this method can be easily applied to any mammal to measure and analyze its LRC ratio.

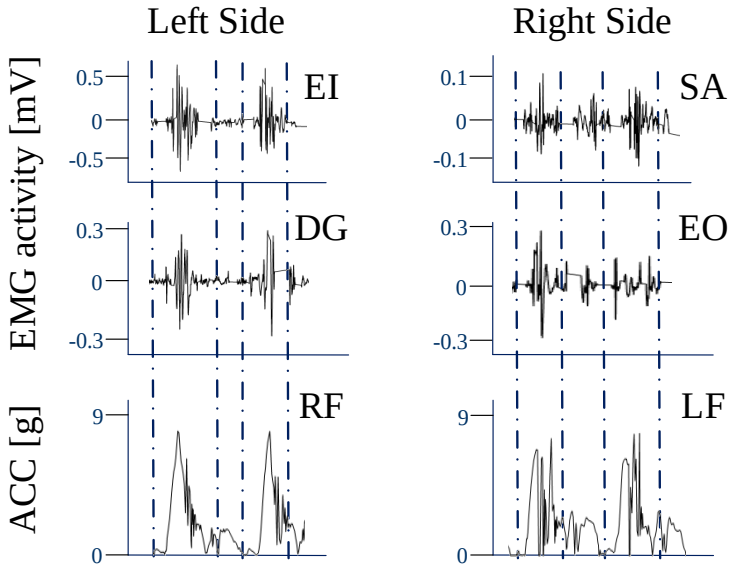

Fig. 4.10 Ensemble averages of electromyographic activity for four respiratory muscles, taken from a subject running at maximum speed (sprint mode). The signals from the right side revealed a synchronization with each step of the right foot, reaching its maximum value. All traces were made at the same time scale.

4.2.2 Analysis of sEMG Signals

The proposed method also allows analyzing the interaction between the muscles of respiration and the locomotion in mammals. As it was explained in Chapter 2, the LRC presents four mechanical impacts which induce changes in the main physiological parameters of the respiration, the thoracic pressure and the lung air volume. One of the impacts is related to different respiratory muscles (abdominal and thoracic) and how intensely some of them are

involved during inhalation and exhalation. In order to be able to analyze the contraction of the respiratory muscles during locomotion, this method used surface electromyography sensors to detect the electrical activity of those muscles. Fig. 4.10 shows a noted synchronization between the muscles and the foot strike on the ground. The sensors located on the right side of the body were the *M. intercostalis externus* (EI) and the *diaphragm* (DG); they show more interaction with each step, reaching different peak values of 0.5 mV for the EI and 0.3 mV for the D. On the other hand, the sensor located on the left side (*M. serratus anterior* (SA) and *M. abdominis obliquus* (EO)) also presented a synchronization, but a different pattern in the interaction with foot strike.

However, the signals like EO have a phase delay of electromyography activity in relation to the breathing cycle. In Fig. 4.11 the maximum amplitude of EO during inhalation is shown. In addition, on the right side of Fig. 4.11, signals confirm the high activity of the muscles (EI and DG) during the breathing cycle. When these signals were collected in static state with a normal breathing cycle, the peak values decreased considerably.

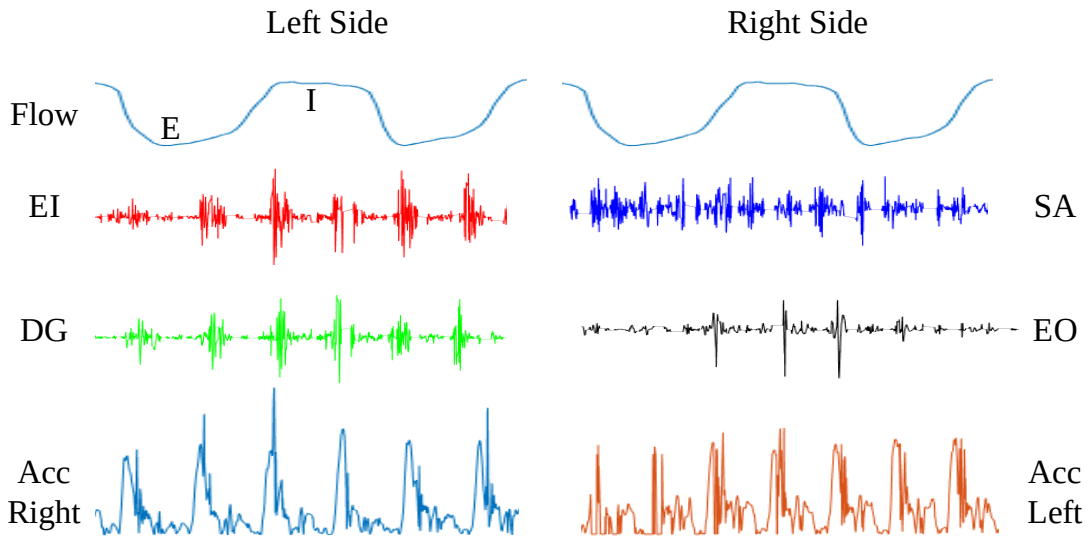

Fig. 4.11 Representative synchronized sEMG signals during the breathing cycle while running in a sprint mode. The EI an DG signals show increased electrical activity during inhalation and exhalation. The EO reached maximum peaks during inhalation. SA presents an unclear analysis of the synchronization with the breathing and movements.

Chapter 5

Discussion

Each electronic component of this developed wireless system is commercially available for medical applications in humans. However, none of these commercial systems allows the integration and synchronization of signals of all modules required to analyze the LRC in mammals. Our implemented system was also designed to integrate additional modules to measure physiological parameters that the study and specialist require.

Two modules (IPM and RFM) were designed and implemented following the mechatronics methodology VDI 2206, fulfilling requirements like allowing wireless transmission. In case of IPM, existing implantable devices with wireless transmission to measure pressure in animals. However, these devices are code closed and do not allow signal synchronization with other modules, and are not designed for long distance transmission, since in the majority of the cases they are used for analysis in laboratories with the animal in a static state. On the other hand, the RFM has similar requirements as a wireless spirometer, except that our device was not developed for medical application in humans (e.g. for diagnostics of lung diseases). Besides, our device was designed to measure the volumetric flow during locomotion outdoors. A spiroergometry device can fulfill the function of measuring the flow in movement. However, the commercial devices are designed only for humans and they also do not allow the signal synchronization with other devices. Although our experimental test was made with humans, it is possible to adapt our system to other mammals.

Finally, we want to remark that this system is not a biomedical device with application in human medicine. However, we consider a valuable tool in areas like veterinary medicine or zoology.

Next we discuss the results of the experiments as well as the advantages and disadvantages of the implemented system. Furthermore, we discuss the obtained errors during experimental evaluation and the possibles reasons for those. Finally, the discussion ends with the review of technical implementation of each module and the GUI for data analysis.

5.1 Discussion of Errors

This system is the first prototype implemented for the LRC analysis. As expected there are some features in the system that can be improved for the correct and accurate data acquisition.

In the following, the obtained errors presented during the experiments in each module of the system will be discussed.

The IPM pressure sensor calibration method presented some errors during measurement collection for calibration. The sensor values were compared with those provided by the digital manometer. These manometer values were taken visually from digital display, causing inaccuracies in the calibration method (linear regression) and therefore an erroneous post data acquisition. In a future prototype it is necessary to use a high precision manometer designed for calibration and to develop a computational comparison with the sensor values.

In case of the IPM test bench, the pressure changes in the chamber are too fast and abrupt due to the mechanical and manual control of the rubber bulb. For a better approximation of the pressure changes in the pleural cavity, this test bench should allow controlled changes. The proposal related to a new test bench is based on a micro-fluidically controlled system.

The RFM could provoke errors in the measured data. The hermetic seal of the mask should minimize losses of air flow during inspiration and expiration. However, due to the different shapes and sizes of the subject's faces, there are air losses in some cases. Other features of the RFM are related to the post processing data. The volume numerical calculation based on the signal integration of the flow signal could accumulate error. So, other algorithms can be implemented, such as the Simpson's rule for integration together with a subdivision strategy like adaptive quadrature algorithms. In this case, the computational resource is not critical as the volume calculation is not in "real time" during the experiments.

Trigno system does not report any error during the data acquisition. However, when it is integrated with other modules, a delay in the data acquisition increases significantly. These errors could arise due to two reasons. First, the communication protocol of each module should be more robust in order to avoid any missing data, and the module should re-send the values to the DCC. Second, the GUI should be run in an embedded DCC. In our case, a laptop was used as a DCC, and it shares computing resources with many other applications.

5.2 Discussion of Results

The discussion of results will focus on two main research questions that were asked at the beginning of this work: (1) Is the method based on a modular multi-sensor system with wireless communication is a reliable tool for the analysis of the interaction between respiration and locomotion in mammals? (2) Will the experiments with exercising mammals in a free space with self-selected running pace have a considerable difference in the results compared to the typical laboratory experiments in the same field, using a treadmill with a steady set speed?

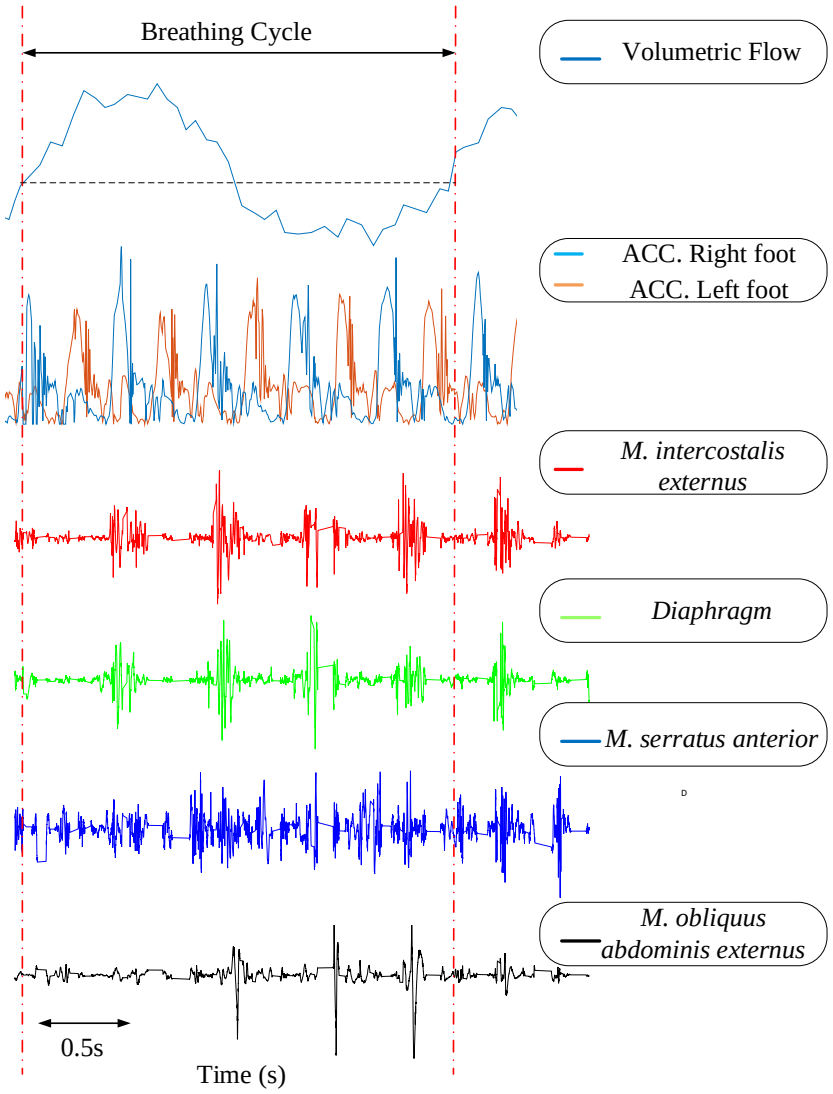

Fig. 5.1 Representative electromyographic (EMG) traces from four respiratory muscles with traces of volumetric airflow and x-axis acceleration. These signals illustrate the method for the coupling analysis and the muscular activity during locomotion. The EMG signals correspond to the electrical activity of the *M. intercostalis externus* and *diaphragm* which are located on the right side of the body. On the other hand the signals of the *M. serratus anterior* and *M. obliquus abdominis externus* are located on the left side of the body.

Regarding the reliability of the system for the LRC study, the obtained results showed that it is possible to identify the synchronization between different physiological parameters in order to understand the phased lock between them during locomotion of mammals. Fig. 5.1 illustrates how the implemented system shows the synchronized signals for all the parameters. In this representative example it is possible to analyze one breathing cycle during a running

mode. If the fourth module (IPM) could have been integrated into this experiment, the thoracic pressure could measured.

This method minimizes the stress of the subject under the test compared to those in laboratories. The fact that the subject can move freely with a preferred self-selected running pace allows the analysis of data that is closer to the subject's natural behavior. In addition, this method could decrease significantly the training period of any mammal using the attached modules, especially the mask with the volumetric flow sensor.

Once the data acquisition is finished, the post data processing can be executed by specialists. The analysis is supported by cameras in order to achieve deeper understanding of each subject behavior while moving. The data segmentation allows the specialist to better understand each phase of the breathing cycle coupling with locomotion and the electrical activity of the muscles. Considering these characteristics for the post analysis, the implemented GUI allows the raw data segmentation and the deep analysis of each signal independently or synchronized with another signals.

Confirming the comments of the manufacturer, all the selected sensors are technically applicable and reliable for this kind of application. Furthermore, as the wireless communication was used, the first prototype has its limitations like the operational distance and the identified delay proportional to the amount of integrated sensors. However, the technical characteristics always could be improved in future designs.

5.3 Discussion of Prototypical Technical Implementation

In the following, the performance of the implemented modules will be discussed. (1) The Implantable Pressure Module (IPM) was based on an implantable device which can measure the pressure in the thoracic cage. This module was designed based on commercial electronic components and following the international standard for implantable devices, like transmission frequency in the range of medradio band (402-405 MHz), low power transmission ($< 25\ \mu W$) and averaged SAR was not exceeding 2 W/kg. Other characteristics were also considered in the implementation of the device, for example, the bio-compatibility of the enclosure material (silicone MED-4011) in order to avoid infections. However, this module during the design presented three main limitation. First, the antennas available on the market were ceramic chip type. These antennas are designed for different applications, and their size is not compatible with the design of a tiny implantable module. Second, the selected battery was lithium coin cell type, and it has a limited battery capacity, which affected the functional life time of the device. Third, the pressure sensor catheter size is determined by the sensor size. Also, the commercial sensors for medical applications are used to measure

blood pressure. These characteristics limited the size of the device, and as a consequence not all mammals can be studied with this implementation of the module.

(2) The respiratory flow module (RFM) measures the air volumetric flow during the breathing cycle. The inhaled and exhaled air volume is calculated by integration of flow over time. For the particular experiment, this module was designed based on human physiology, taking into account the species-specific lung volume and vital capacity. According to the manufacturer, the selected sensor is designed for spirometry or another particular respiratory device. In order to adapt the system for specific mammal species, there are two main factors to be considered in the new module design. The sensor selection, which accomplishes the physiological requirements of each species, and the ergonomic mask, which has to be designed considering the anatomical characteristics of the mammals under test.

(3) The Trigno Lab is a commercial wireless system capable of measuring the electrical activity of muscles and the acceleration of any object. This system was selected because of reliable data acquisition and the possibility of easy integration with external systems. However, the system model is not portable and has limited operational distance, as this became obvious in the performed experiments.

Regarding the results of our experiment, the post data analysis allows us to identify the synchronization of different physiological parameters without any restrictions. Only analyzing the flow and acceleration signal, it is possible to calculate the LRC ratio and to establish the existence of a coupling between respiration and locomotion. First results confirm what other researchers previously affirmed, that LRC ratio in humans is flexible and vary in the range of 2:1, 3:1, 4:1. Although, the range values of the locomotor driven volume (LDV) in some cases reached almost the maximum vital capacity of the subject. On the other hand, the analysis of EMG signals showed a phased locked with breathing. In addition, the magnitude of the signal increased when the subject was in motion, as the respiration contraction became stronger during respiration. However, as the biological analysis was out of scope of this work, the achieved results should be further analyzed by specialist in this area.

Finally, we can conclude that the developed method is suitable for the analysis of LRC in humans. Also, we confirmed the possibility to adapt this system to study the LRC in different type of mammals. However, it is necessary to previously study physiological and anatomical parameters for each species.

To summarize: This implemented method is based on a modular multi-sensor system which uses wireless communication for data transfer. This system has integrated four modules and its target is to collect specific physiological parameters of mammals in running mode. However, the implemented technology allows the integration of more modules, which

measure similar or different parameters. The selected wireless communication (protocol WiFi 802.11.x) presented several advantages compared to similar technologies like Zigbee protocols or Bluetooth. First, it allows faster data transmission and the integration of several modules in a local network. Second, it allows the implementation of GUI on any server connected to Internet, thereby enabling any specialist in the world to follow the experimental test on line and making the data always available for post processing. The operation distance is limited and can not exceed 50 m. This last characteristic can be solved by using several network repeaters to increase the transmission range. In the developed prototype, the GUI was installed on a Laptop (DCC). However, in order to improve the operation range of wireless transmission and to avoid delays during the data collection, it is recommended to implement DCC on an dedicated embedded system. This system is portable and has powerful computing device.

Chapter 6

Summary and Outlook

This chapter summarizes the thesis, and outlines directions for future research.

6.1 Summary

This thesis focuses on technology to evaluate the concept of neuromuscular and mechanical linkage between locomotion and respiration in mammals. This interaction is called Locomotor-Respiratory Coupling (LRC). This work showed the development of an experimental method for the study of LRC during free-running mode in mammals. These experiments were developed using a wireless modular multi-sensor system to collect data from different physiological parameters of respiration during locomotion. Unlike earlier experimental studies in several animals, here the focus was exclusively on the study of the LRC and its changes not only in air volume changes in lungs, but also on pressure changes in the thoracic cavity, and the neuromuscular reaction of breathing muscles during the locomotion. On the other hand, unlike all previous studies using experimental tests in conditioned laboratories, inducing to a fixed speed of locomotion on a treadmill, we wanted to developed a study method considering the natural environment in the movement of any species, minimizing the stress of experiments in the animal. In order to identify technical and theoretical requirements, the state of the art was analyzed.

Regarding previous experimental studies, they were focused on several animals as mammals (bipedal and quadrupedal), birds and reptiles. They provide a better understanding of how the principal parameters of respiration (pressure and volume) are affected during locomotion. The outcome of the literature and previous works analysis was that LRC has a number of important physiological effects such as increasing breathing performance as well as reducing the energy cost of breathing. They also concluded that in various quadrupedal mammals the LRC ratio (strides/breaths) is 1:1 during their highest speed such as galloping or trotting. However, the human breathing pattern is more flexible during running and varies between 2:1, 3:1, 4:1 and 5:1. Furthermore, the discussion is focused on whether the locomotor driven volume (LDV) is significant or not for breathing. For some researchers the volume change provided by stride in trotting and galloping horses ranges up to 20% of

tidal volume. In humans it was from 1% to 2% of tidal volume or in trotting dogs it was on 3%-16%.

This work was based on the premise of whether the quantitative results obtained in previous studies could vary, if the experimental tests in animals were carried out outdoors with a self-selected running pace instead of running on a treadmill with a steady speed. Furthermore, exercises-associated forces (mechanical interaction mechanism) of locomotion affect respiration parameters (ventilatory pressures and volume flows), as was mentioned in literature. However, previous studies did not considered pressure changes in the thoracic cavity, leaving a question about the pressure values reached during the experiments. For these reasons, we propose to implement a wireless modular system based on multiple sensors that allows measuring the changes of pressure and respiratory volume during locomotion for the LRC analysis. In addition, to get a better understanding of the coupling, this system includes the electrical activity of the ventilatory muscles to analyze the neuromuscular effects during motion.

The system consists of four modules interconnected, each module measuring a specific physiological parameter in the respiration and locomotion. The data collected from all modules were sent wirelessly using the Wi-Fi protocol IEEE 802.11 a/b/g/n to the DCC. A GUI installed in the DCC manages the data acquisition and the post data processing. In summary, the whole system (DDC + modules) is connected to a local network (WLAN) for intercommunication. In the following, we review each part of the system:

(1) The GUI was installed on a Laptop (DCC) with an integrated Wi-Fi transceiver. The main two functions of the GUI are the data acquisition of each module and the post processing of the collected data for the LRC analysis.

(2) The IPM was based on an implantable device to measure the pressure within the thoracic cavity in order to collect data of the pressure changes during respiration of the mammal in locomotion. IPM transmits data wirelessly over the frequency band $f < 1$ GHz. The IPM receptor re-transmits the pressure values to the DCC using frequency band of 2.4 GHz via the Wi-Fi protocol.

In addition, a test bench was implemented to calibrate and to test the functionality of the module. This bench consisted of a chamber filled with pork meat. Besides, the pressure sensor was within the chamber and the measurements were compared with a digital manometer installed. Also, a rubber bulb was connected externally to change the pressure within the chamber. The results obtained showed a continuous data transmission between the transmitter (IPM-Tx) and the receiver (IPM-Rx). However, the operational distance was limited to ≈ 1.5 m when the sensor was inside the chamber. Our conclusion regarding this module was that

the IPM-Rx has to be as close as possible with the IPM-Tx, which means a portable device carried by the subject under test.

(3) The RFM was based on a flow mass sensor for respiratory application in humans. As the experimental test was implemented with humans, the sensor holder was attached in a hermetic mask. The data is also transmitted wirelessly using Wi-Fi protocol to the DCC. This module was tested with a participant running outdoors and indoors. The results obtained presented a continuous data transmission between the module and the DCC along an operational distance of $\approx$ 60 m indoors in a closed sport center and $\approx$ 20 m outdoors without any WLAN repeater to increase the distance of operation. After the experiments, we conclude that this module has to be re-designed to study other animals due to the different features in anatomy and physiology of each species. For example, the lung volume capacity should be considered to select the correct sensor as well as the snout shape and size to design the sensor holder and the mask.

(4) Regarding the last two modules, the SIM and RMM are implemented based on the wireless system Trigno™ Lab. Trigno has 16 hybrid transducers (Trigno™ sensor) that combine a surface EMG and a triaxial wireless accelerometer. Trigno™ Lab receives the measurements from the corresponding Trigno™ sensor, and it re-transmits the data to the DCC. The main disadvantage of this system is the size of the Trigno™ Lab, which limited the transmission distance of the whole system. However, the company Delsys© also offers the portable version called Trigno™ Mobile, allowing an extensive experimental distances.

Next the implemented system was experimentally evaluated in order to calculate the LRC ratio and to analyze the electrical activity of some respiratory muscles (*M. intercostalis externus*, *M. serratus anterior*, *M. abdominis obliquus externus* and *diaphragm*) and their direct relation to the locomotion. The experiments took place in the closed sports center of the Technische Universität Ilmenau. 15 healthy (12 men and 3 women) participated in the experiment (23-35 years, median 28 years). Each participant performed 12 sprint tests, running with the fastest constant speed that could be reached along 30 m in a straight line. After the data analysis, we could confirm what other researchers previously affirmed, that LRC ratio in humans is flexible and varies in the range of 2:1, 3:1, 4:1. The obtained values of LDV in some cases reached almost the maximum vital capacity of the subject. On the other hand, the analysis of EMG signals showed a phased lock with breathing. In addition, the magnitude of the signal increased when the subject was in motion as the respiration contraction became stronger during respiration. However, as the biological analysis was out of scope of this work, the results achieved should be further analyzed by specialists in this area.

Finally, we presented the discussion about our results, error and technical implementation of our system. In this discussion we concluded that the developed system is suitable for the analysis of LRC in humans. Also, we confirmed the possibility to adapt this system to study the LRC in different type of mammals including previous study of physiology and anatomy of the species.

6.2 Outlook

Besides possible technical improvements of the system, the presented research in this thesis has opened a number of research lines that should be explored in the future. This work was developed as an alternative system to allow the LRC study of animals during outdoor locomotion. Quadrupedal mammal of medium or large body size, as with dogs or horses, should be considered for future experiments in order to confirm the system viability in areas such as veterinary medicine or zoology. To develop these experiments, the IPM calibration method must be improved to guarantee an accurate data acquisition. Also, the RFM should be adapted to the animal facial anatomy, as well as selecting the flow sensor according the volumetric capacity of the animals lungs.

Considering complementary studies to our research, the field of system identification is based on statistical methods to build mathematical model of LRC of the species under study like dogs or horses. For instance, computational methods such as neural networks can be used to predict certain physiological phenomena under certain conditions. LRC is a complex system with multiple variables and conditions; an artificial neural network is a technique that mimics the operation of the human brain (nerves and neurons). These networks are programmed to "learn" by sifting data repeatedly, looking for relationships method to build mathematical models.

Another complementary study is the development of the LRC biomechanic model of quadruped mammals, considering the four exercises-associated forces or mechanical impacts (lumbar flexion, viscera piston, ventilatory muscles and rib cage loading by the forelimbs) explained in Chapter 2. The saved data from the experiments could be used as input values to check the accuracy of the developed model.

Finally, the possibility is attractive to develop studies with the integration of other modules to our system in order to extend the LRC study, such as heart rate measurement during locomotion or an advanced running gait analysis based on motion tracking system.

Bibliography

[1] Ainsworth, D. M., Smith, C. A., Henderson, K. S., and Dempsey, J. A. (1996). Breathing during exercise in dogs–passive or active? *Journal of Applied Physiology*, 81(2):586–595.

[2] Alexander, R. (1989). On the synchronization of breathing with running in wallabies (macropus spp.) and horses (equus caballus). *Journal of Zoology*, 218(1):69–85.

[3] Aliverti, A. (2016). The respiratory muscles during exercise. *Breathe*, 12(2):165–168.

[4] Anders, C., Wagner, H., Puta, C., Grassme, R., Petrovitch, A., and Scholle, H.-C. (2007). Trunk muscle activation patterns during walking at different speeds. *Journal of Electromyography and Kinesiology*, 17(2):245–252.

[5] Banzett, R. B., Mead, J., Reid, M. B., and Topulos, G. P. (1992). Locomotion in men has no appreciable mechanical effect on breathing. *Journal of Applied Physiology*, 72(5):1922–1926.

[6] Barnes, K. and Kilding, A. (2015). Running economy: measurement, norms, and determining factors. *Sport Medicine*, 10(2):1186.

[7] Barrow, A. and Pandit, J. J. (2014). Lung ventilation and the physiology of breathing. *Surgery (Oxford)*, 32(5):221–227.

[8] Bates, J. H. T. (2009). *Lung Mechanics: An Inverse Modeling Approach*. Cambridge University Press.

[9] Baudinette, R. (1991). The energetics and cardiorespiratory correlates of mammalian terrestrial locomotion. *Journal of Experimental Biology*, 160(1):209–231.

[10] Bazaka, K. and Jacob, M. V. (2012). Implantable devices: issues and challenges. *Electronics*, 2(1):1–34.

[11] Bernasconi, P. and Kohl, J. (1993). Analysis of co-ordination between breathing and exercise rhythms in man. *The Journal of physiology*, 471:693.

[12] Bhunia, S., Majerus, S., and Sawan, M. (2015). *Implantable Biomedical Microsystems: Design Principles and Applications*. Elsevier.

[13] Birlenbach, U., Banzett, R., Loring, S., and Carrier, D. (1994). A modest fraction of tidal volume is step-related in trotting dogs. *Physiologist*, 37:51.

[14] Bock, D. C., Marschilok, A. C., Takeuchi, K. J., and Takeuchi, E. S. (2012). Batteries used to power implantable biomedical devices. *Electrochimica acta*, 84:155–164.

[15] Boggs, D., Seveyka, J., Kilgore, D., and Dial, K. (1997). Coordination of respiratory cycles with wingbeat cycles in the black-billed magpie (pica pica). *Journal of Experimental Biology*, 200(9):1413–1420.

[16] Boggs, D. F. (1997). Coordinated control of respiratory pattern during locomotion in birds. *American Zoologist*, 37(1):41–53.

[17] Boggs, D. F. (2002). Interactions between locomotion and ventilation in tetrapods. *Comparative Biochemistry and Physiology Part A: Molecular & Integrative Physiology*, 133(2):269–288.

[18] Boggs, D. F., Butler, P. J., and Wallace, S. E. (1998). Differential air sac pressures in diving tufted ducks aythya fuligula. *Journal of experimental biology*, 201(18):2665–2668.

[19] Boutaayamou, M., Schwartz, C., Stamatakis, J., Denoël, V., Maquet, D., Forthomme, B., Croisier, J.-L., Macq, B., Verly, J. G., Garraux, G., et al. (2015). Development and validation of an accelerometer-based method for quantifying gait events. *Medical engineering & physics*, 37(2):226–232.

[20] Bramble, D. M. (1989). Axial-appendicular dynamics and the integration of breathing and gait in mammal. *American Zoologist*, 29(1):171–186.

[21] Bramble, D. M. and Carrier, D. R. (1983). Running and breathing in mammals. *Science*, 219(4582):251–256.

[22] Bramble, D. M. and Jenkins Jr, F. A. (1993). Mammalian locomotor-respiratory integration: implications for diaphragmatic and pulmonary design. *Science*, 262(5131):235–240.

[23] Carrier, D. (1990). Activity of the hypaxial muscles during walking in the lizard iguana iguana. *Journal of Experimental Biology*, 152(1):453–470.

[24] Carrier, D. R. (1987). The evolution of locomotor stamina in tetrapods: circumventing a mechanical constraint. *Paleobiology*, 13(3):326–341.

[25] Carrier, D. R. (1991). Conflict in the hypaxial musculo-skeletal system: documenting an evolutionary constraint. *American Zoologist*, pages 644–654.

[26] Carrier, D. R. (1996). Function of the intercostal muscles in trotting dogs: ventilation or locomotion? *The Journal of experimental biology*, 199(7):1455–1465.

[27] Chiang, C.-C., Lin, C.-C. K., and Ju, M.-S. (2007). An implantable capacitive pressure sensor for biomedical applications. *Sensors and Actuators A: physical*, 134(2):382–388.

[28] Chow, E. Y., Morris, M. M., and Irazoqui, P. P. (2013). Implantable rf medical devices: The benefits of high-speed communication and much greater communication distances in biomedical applications. *IEEE Microwave Magazine*, 14(4):64–73.

[29] Chowdhury, R. H., Reaz, M. B., Ali, M. A. B. M., Bakar, A. A., Chellappan, K., and Chang, T. G. (2013). Surface electromyography signal processing and classification techniques. *Sensors*, 13(9):12431–12466.

[30] Cotes, J. E., Chinn, D. J., and Miller, M. R. (2009). *Lung Volumes*, pages 111–117. Blackwell Publishing Ltd.

[31] Crawford, E. C. (1962). Mechanical aspects of panting in dogs. *Journal of applied physiology*, 17(2):249–251.

[32] Daffertshofer, A., Huys, R., and Beek, P. J. (2004). Dynamical coupling between locomotion and respiration. *Biological cybernetics*, 90(3):157–164.

[33] Daley, M. A., Bramble, D. M., and Carrier, D. R. (2013). Impact loading and locomotor-respiratory coordination significantly influence breathing dynamics in running humans. *PloS one*, 8(8):e70752.

[34] De Luca, C. J., Adam, A., Wotiz, R., Gilmore, L. D., and Nawab, S. H. (2006). Decomposition of surface emg signals. *Journal of neurophysiology*, 96(3):1646–1657.

[35] De Troyer, A., Kirkwood, P. A., and Wilson, T. A. (2005). Respiratory action of the intercostal muscles. *Physiological Reviews*, 85(2):717–756.

[36] Deban, S. M. and Carrier, D. R. (2002). Hypaxial muscle activity during running and breathing in dogs. *Journal of Experimental Biology*, 205(13):1953–1967.

[37] Delsys, Inc (2014). Trigno™ wireless system user's guide. "Rev. MAN-012-2-7". Delsys Incorporated.

[38] Duncker, H.-R. (2004). Vertebrate lungs: structure, topography and mechanics: A comparative perspective of the progressive integration of respiratory system, locomotor apparatus and ontogenetic development. *Respiratory physiology & neurobiology*, 144(2):111–124.

[39] Ebert, D., Raßler, B., and Hefter, H. (2000). Coordination between breathing and forearm movements during sinusoidal tracking. *European Journal of Applied Physiology*, 81(4):288–296.

[40] Fang, Q. (2010). Body emf absorption: a design issue for implantable medical electronics. *International Journal of Bioelectromagnetism*, 12(1):7–11.

[41] Federal Communications Commission (2012). Medical device radiocommunications service (MedRadio).

[42] Fernandes, C. R. (2006). Importance of pleural pressure for the evaluation of respiratory mechanics. *Revista brasileira de anestesiologia*, 56(3):287–303.

[43] Frevert, C., Nations, C., Seeherman, H., Loring, S., and Banzett, R. (1990). Airflow associated with stride in the horse. *Physiologist*, 33:A83.

[44] Funk, G. D., Valenzuela, I. J., and Milsom, W. K. (1997). Energetic consequences of coordinating wingbeat and respiratory rhythms in birds. *Journal of Experimental Biology*, 200(5):915–920.

[45] Gilleo, K., ET-Trends, L., and Warwick, R. (2005). Mems in medicine. *Circuits Assembly*, 16(8):32.

[46] Godfrey, A., Del Din, S., Barry, G., Mathers, J., and Rochester, L. (2015). Instrumenting gait with an accelerometer: A system and algorithm examination. *Medical engineering & physics*, 37(4):400–407.

[47] Grayson, A. R., Shawgo, R. S., Johnson, A. M., Flynn, N. T., Li, Y., Cima, M. J., and Langer, R. (2004). A biomems review: Mems technology for physiologically integrated devices. *Proceedings of the IEEE*, 92(1):6–21.

[48] Hawkes, E. Z., Nowicky, A. V., and McConnell, A. K. (2007). Diaphragm and intercostal surface emg and muscle performance after acute inspiratory muscle loading. *Respiratory physiology & neurobiology*, 155(3):213–219.

[49] Hedenstierna, G. (2012). Esophageal pressure: benefit and limitations. *Minerva anestesiologica*, 78(8):959–966.

[50] Henrik Casimir Ahn, Baz Delshad, J. B. (2016). An implantable pressure sensor for long-term wireless monitoring of cardiac function -first study in man. *Journal of Cardiovascular Diseases & Diagnosis*, 4(4):252.

[51] HEPPER, N., FOWLER, W., and HELMHOLZ, H. (1960). Relationship of height to lung volume in healthy men. *Diseases of the chest*, 37:314—320.

[52] Higgs, B., Behrakis, P., Bevan, D., and Milic-Emili, J. (1983). Measurement of pleural pressure with esophageal balloon in anesthetized humans. *Anesthesiology*, 59(4):340–343.

[53] Hodges, P. W. and Gandevia, S. C. (2000). Changes in intra-abdominal pressure during postural and respiratory activation of the human diaphragm. *Journal of applied Physiology*, 89(3):967–976.

[54] ICNIRP (2009). Guidelines for limiting exposure to time-varying electric, magnetic, and electromagnetic fields (up to 300 ghz). *Health physics*, 97(3):257–258.

[55] IEEE (2006). Standard for safety levels with respect to human exposure to radio frequency electromagnetic fields, 3 khz to 300 ghz. *IEEE Std C95.1-2005 (Revision of IEEE Std C95.1-1991)*, pages 1–238.

[56] Islam, M. N. and Yuce, M. R. (2016). Review of medical implant communication system (mics) band and network. *ICT Express*, 2(4):188–194.

[57] Itoh, Y., Miyamoto, M., Hojo, T., Hirasawa, Y., and Kubota, T. (2008). Convenient use of accelerometer for gait analysis. *Bull Osaka Med Coll*, 54:21–31.

[58] ITU (2014). ITU-T K.52: Guidelines on complying with limits for humans exposure to electromagnetic field. International Telecomunication Union.

[59] Johnson, P. J., Rosenbluth, E. M., Nygaard, I. E., Parikh, M. K., and Hitchcock, R. W. (2009). Development of a novel intra-vaginal transducer with improved dynamic response. *Biomedical microdevices*, 11(6):1213–1221.

[60] Kim, S. H., Moon, J.-H., Kim, J. H., Jeong, S. M., and Lee, S.-H. (2011). Flexible, stretchable and implantable pdms encapsulated cable for implantable medical device. *Biomedical Engineering Letters*, 1(3):199–203.

[61] Kiourti, A. and Nikita, K. S. (2012a). Recent advances in implantable antennas for medical telemetry [education column]. *IEEE Antennas and Propagation Magazine*, 54(6):190–199.

[62] Kiourti, A. and Nikita, K. S. (2012b). A review of implantable patch antennas for biomedical telemetry: Challenges and solutions [wireless corner]. *IEEE Antennas and Propagation Magazine*, 54(3):210–228.

[63] Kirsten, S., Schubert, M., Braunschweig, M., Woldt, G., Voitsekhivska, T., and Wolter, K.-J. (2014). Biocompatible packaging for implantable miniaturized pressure sensor device used for stent grafts: Concept and choice of materials. In *Electronics Packaging Technology Conference (EPTC), 2014 IEEE 16th*, pages 719–724. IEEE.

[64] Kohl, J., Koller, E., and Jäger, M. (1981). Relation between pedalling-and breathing rhythm. *European journal of applied physiology and occupational physiology*, 47(3):223–237.

[65] Lafortuna, C. L., Reinach, E., and Saibene, F. (1996). The effects of locomotor-respiratory coupling on the pattern of breathing in horses. *The Journal of physiology*, 492(Pt 2):587.

[66] Lee, H. and Banzett, R. B. (1997). Mechanical links between locomotion and breathing: can you breathe with your legs? *Physiology*, 12(6):273–278.

[67] Lin, C. C., Jea, D., Dabiri, F., Massey, T., Tan, R., Sarrafzadeh, M., Srivastava, M., Schulam, P., Schmidt, J., and Montemagno, C. (2007). The development of an in-vivo active pressure monitoring system. In *4th International Workshop on Wearable and Implantable Body Sensor Networks (BSN 2007)*, pages 105–110. Springer.

[68] Mead, J. (1960). Control of respiratory frequency. *Journal of Applied Physiology*, 15(3):325–336.

[69] Mead, J. and Gaensler, E. (1959). Esophageal and pleural pressures in man, upright and supine. *Journal of Applied Physiology*, 14(1):81–83.

[70] Merletti, R. and De Luca, C. (1989). New techniques in surface electromyography. *Computer aided electromyography and expert systems*, 2:115–124.

[71] Milic-Emili, J., Mead, J., Turner, J., and Glauser, E. (1964). Improved technique for estimating pleural pressure from esophageal balloons. *Journal of Applied Physiology*, 19(2):207–211.

[72] Nassar, P. N., Jackson, A. C., and Carrier, D. R. (2001). Entraining the natural frequencies of running and breathing in guinea fowl (numida meleagris). *Journal of Experimental Biology*, 204(9):1641–1651.

[73] NXP (2014). UM10204, I2C-bus specification and user manual. "Rev. 6", NXP Semiconductors.

[74] O'Halloran, J., Hamill, J., McDermott, W. J., Remelius, J. G., and Van Emmerik, R. E. (2012). Locomotor-respiratory coupling patterns and oxygen consumption during walking above and below preferred stride frequency. *European journal of applied physiology*, 112(3):929–940.

[75] Patterson, M. R. and Caulfield, B. (2013). Using a foot mounted accelerometer to detect changes in gait patterns. In *Engineering in Medicine and Biology Society (EMBC), 2013 35th Annual International Conference of the IEEE*, pages 7471–7475. IEEE.

[76] Persegol, L., Jordan, M., and Viala, D. (1990). Evidence for the entrainment of breathing by locomotor pattern in human. *Journal de physiologie*, 85(1):38–43.

[77] Purcell, B., Channells, J., James, D., and Barrett, R. (2005). Use of accelerometers for detecting foot-ground contact time during running. In *Proc. SPIE*, volume 6036, pages 292–299.

[78] Qin, Y., Howlader, M. M., Deen, M. J., Haddara, Y. M., and Selvaganapathy, P. R. (2014). Polymer integration for packaging of implantable sensors. *Sensors and Actuators B: Chemical*, 202:758–778.

[79] Raßler, B., Ebert, D., Waurick, S., and Junghans, R. (1996). Coordination between breathing and finger tracking in man. *Journal of motor behavior*, 28(1):48–57.

[80] Raßler, B. and Kohl, J. (1996). Analysis of coordination between breathing and walking rhythms in humans. *Respiration physiology*, 106(3):317–327.

[81] Reaz, M. B., Hussain, M., and Mohd-Yasin, F. (2006). Techniques of emg signal analysis: detection, processing, classification and applications. *Biological procedures online*, 8(1):11–35.

[82] Saladin, K. S. and Miller, L. (2015). *Anatomy & physiology: the unity of form and function*. WCB/McGraw-Hill New York (NY).

[83] Sensirion (2016). Low pressure drop digital flow meter - SFM3000. "Rev. 2.2". Sensirion- The Sensor Company.

[84] Simons, R. S. (1999). Running, breathing and visceral motion in the domestic rabbit (oryctolagus cuniculus): testing visceral displacement hypotheses. *The Journal of experimental biology*, 202(5):563–577.

[85] Tan, R., McClure, T., Lin, C., Jea, D., Dabiri, F., Massey, T., Sarrafzadeh, M., Srivastava, M., Montemagno, C., Schulam, P., et al. (2009). Development of a fully implantable wireless pressure monitoring system. *Biomedical microdevices*, 11(1):259–264.

[86] Technology, I. D. (2016). ZSC31014 - RBic$_{ilite}$™ digital output sensor signal conditioner. "Rev. 1.65". Integrated Device Technology.

[87] Teo, A. J., Mishra, A., Park, I., Kim, Y.-J., Park, W.-T., and Yoon, Y.-J. (2016). Polymeric biomaterials for medical implants and devices. *ACS Biomaterials Science & Engineering*, 2(4):454–472.

[88] Valdastri, P., Menciassi, A., Arena, A., Caccamo, C., and Dario, P. (2004). An implantable telemetry platform system for in vivo monitoring of physiological parameters. *IEEE Transactions on Information Technology in Biomedicine*, 8(3):271–278.

[89] World Health Organization (2002). *Establishing a dialogue on risks from electromagnetic fields*. Radiation and Environmental Health, Dept. of Protection of the Human Environment, World Health Organization Geneva.

[90] Xu, L., Meng, M. Q.-H., Ren, H., and Chan, Y. (2009). Radiation characteristics of ingestible wireless devices in human intestine following radio frequency exposure at 430, 800, 1200, and 2400 mhz. *IEEE Transactions on Antennas and Propagation*, 57(8):2418–2428.

[91] Young, I. S., Alexander, R., Woakes, A., Butler, P., and Anderson, L. (1992). The synchronization of ventilation and locomotion in horses (equus caballus). *Journal of Experimental Biology*, 166(1):19–31.

[92] Zsoldos, R., Kotschwar, A., Kotschwar, A., Rodriguez, C., Peham, C., and Licka, T. (2010). Activity of the equine rectus abdominis and oblique external abdominal muscles measured by surface emg during walk and trot on the treadmill. *Equine Veterinary Journal*, 42(s38):523–529.

Acknowledgements

Firstly, I would like to express my sincere gratitude to my advisor Prof. Hartmut Witte for the continuous support of my Ph.D study and related research, for his patience, motivation, and immense knowledge. His guidance helped me all the time during the last years of research and writing of this thesis. I could not have imagined having a better advisor and mentor for my Ph.D study.

The members of the "Biomechatronik" group have contributed immensely to my personal and professional time at Ilmenau. The group has been a source of friendships as well as good advice and collaboration. I am especially grateful to Mrs. Kerstin Schmidt for her invaluable friendship and advice as well as her selfless patience and help. A very special gratitude goes to José Luis Zárate Moya for his friendship and collaboration.

And most of all I would like to acknowledge my loving, supportive, encouraging, and patient wife Alina who faithfully supported me during the final stages of this Ph.D, and her constant encouragement throughout my research period is so much appreciated.

I gratefully acknowledge the funding sources that made my Ph.D. work possible. I was funded by the Peruvian organization INNÓVATE PERU (ex FINCYT) during my first three years of my Ph.D studies. My work in the end of this research was also supported by the Thuringian Graduate Funding (ThürGFVO).

Finally I would like to highlight my home land Peru, where the most basic source of my life energy resides: my family, for all their love and encouragement. And my parents who raised a love for science in me and supported me in all my pursuits.

Appendix A

Characteristics of Implantable Pressure Module

A.1 Electronics Circuits Schematic Diagram

The following sections show the electronic circuit of the IPM transmitter and receiver.

A.1.1 Pressure Transmitter

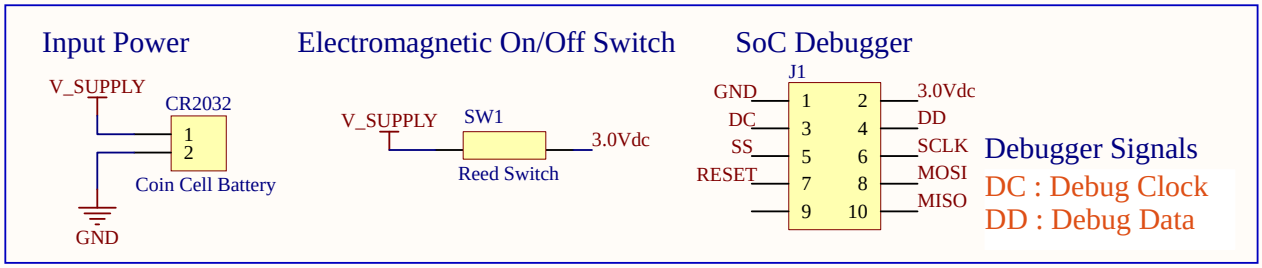

Fig. A.1 PTx electronic schematic : power circuit and SoC Debugger

1. The implantable transmitter uses a coin cell lithium battery of 3VDC as a power supply. The selected cell (CR2032) has a diameter = 20 mm has capacity of 240 mAh.

2. The reed switch is used to power on-off the device. When the device is exposed to a magnetic field, the two ferrous materials inside the switch pull together and the switch closes.

3. The device used as a debugger connector programs the SoC *in situ*. The main signals to download in the firmware in the chip are DC and DD. However, the SPI signals allow debugging the firmware with an external software called SmartRF^{TM} Studio developed by Texas Instrument.

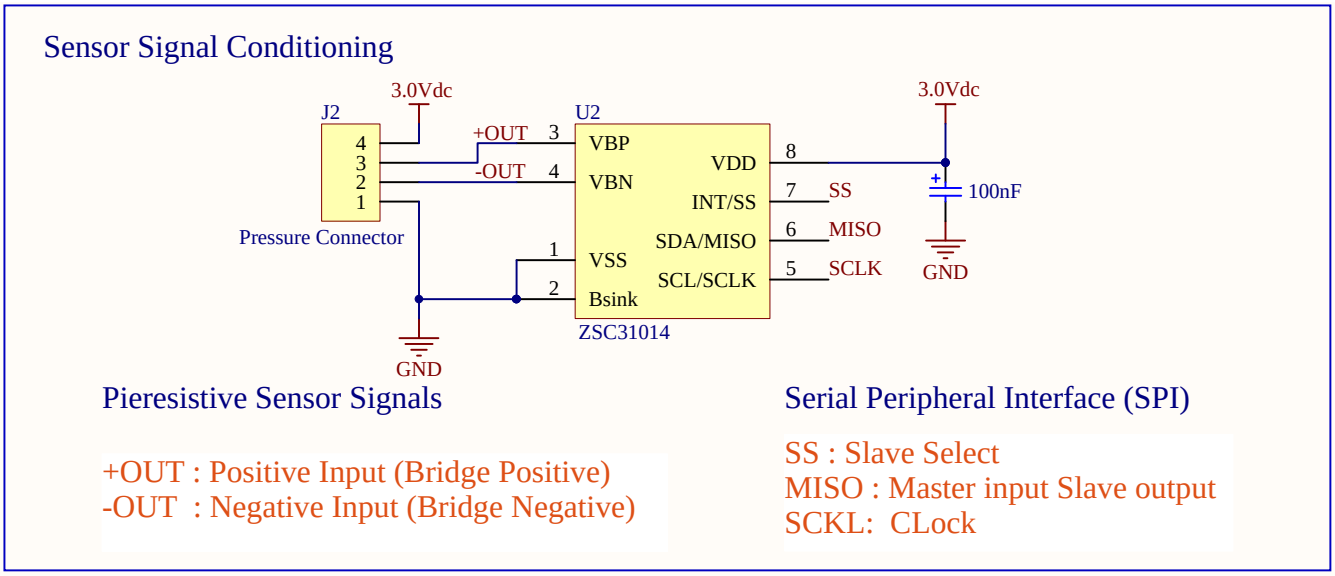

Fig. A.2 PTx circuit Schematic : Sensor Signal Conditioning

The sensor signal conditioner sends data via SPI bus. It receives the analog raw values from the piezoresistive sensor. The tension difference of the inputs $+Out$ and $-Out$ is amplified and digitalized. When the master (SoC) activates the signal SS, during each SPI clock (SCLK) cycle a data transmission occurs via MISO.

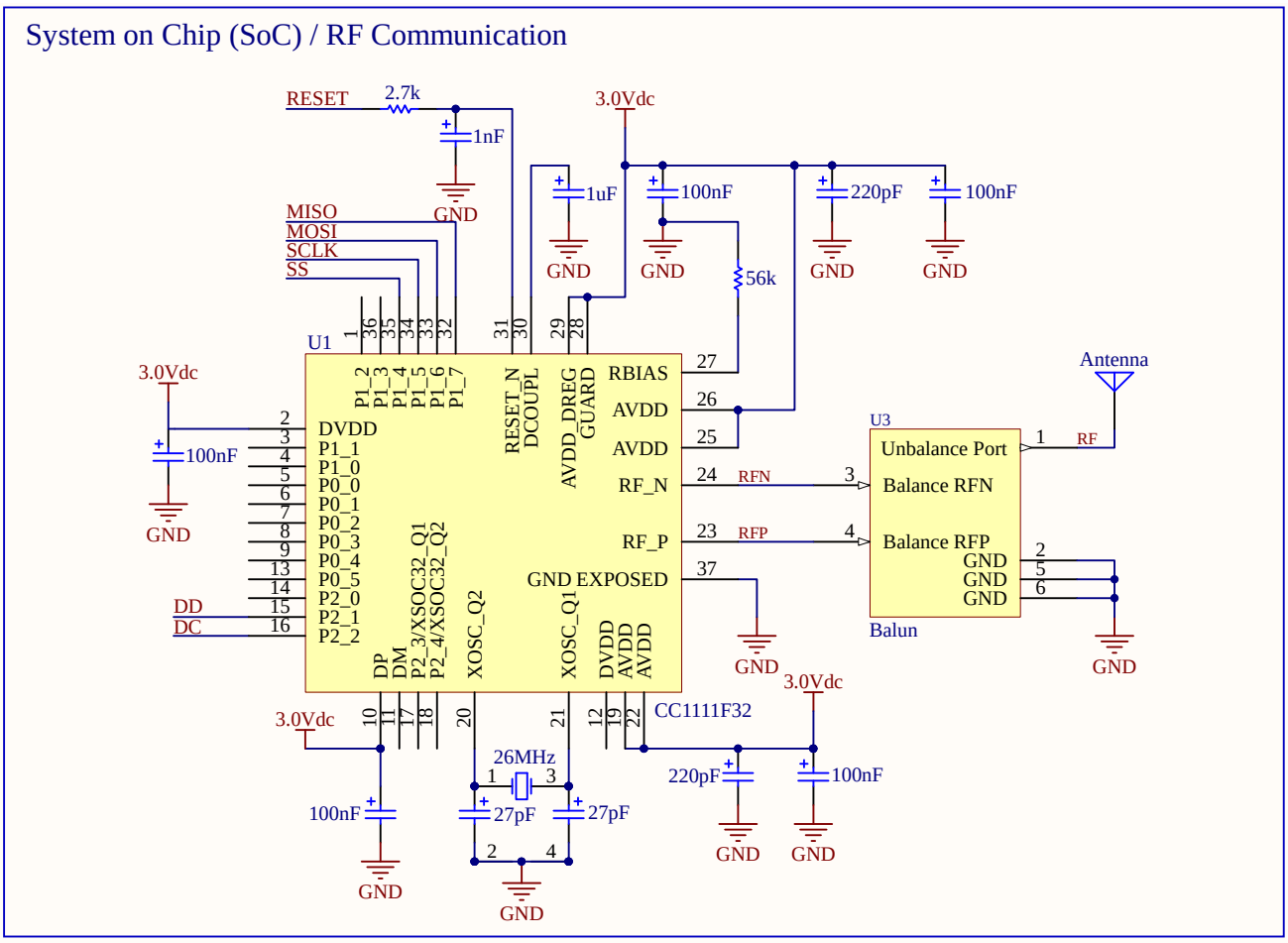

Fig. A.3 PTx circuit Schematic : SoC and RF Communication

1. The SoC uses a crystal oscillator of 26 MHz (NX3225GA). This provides a stable clock signal and stabilizes the operation frequency of the transmitter and receiver.

2. A Balun device is used to convert a balanced signal (two conductors RFN and RFP) to an unbalanced signal (a single signal working against ground). This impedance transformer converts differential to 50 Ω single-ended RF signal (antenna).

A.1.2 Pressure Receiver

The receiver electronic circuit is similar to the transmitter (Fig. A.4). However, some characteristics are different:

1. As the receiver is external, a normal power on/off switch is used.

2. The power supply used is a Li-Po (3.7 VDC) battery which allows more energy capacity (1000 mAh).

3. A Wi-Fi module is connected via UART bus. This device transmits data to the DCC.

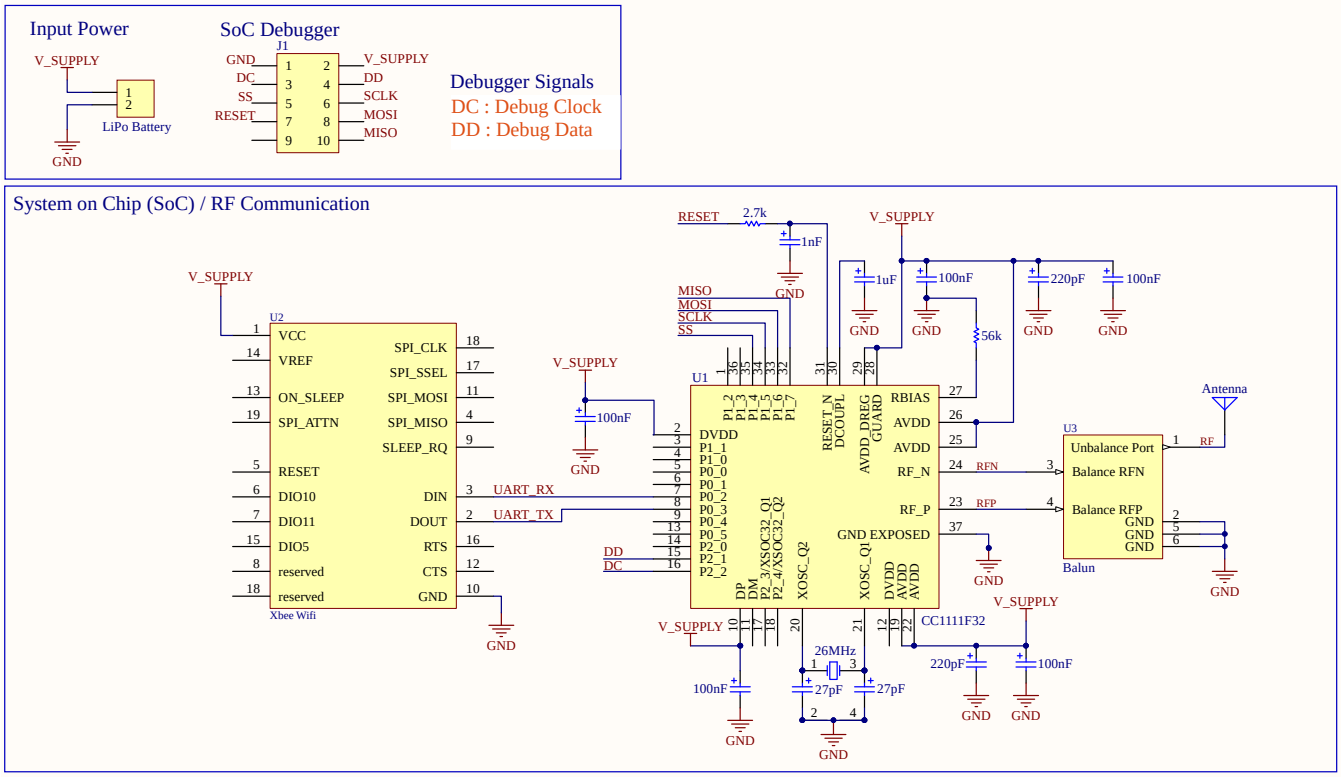

Fig. A.4 PRx circuit Schematic : SoC and Wireless Communication

A.2 Operation Algorithm

A.2.1 Receptor Firmware

The program algorithm (firmware) in the IPM receptor is shown in Fig. A.5.

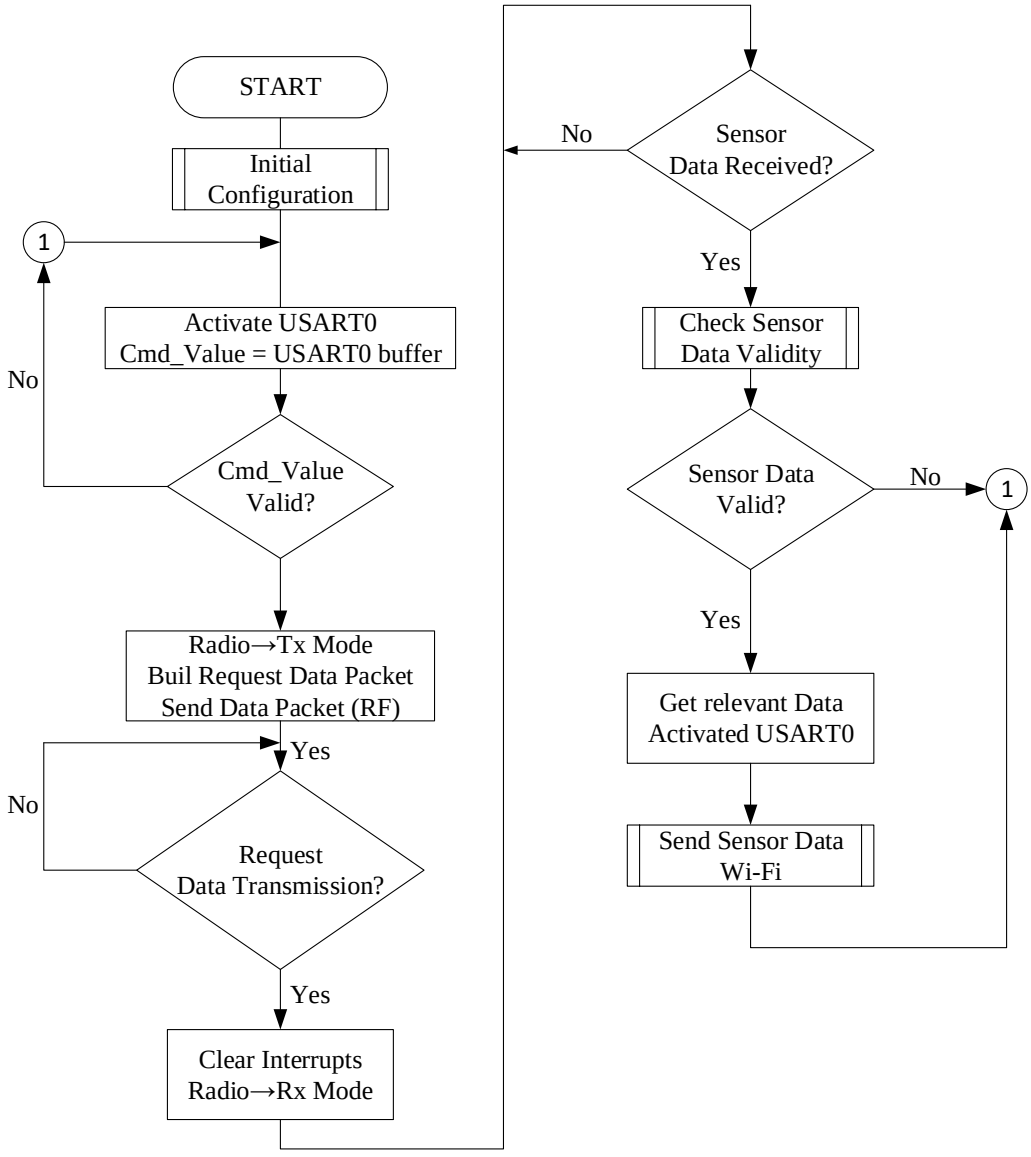

Fig. A.5 Receiver Operation Flowchart

The following steps explain the receptor operation algorithms, after the device is activated.

1. *Initial Configuration* functions: The PRx SoC sets the hardware setup.

Listing A.1 PRx Code - Hardware initilization

```
INIT_PORTS(); // initializes ports as input or output.
INIT_CLK(); //  sets the clock of operation.
INIT_USART0(); // sets communication protocol Wi-Fi.
RADIO_CONFIGURATION(); // set RF communication.
```

2. The DCC sends a request sensor data via Wi-Fi to the PRx. The Wi-Fi transceiver sends via UART0 a request command (*Cmd_Value* = 0x24) to the SoC.

3. If the Cmd_Value is not valid, the SoC still waits for the correct command.

4. If the Cmd_Value is valid, SoC changes to transmission mode (*Tx Mode*) to send a request command (Cmd_Value = 0x24) to the transmitter. The packet is built and sent.

Listing A.2 Prx Code - Data Frame construction

```
if (dato==0x24){
// 0x24 request command from the Wi-Fi Transceiver
mode = RADIO_MODE_TX;     // change to Transmission mode
radioPktBuffer[0] = PACKET_LENGTH;  // # of byte = 17
radioPktBuffer[1] = (BYTE) (NETWORK_ID_KEY>>8);
radioPktBuffer[2] = (BYTE) NETWORK_ID_KEY;// Identification
```

```
for (i = 3; i <= PACKET_LENGTH; i++) {
radioPktBuffer[i] = 0x24;} // request command to the PTx
RFST = STROBE_TX;              // Switch radio to TX
while(!pktSentFlag); // Wait until the packet is sent.
```

5. After the command is transmitted, the interruption flag are cleared for the next transmission. The SoC changes to reception mode, waiting for sensor data values.

Listing A.3 PRx Code - Prepare to receive data

```
pktSentFlag = FALSE; // clear interruption flag
// The Soc change to reception mode to wait for sensor values.
mode = RADIO_MODE_RX;  // Reception mode
RFST    = STROBE_RX;      // Switch radio to RX
```

6. The packet is received from the PTx. Then the PRx SoC verifies the validity of the packet.

7. If the packet is not valid, the SoC requests sensor data again. Otherwise it waits for an order from the Wi-Fi transceiver.

8. If the Data is valid, the SoC extracts the sensor values from the packet. Finally, the SoC sends data to Wi-Fi transceiver.

Listing A.4 PRx Code - Sensor data extraction from the frame and wireless transmission

```
for (i=0;i<=3;i++){
TxBufferSlave[i]=radioPktBuffer[i+3];} // The sensor data is
    extracted from the received packet.
send_usart0((uint16*)TxBufferSlave, lenght); // This function
    sends the data to the Wi-Fi tranceiver. Finally, it sends
    data to the DCC.
```

A.2.2 Transmitter Firmware

The program algorithm (firmware) in the PIM transmitter is shown in Fig. A.6.

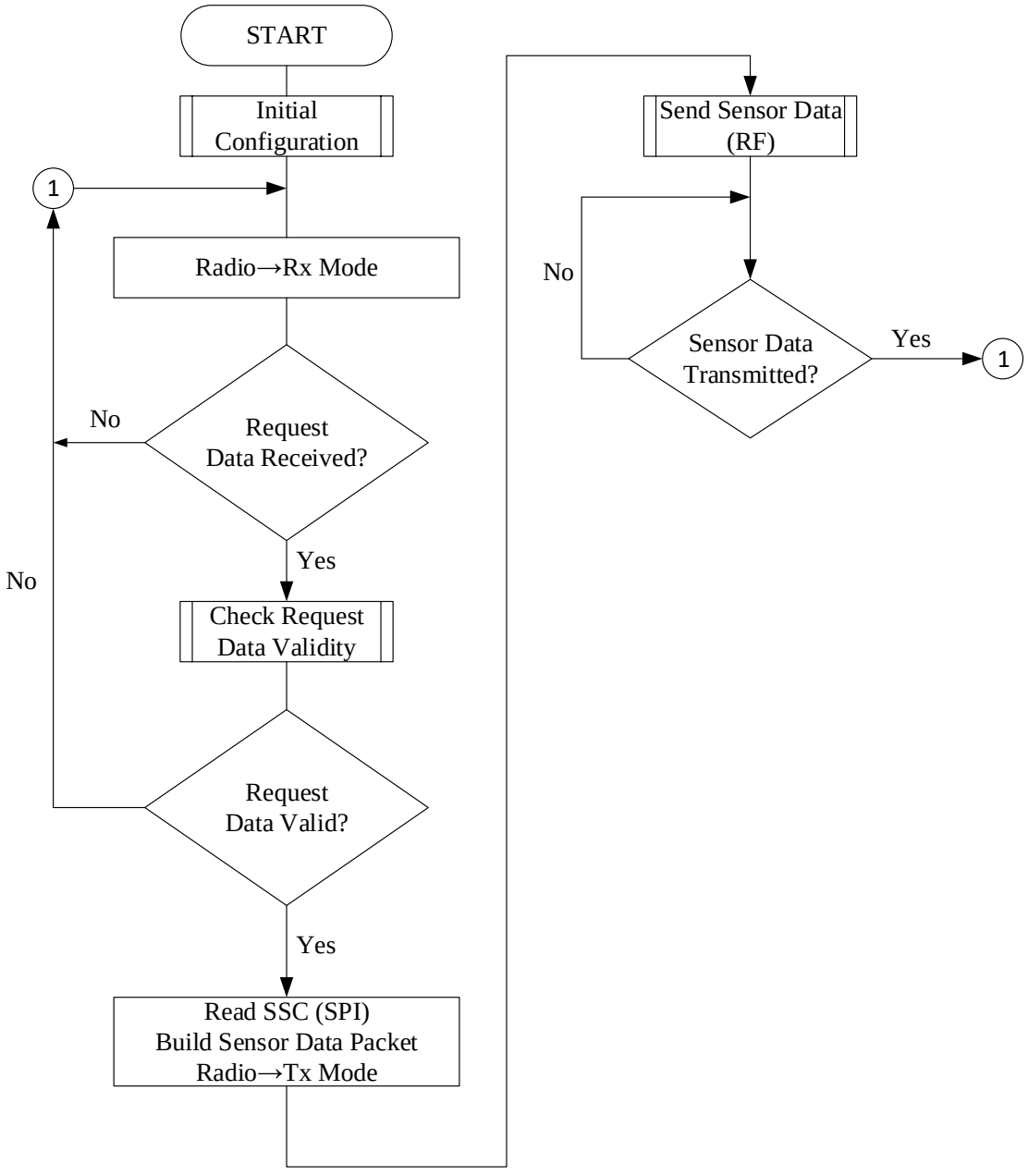

Fig. A.6 Transmitter Operation Flowchart

The following steps explain the transmitter operation algorithms, after the device is activated.

1. The hardware setup is almost the same of the PRx SoC. *Initial Configuration* function includes the SPI bus initialization.

2. The PTx SoC actives the reception mode. It waits to receive the request command from the PRx.

Listing A.5 PTx Code - Prepare to receive commands

```
mode = RADIO_MODE_RX; // Reception mode activated
RFST    = STROBE_RX;       // Switch radio to RX
while (!pktRcvdFlag); // complete packet is received?.
```

3. If the Cmd_Value is not valid, the SoC still waits for the correct command.

4. If the Cmd_Value is valid, the SoC reads via SPI the digital sensor value from the SSC. Furthermore, the SoC changes to transmission mode (*Tx Mode*) to built the packet which includes the sensor data.

Listing A.6 PTx Code - SoC read sensor data through SPI bus

```
for (int j=0 ;j <= N ; j++)
{

SSN = LOW; // Activate the input of SPI bus
while(!U1TX_BYTE); // is the byte transmitted ?
RxBufferSlave[j]=U1DBUF ; // save value byte in buffer

}

SSN=HIGH; // desactivar SPI input
RxBufferSlave[0x00]= RxBufferSlave[0x00]&0x3F; // From the SSC
    frame is extracted the Sensor values.
for (i = 0; i <= N; i++) {

radioPktBuffer[i+3] = RxBufferSlave[i]; // The sensor value is
    located in the RF transmission packet.
}
```

5. The PTx SoC sends the packets and wait until is complete transmitted.

Listing A.7 PTx Code - Data transmission

```
DMAARM |= DMAARM_CHANNEL0;   // Arm DMA channel 0
RFST = STROBE_TX;   // Switch radio to TX
while(!pktSentFlag); // Wait until the packets is sent.
```

Appendix B

Characteristics of Respiratory Flow Module

B.1 Electronics Circuits Schematic Diagram

Electrical characteristics of the transmitter are shown in Fig. B.1.

1. The complete system is powered by a Li-Po battery of 7.4 V DC (1000 mAh).
2. A step down voltage regulator of 5 V DC (AMS117-5.0) is used to supply the sensor and the WCC.
3. The sensor connector is a 4-pin 2 mm pitch. It is compatible with Molex DuraClik™ socket (502351-0400).
4. Two pull up resistors of 4.7 kΩ were used.
5. The resistor are connected between the signal (SDA and SCL) and a positive power supply voltage (3.3 V DC).
6. The power supply of 3.3 V DC are taken from the WCC (ESP32).

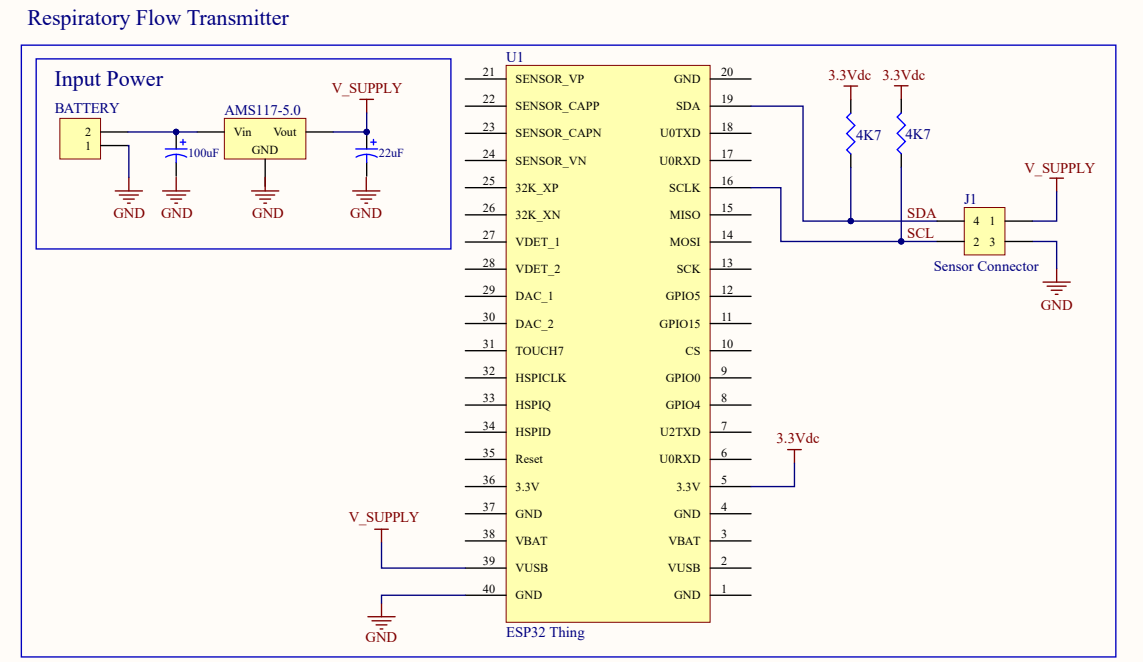

Fig. B.1 RFM Electronic Circuit Schematics: Transmitter

B.1.1 Pull-Up Resistor Calculation

The supply voltage limits the minimum value of resistor $R_{p(min)}$ due to the specified minimum sink current for Standard-mode and Fast-mode.

$$R_{p(min)} = \frac{V_{DD} - V_{OL(max)}}{I_{OL}} \quad , \quad [\Omega] \tag{B.1}$$

where V_{OL} is low level output voltage (0.4 V) at the device current sink (I_{OL}) and supply voltage of $V_{DD} > 2$ V.

The maximum pull up resistance is limited by the bus capacitance (C_b) due to I2C standard rise time specifications. The maximum pull up resistor is a function of the maximum rise time (t_r) and the estimated bus capacitance (C_b) [73]:

$$R_{p(max)} = \frac{t_r}{0.8473 \times C_b} \quad , \quad [\Omega] \tag{B.2}$$

The selected sensor works at operation frequency of 100 kHz (standard-mode). According to the electrical characteristic of the WCC and the sensor, the c_p=20 pF and t_r=1 μs. The calculated pull up resistor has to be in range of 966.7 Ω< Rp <57 kΩ. However, the sensor manufacturer recommends commercially available resistor values of 10 kΩ or 4.7 kΩ.

B.2 RFM Operation Algorithm

The selected Wireless Communication Controller (WCC) is the SparkFun ESP32 Thing. This device obtains the data from the sensor and transmits data wirelessly to the DCC. The following steps show the WCC functions: (i) Enable connection with the DCC through Wi-Fi protocol. (ii) Enable communication with the sensor through I2C protocol. (iii) Receive the external control command from the DCC to start/stop data acquisition.

SparkFun ESP32 Thing is based on Arduino software. The device firmware was programmed using the libraries *Wire* and *WiFi*. These manage the I2C and Wi-Fi protocol commands respectively. Besides, the WCC is connected to a private WLAN. The network setup variables used are shown in Table B.1.

RFM Network Characteristics	
Network_Name	Bio3150bmtk
Network_Password	123456789
Server Ip_Address*	192.168.137.1
HostPort	30000

* If the connection is realized through an access point or router, it has to be define a static Ip-Address for server.

Table B.1 Wireless Local Area Network (WLAN) setup variables.

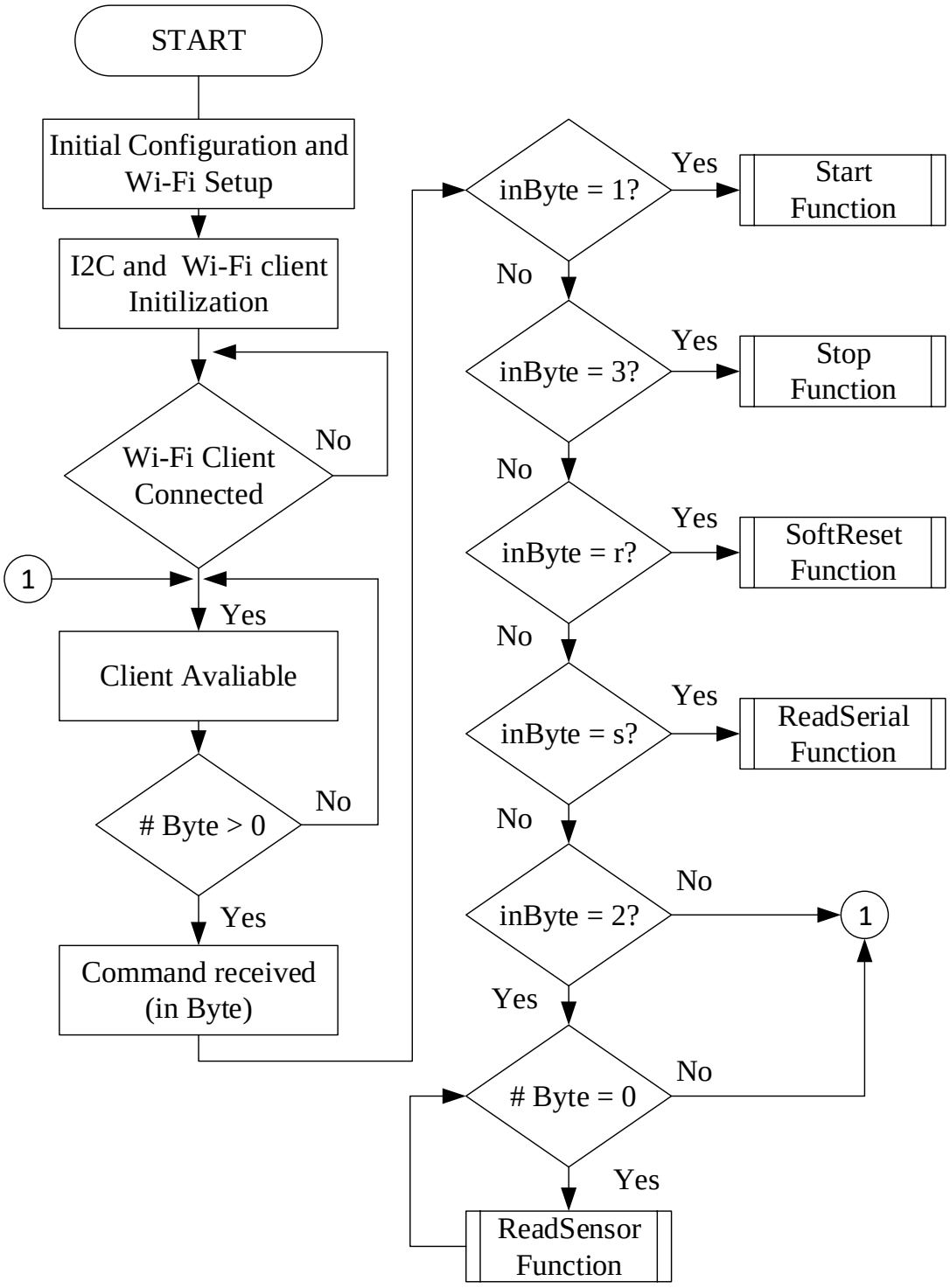

Fig. B.2 RFM Operation Flowchart

The following step explains the RF transmitter operation algorithms.

1. *Initial Configuration* functions: Libraries *Wire* and *WiFi* are included in the main program. Also, the network variables of Wi-Fi communication are set. These libraries belong to Arduino IDE.

Listing B.1 ESP32 code - Arduino IDE Libraries

```
#include <Wire.h>
#include <WiFi.h>
```

2. The program starts with the initialization of the I2C and the Wi-Fi client protocols.

Listing B.2 ESP32 code - I2C and Wi-Fi protocol initilization

```
Wire.begin(); // I2C bus initilization.
WiFi.begin(Network_Name, Network_Paasword);
```

3. Then, the WCC initializes connection with the WLAN. The DCC has to be connected with the same WLAN. Beside, the server it reads the hostport to start data transfer.

Listing B.3 ESP32 code - WLAN connection

```
if (!client.connected()) {
Serial.println("\nStarting␣connection␣to␣server...");
        if (client.connect(server, hostPort)) {
        Serial.println("connected␣to␣server");
        }
}
else
```

4. If the server is connected with the module, the WCC waits for any command from the server. The command is saved in the variable *inByte*. Depends on the command, the WCC executes one of the following functions: *Start*, *softReset*, *ReadSerial* and *readSensor*.

Listing B.4 ESP32 code - Command reception

```
if (client.available() > 0){
int inByte = client.read();
```

Listing B.5 ESP32 code - Operational functions

```
switch (inByte){

 case '1':
        Start();// Function "Start"
 break;

 case '2':
        while(client.available()){
         readSensor(); // read sensor data
         sprintf(tbs, "%04d", Flow);
         Serial.println(tbs);
                if (client.connected()){
                client.println(t);} // Send data
                   wirelessly
        }
 break;

 case 'r': // Function Reset WCC
        SoftReset();
 break;

 case 's': // Function read Serial
        ReadSerial();
 break;

 case '3':
        if (!client.connected()) {
         Serial.println();
         Serial.println("disconnecting.");
         client.stop();
        }
 break;
 default; break;
}
```

5. The received command execute these functions in the WCC:

   <Start> According to sensor data-sheet, the first measurement performed after sensor controller initialization is not valid. This function sends the command "1000" [HEX].

   <softReset> This function resets the WCC in case of the I2C communication between the master and sensor stops. This function sends the command "2000" [HEX].

   <ReadSerial> This function reads 32 bits corresponding to the serial number of the airflow sensor. This function sends the command "31AE" [HEX].

   <readSensor> This function reads 2 Bytes corresponding to the flow sensor. In order to obtain the final flow value in slm, the Eq. 3.6 is applied. The formatting operator string %04d is using to convert data to string. According to the acquired measurement, values need maximum 3 Bytes for each digit. However, if it is a negative value, one more Byte is needed. To avoid the change size in the package when the values are positive, the formatting operator adds a "0". Finally, the DCC received and process the data packets.

Listing B.6 ESP32 code - Reading Formatting and Sending Data.

```
# Declaration of variables
int Flow=0;
int ScaleFactorFlow= 140;
int OffsetFlow=32000;
char tbs[16];
int reading = 0;
...
# Resquest data from the sensor
while(Wire.available()){
 if (2 <= Wire.available()) { // two bytes received
 reading = Wire.read(); //
 reading = reading << 8;// shift 8 bits to the right
 reading |= Wire.read();// Compound reading
 Flow = (reading - OffsetFlow)/ScaleFactorFlow;
}
...
# Send packets
sprintf(tbs, "%04d", Flow);
Serial.println(tbs);
```

Listing B.7 Matlab code – Reading packets from ESP32.

```
# Function MultiplexedFlowData
bytesReady1 = S.obj.BytesAvailable;
bytesReady = bytesReady1 - mod(bytesReady1, 6); // 6
    bytes per value
data_byte = fread(S.obj,bytesReady);
data = sscanf(char(data_byte),'%04d');
```

B.3 Volume Flow Module Prototypes

The final experimental test was performed with the second transmitter holder designed, and its CAD drawings are shown in the next section. However, another transmitter holder was tested. Fig.B.3 shows a first prototype implemented and tested in free-running mode. This model is similar to a commercial gas mask filter. The device has the following characteristics: diameter = 20 cm, length = 9 cm and weight ≈ 280 gr. This prototype reaches a range over 60 m with continuous data transfer. However, during the outdoor test a slight swing was observed. The main reason is due to the fact that the center of mass is located in front of the mask.

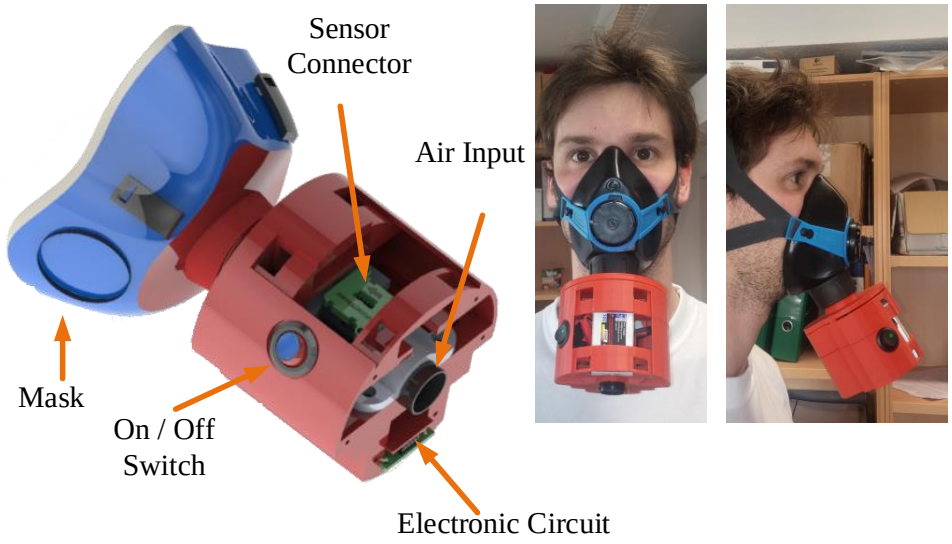

Fig. B.3 Design description and implementation - First prototype of the respiratory flow transmitter.

B.4 Volume Flow Module Drawings

The followings drawings are the result of the semester work project (2017-1) by Marc Bourillon.

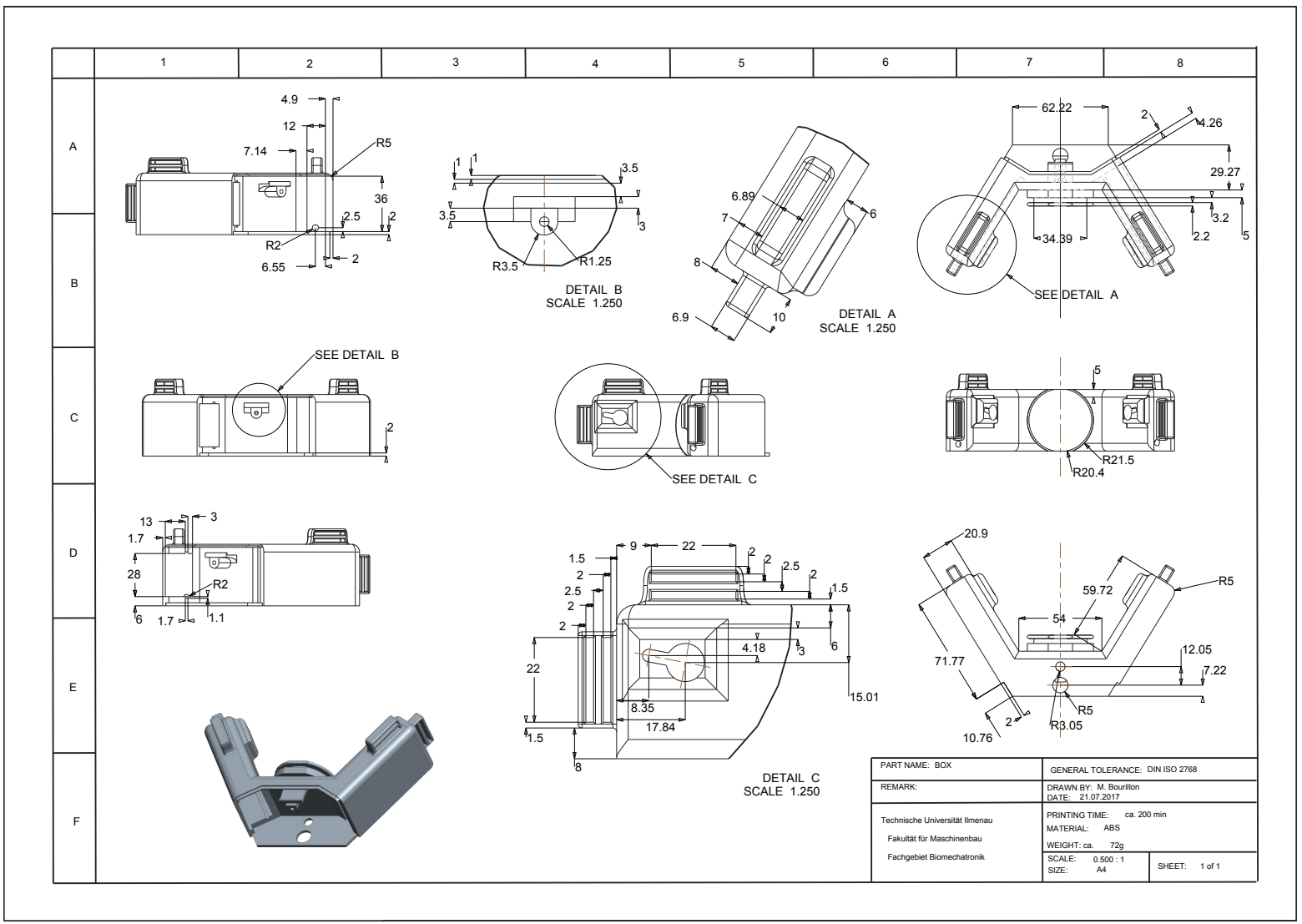
1
2
3
4
5
6
7
8
A
B
C
D
E
F
4.9
12
7.14
R5
36
2.5
2
R2
6.55
2
1
1
3.5
3.5
3
R3.5
R1.25
DETAIL B
SCALE 1.250
6.89
7
6
8
6.9
10
DETAIL A
SCALE 1.250
62.22
2
4.26
29.27
3.2
34.39
2.2
5
SEE DETAIL A
SEE DETAIL B
2
SEE DETAIL C
5
R21.5
R20.4
13
3
1.7
28
R2
6
1.7
1.1
9
22
2
2
2.5
2
1.5
1.5
2
2.5
2
2
4.18
3
6
22
15.01
8.35
17.84
1.5
8
DETAIL C
SCALE 1.250
20.9
R5
59.72
54
12.05
71.77
7.22
R5
2
R3.05
10.76
PART NAME: BOX
GENERAL TOLERANCE: DIN ISO 2768
REMARK:
DRAWN BY: M. Bourillon
DATE: 21.07.2017
Technische Universität Ilmenau
Fakultät für Maschinenbau
Fachgebiet Biomechatronik
PRINTING TIME: ca. 200 min
MATERIAL: ABS
WEIGHT: ca. 72g
SCALE: 0.500 : 1
SIZE: A4
SHEET: 1 of 1

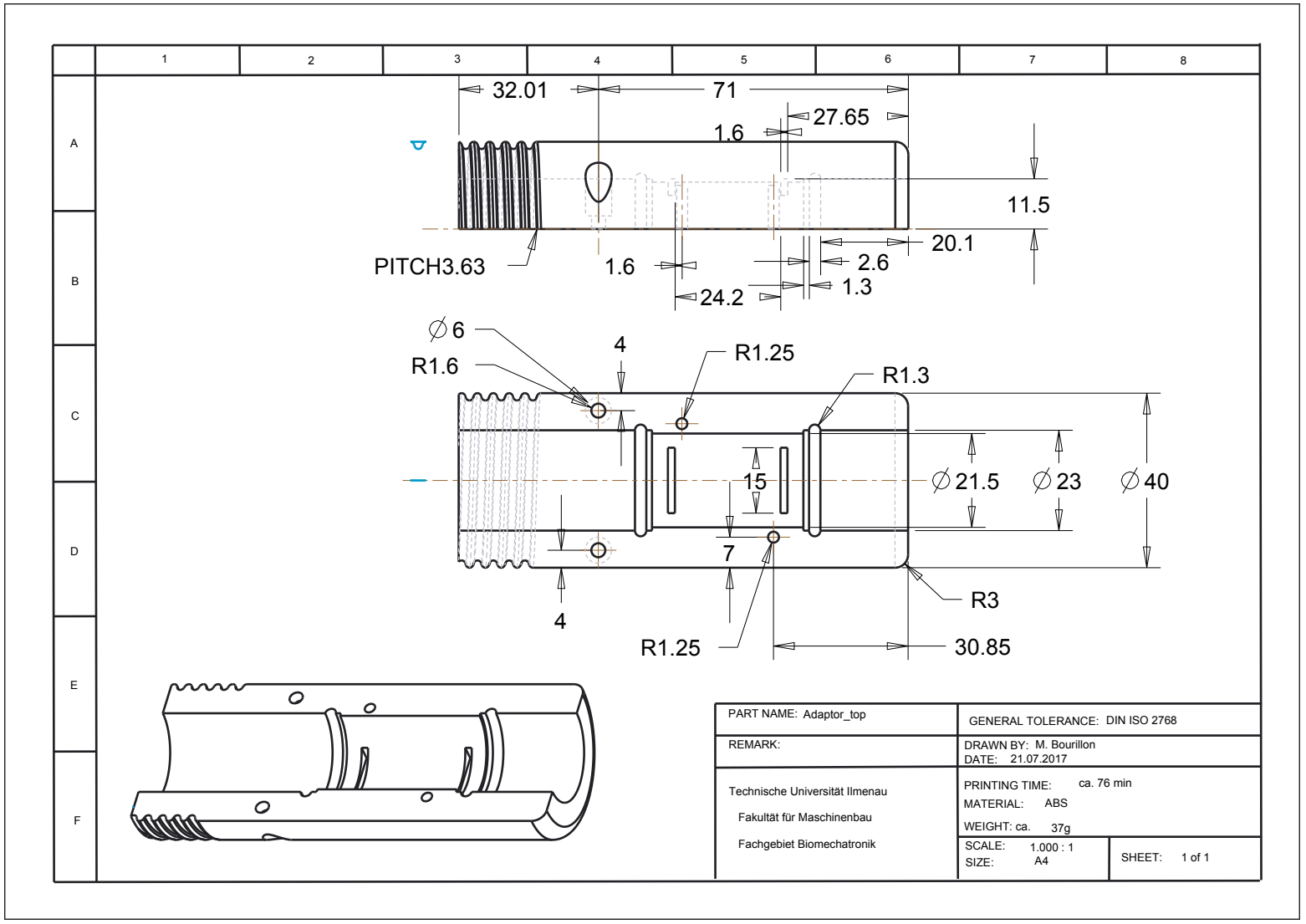
32.01
71
27.65
1.6
11.5
20.1
PITCH3.63
1.6
2.6
1.3
24.2
∅6
R1.6
4
R1.25
R1.3
15
∅21.5
∅23
∅40
7
R3
4
R1.25
30.85
PART NAME: Adaptor_top
GENERAL TOLERANCE: DIN ISO 2768
REMARK:
DRAWN BY: M. Bourillon
DATE: 21.07.2017
Technische Universität Ilmenau
Fakultät für Maschinenbau
Fachgebiet Biomechatronik
PRINTING TIME: ca. 76 min
MATERIAL: ABS
WEIGHT: ca. 37g
SCALE: 1.000 : 1
SIZE: A4
SHEET: 1 of 1

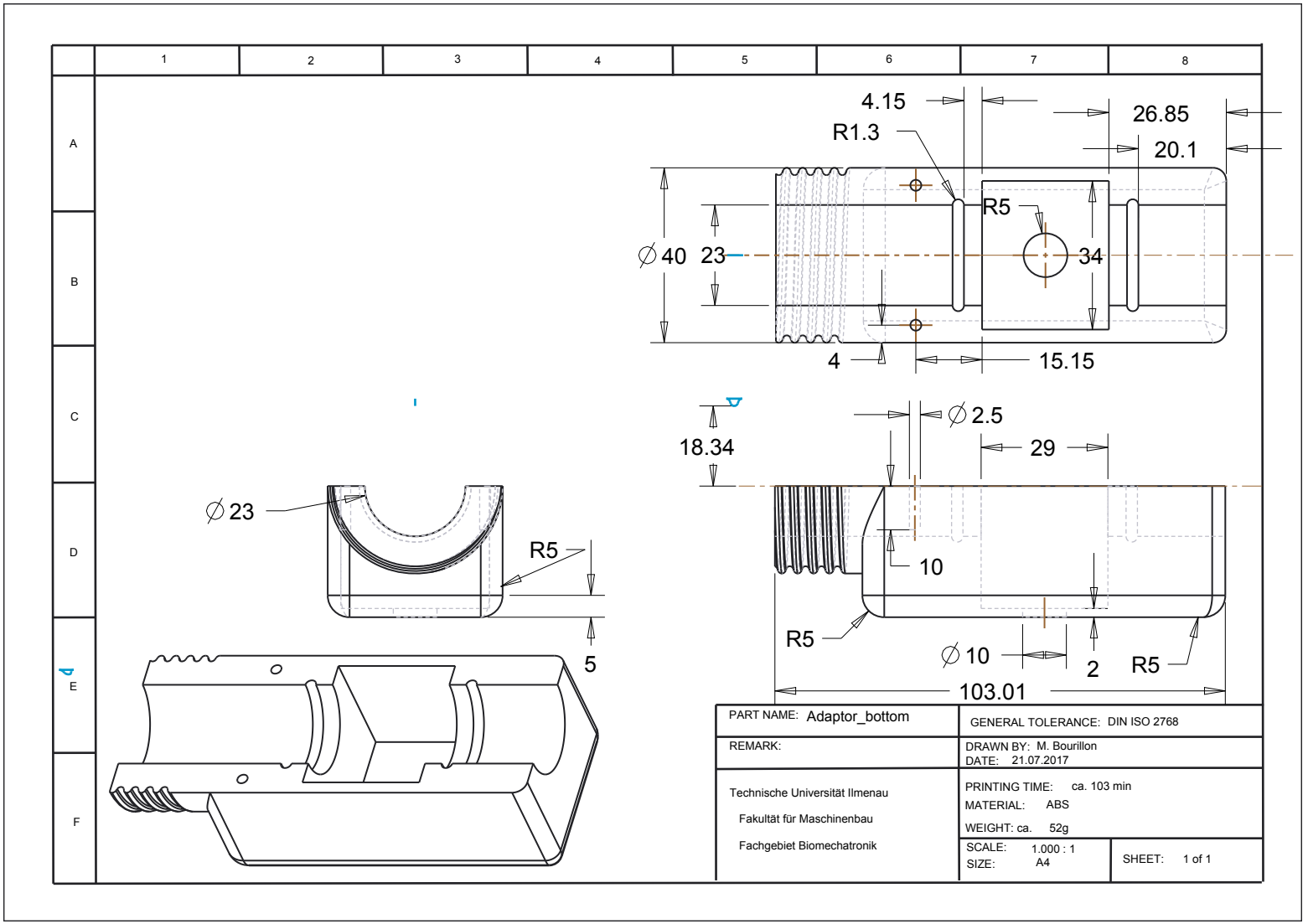
4.15
R1.3
26.85
20.1
R5
∅40
23
34
4
15.15
18.34
∅2.5
29
∅23
R5
10
5
R5
∅10
2
R5
103.01
PART NAME: Adaptor_bottom
GENERAL TOLERANCE: DIN ISO 2768
REMARK:
DRAWN BY: M. Bourillon
DATE: 21.07.2017
Technische Universität Ilmenau
Fakultät für Maschinenbau
Fachgebiet Biomechatronik
PRINTING TIME: ca. 103 min
MATERIAL: ABS
WEIGHT: ca. 52g
SCALE: 1.000 : 1
SIZE: A4
SHEET: 1 of 1

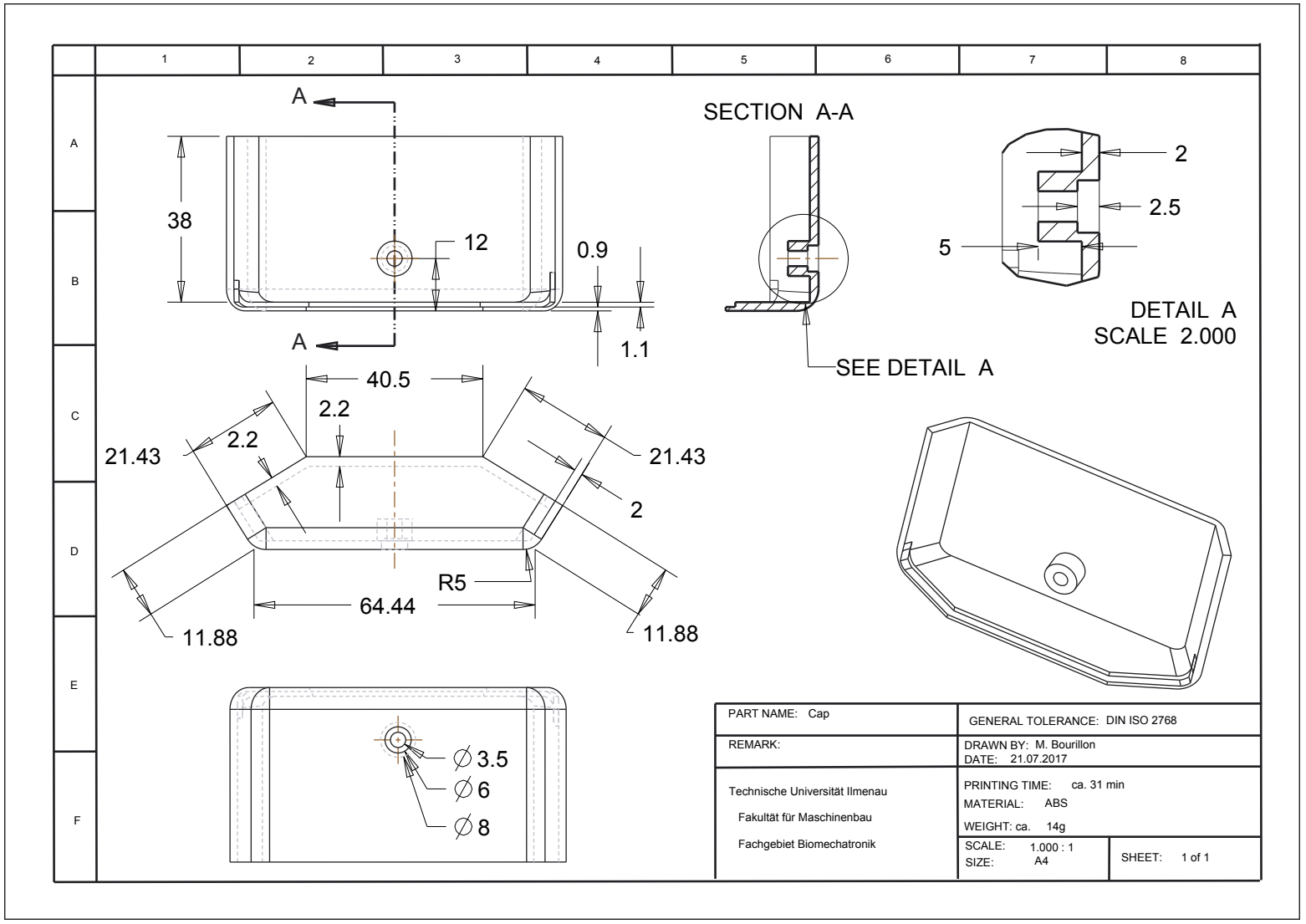
A
38
12
0.9
1.1
A
SECTION A-A
SEE DETAIL A
2
2.5
5
DETAIL A
SCALE 2.000
40.5
2.2
21.43
2.2
21.43
2
R5
64.44
11.88
11.88
∅3.5
∅6
∅8
PART NAME: Cap
GENERAL TOLERANCE: DIN ISO 2768
REMARK:
DRAWN BY: M. Bourillon
DATE: 21.07.2017
Technische Universität Ilmenau
Fakultät für Maschinenbau
Fachgebiet Biomechatronik
PRINTING TIME: ca. 31 min
MATERIAL: ABS
WEIGHT: ca. 14g
SCALE: 1.000 : 1
SIZE: A4
SHEET: 1 of 1

Appendix C

Characteristics of the Graphic Unit Interface (GUI)

C.1 Data Acquisition Interface (DAQ-I)

The GUI controls all the implemented modules, it allows the real time data acquisition and visualization. Also, it saves the data for post processing analysis. Besides, the GUI has the characteristic of being modular. Thus, more devices can be added for future applications.

C.1.1 Signal Visualization

According to the tests, 5 seconds of data correspond to 36480 bytes by Trigno system. To visualize the data in real time, the FIFO[1] principle is used, allowing adding data in an array (buffer), and in case of over-memory, the oldest entries are overwritten (see Fig. C.1).

First the array is filled with new packets (size in multiples of 384 bytes). The array is full of data when it reaches 36480 bytes. Depending on the size of the new packet (384*n), it shifts bytes in 384n position to the left, and it writes the new 384n bytes.

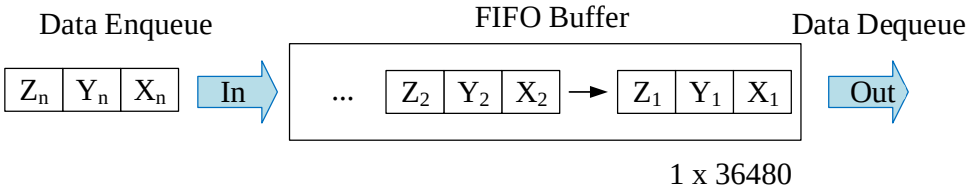

Fig. C.1 Representation of a FIFO (queue) with enqueue and dequeue operations.

C.1.2 Description of the DAQ-I Functions

This section explains each function implemented in the DAQ-I. (Matlab script).

[1] FIFO is an acronym for first in, first out, a method for organizing and manipulating a data buffer, where the oldest (first) entry, or 'head' of the queue, is processed first

<create> This function describes the whole graphic interface. Here buttons are defined, popup menus and other UI-controls. Also, position, size and special properties of each UI-Control were initialized.

<createGraph> This function creates the axes for each signal plot (accelerometer, flow, emg, pressure). To call and update these axes with new data, it sets a handle for each plot. There are additional handles (plot) for post processing. Besides, before the function is called, the number of sensor has to be defined. Thus, one plot can be set for each sensor. Other characteristic in this function is the selection of the number of axis shown. For example, in case of the three axis from each accelerometer, it displays one of the signals (X -axis) to reduce the consumption of computing resources and to facilitate the step identification.

For post processing analysis, markers have been added to help step identification and two additional plots for airflow (filtered signal and volume). In the same way it is possible to add more plots to show other properties or to add more plot-handles. Two other characteristics were considered: (1) The acceleration plot, the y-limits are between ± 9 g. These limit are due to the Trigno sensor's limitations. (2) The airflow plot, the y-limits depend on different factors like type of locomotion, speed and individual performance. After some tests running, they were defined also at its maximum, between ± 200 slm.

<pbNewIP_call> This callback assigns the value of the editable text field to "Trigno-IP Address" variable. Also, it shows the saved value in the static text field at the side.

<pbOwnIP_call> This callback assigns the own IP Address (localhost) to "Trigno IP Address" variable.

<popupmenuMode> This callback assigns the value from popupmenu to the "Module" variable. Depending on the case, it makes visible or/and it enables determined UI setup and axes.

<popupmenuNumS_Callback> This callback assigns the value from popupmenu to Num-Sensor variable. Depending on the case it makes visible or/and it enables determined UI setup. This value defines the number of signals to plot and save.

<popupmenuS1_Callback> This callback assigns the value from popupmenu to Sensor1 (first sensor). This defines the first Trigno sensor number to get data.

<pbStart_call> This function takes the date and the hour to create a new folder named year_month_day_hour_minutes. This folder saves the files with extension $*.txt$ for each sensor.

The communication between Trigno system and GUI works through TCP/IP protocol. The protocol TCP/IP refers to the Transmission Control Protocol (TCP) and the Internet Protocol (IP). This protocol suite provides end-to-end data communication specifying how data should be packetized, addressed, transmitted, routed and received. Thus, the ports define the end point of the transmission. Each Port is included in a TCP/IP Object, which are called interfaceObjects in the Matlab script. The ports assigned to the modules are:

- The command interface between the Trigno Lab and the DCC is implemented on a single port 50040.
- The EMG data are streamed (output only) on port 50041.
- The Accelerometer data are streamed (output only) on port 50042.
- The Airflow Sensor data is stremmed on the port 30000.
- The Pressure Sensor data is stremmed on the port 30001.

In addition, a timer object is included, that schedules the execution of functions in a loop. Using an "fixedSpacing" execution "Mode", a period of 0.01 seconds between each execution is set. That means, plots are every 0.01 seconds updated.
The amount of bytes available to read and to run localReadAnPlotMultiplexed functions are defined by the following conditions:

1. For accelerometer from Trigno System. Because of Trigno Protocol, each value needs eight bytes to be transmitted, with 48 accelerometer channels. Trigno System has 16 sensors, each one with one embedded triaxial accelerometer. That makes 384 bytes to accomplish transmission from 16 accelerometers.
2. For air flow sensor. According to string format from ESP32 with six bytes accomplish transmission from one signed integer value. To start transmissions, the Timer-Objects starts working and the "interfaceObjects" is opened to received data. Each device requires a command to begin the transmission of acquired data.

To start the data acquisition, Trigno System uses a formatted string ['START\r\n\r'] and Air flow sensor uses two commands, “1” and “2”, with breaks of 2 seconds between them. Breaks are necessary to set the sensor in write mode and to begin acquisition. Function "tic-toc" from Matlab is used to fill timelines, time "zero" is defined to be when all objects start.

<pbStop_call> This function stops, deletes "Timer-Objects" and "interfaceObjects" of all module.

<localReadAnPlotMultiplexedFlow> This function is called each time that each "Interface-Object" found bytes available. For avoiding to receive incomplete packet, it is subtracted the remaining bytes (module of available data). This function has the following characteristics:

1. To read formatted data it is necessary to know the format of each system. As shown in Section B.2, the format “%04d”, signed integer with three digits plus sign, defines the format for air flow sensor data. The format “uint8”, 8-bit unsigned integer, defines the format for Trigno data. Without this format it is not possible to make a casting of received bytes.

2. To generate a timeline it the Matlab functions, tic toc is used. The function "tic" defines the zero time, and each "toc" sets the elapsed time between the last data packet received and the new one. Packets have do not the same size, which depends on factors like quality and range of transmission. Therefore, to establish a delta time between data from same packet, the following idea is used, shown in Fig.C.2: Trigno System sends an array with three component each sensor, if it knows a reference time point in the past and an current reference time point. It is possible to calculate the interval time between both.

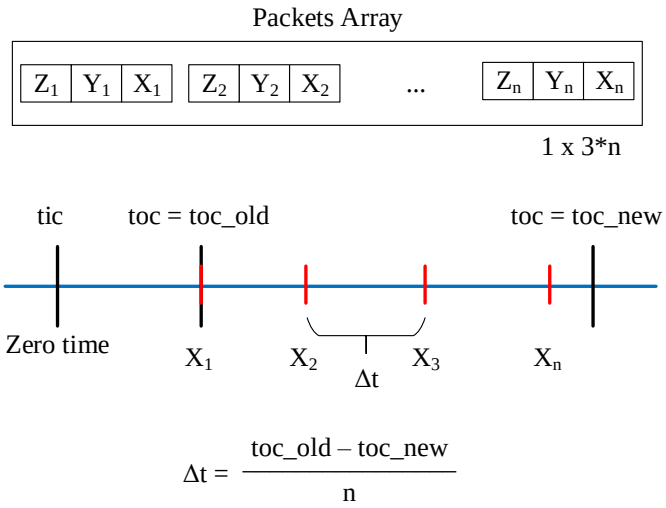

Fig. C.2 Determining the delta time for each sensor value during the data acquisition.

<WriteFile.m> and <WriteFile2.m> These two functions are external functions, as parameters WriteFile receives a values matrix (time, measured value) and a name. In the case of

WriteFile2 is a similar structure, but the indexing of signals change according the number of active sensors.

<updatePlots> This function updates the signal plots setting timeline in x-axis and acquired values in y-axis.

C.1.3 Saving Data

The process of saving data has to repeat in each loop. The buffer is overwritten each time it gets new data. It is not possible to save the data from Trigno and air flow sensor together. The reason is the difference in acquisition rate. Trigno works faster and gets more data than pressure and flow sensor, in the same time interval. Additionally, two different transmission channel are used, that means the data between them arrives with some delay. Saving in separate files increases computation time consumption of the DCC.

C.2 Post Analysis Interface (PA-I)

The Post processing Interface allows the user to load saved data and to visualize the most important signals and characteristics to analyze each experiment. After data loading, it shows one raw signal per sensor.

C.2.1 Description of the PA-I Functions

This section explains the function of the post processing interface (Matlab script).

<helpfigure> This function provides an image which describes how to interpret plotted signals, including the circles of the peaks.

<pbLoad_call> This function loads the data saved. First step is to find the folder where the files are located. Through an "uiget" function (user interface get window) the folder and its location are selected. The files are imported in separate arrays. These arrays are modified, taking the not available numbers (NAN) values out. Also, it initializes the first and last index for both timelines.

<pbPost_call> This callback plots the sensor signals. In case of the accelerometers, this callback reads the size of acceleration matrix to define the amount of values consider in the virtual timeline. Then it proceeds to make new array with just the signal (x,y or z) wanted for the step identification. Furthermore, in the GUI panel, there are sliders associated to set

the parameters "minpeakheight" (threshold) and "minpeakdistance"(ratio) of "findpeaks" function. "Findpeaks" returns the maximal values and their index in the array.

Another characteristic is to use filters to make a smooth curve. In addition, the flow signal can be integrated to calculate the volume. For discrete values an accumulative trapezoidal integration is used. A disadvantage of this procedure is the error accumulation.

Erklärung

Ich versichere, dass ich die vorliegende Arbeit ohne unzulässige Hilfe Dritter und ohne Be-nutzung anderer als der angegebenen Hilfsmittel angefertigt habe. Die aus anderen Quellen direkt oder indirekt übernommenen Daten und Konzepte sind unter Angabe der Quelle ge-kennzeichnet.

Bei der Auswahl und Auswertung folgenden Materials haben mir die nachstehend aufgeführten Personen in der jeweils beschriebenen Weise unentgeltlich geholfen:

1. Die fachliche Betreuung der Promotion Arbeit erfolgte durch Univ.-Prof. Hartmut Witte.

2. Der erste Prototyp des Druckmessmoduls und des Drucksensor-Kalibrierverfahrens wurde von Herrn Antonio Fiestas im Rahmen seiner Masterarbeit entwickelt.

3. Das Design und die Implementierung des volumetrischen Durchflussmessmoduls und die Integration vom Software mit dem TrignoTM Lab-System wurden von Diego Bahena, Marc Bourillon und Sergio Gomez im Rahmen ihrer Arbeit am mechatronischen Projektseminar entwickelt.

4. Der experimentelle Test des globalen Systems wurde mit Unterstützung des Studenten Herrn Jean Paul Barreto an der TU Ilmenau im Rahmen seiner studentischen Hilfkrafttätigkeit durchgeführt.

Weitere Personen waren an der inhaltlich-materiellen Erstellung der vorliegenden Arbeit nicht beteiligt. Insbesondere habe ich hierfür nicht die entgeltliche Hilfe von Vermittlungs- bzw. Beratungsdiensten (Promotionsberater oder anderer Personen) in Anspruch genommen. Niemand hat von mir unmittelbar oder mittelbar geldwerte Leistungen für Arbeiten erhalten, die im Zusammenhang mit dem Inhalt der vorgelegten Dissertation stehen.

Die Arbeit wurde bisher weder im In- noch im Ausland in gleicher oder ähnlicher Form einer Prüfungsbehörde vorgelegt.

Ich bin darauf hingewiesen worden, dass die Unrichtigkeit der vorstehenden Erklärung als Täuschungsversuch bewertet wird und gemäß § 7 Abs. 10 der Promotionsordnung den Abbruch des Promotionsverfahrens zur Folge hat.

Ilmenau, den 08.01.2018 Nelson Enrique Bances Purizaca